



Universidad Autónoma
de Madrid

Departamento de Bioquímica
Facultad de Medicina
Universidad Autónoma de Madrid

Deciphering the mechanism of the arrhythmogenic R735X nonsense PKP2 mutation

PhD candidate: Cristina del Carmen Roselló. Degree in Biotechnology.

Thesis director: Dr. Juan Antonio Bernal

Spanish National Center for Cardiovascular Research (CNIC), Madrid

A mis padres

Estudia las frases que parecen ciertas y ponlas en duda.

David Riesman

AGRADECIMIENTOS-ACKNOWLEDGEMENTS

AGRADECIMIENTOS-ACKNOWLEDGEMENTS

Gracias a mi director de tesis, el Dr. Juan Antonio Bernal, por darme la oportunidad de trabajar en su laboratorio. Por hacerme ver que estaba en el lugar adecuado. Por todo lo aprendido. Gracias por ayudarme a convertirme en una mujer fuerte y con criterio propio.

Gracias al Dr. José Jalife por compartir conmigo su gran sabiduría y experiencia. Por acogerme en su laboratorio como a una más. Por ayudarme cuando ha sido necesario. Por tener la puerta de su despacho o la ventana de *Skype* siempre abierta para mí. Ha sido una suerte y todo un honor.

A todos mis compañeros de laboratorio pasados y presentes, gracias por vuestra inestimable ayuda. Gracias a Cristina, mi amiga y compañera, porque has estado conmigo, y estoy segura de que siempre estarás, en los peores agobios y en las mejores risas. Por compartir conmigo tu inteligencia, tu sensatez y tu prudencia. Por ser brillante y hacer brillar a los demás. A Silvia, la bondad personificada, gracias por tu inocencia y tus ganas de ayudar siempre. Por fijarte en todos los detalles. Por ver siempre el lado positivo de las cosas. Gracias a ambas por acompañarme a llegar hasta aquí. Sin vosotras, no habría sido capaz. A Ana, por tu buen humor, por tu cariño, por hacerme reír hasta el infinito. Gracias *cruso!* A Mariya, gracias por tu desparpajo, por tu fidelidad, por cubrirme siempre. A Diego y María, gracias por enseñarme sobre cardiología, por ser tan buena gente.

A Briane, my partner of adventures, crêpes, make-up, feminism... It has been amazing to meet you and grow up with you during this process. Thanks for having such a glowing heart. A Ghislaine, merci pour ton grand sourire et ton courage, pour être un exemple pour toutes les autres. A Melisa, mi primera amiga en esto de la ciencia. Gracias por acogerme cuando llegué a CNIC, por tu empatía, tu salsa y tus patines. A Julio, Sergio y Jesús, por demostrar que una feria de abril en CNIC es posible. Por ser los mejores compañeros de ciencia y de fiesta. Gracias a María Galardi, María "Manzanares", David, Claudio, Jose, Javito, Itziar, Noelia, Carles, Ruth, Ali, Marcos y a todos aquellos que me han hecho pasar buenos momentos en estos 4 años.

A Giovanna, Nines y Belén, gracias por acogerme en el CC4, enseñarme a trabajar con hiPSCs y compartir conmigo vuestra experiencia. A Paco, por enseñarme y ayudarme cuando no sabía ni

abrir una pipeta dentro de la campana. Por los buenos ratos a ritmo de 3x4. A Cris Sánchez, por tu coherencia, sensatez y prudencia. A Dani, por las risas campana con campana a son de copla o de chiste malo, aunque a veces te arriesgaras a entrar en los desagradacimientos de mi tesis. A ambos, por vuestros inestimables consejos, porque sé que siempre puedo recurrir a vosotros. A Elvira y Verónica, por vuestra profesionalidad y ayuda, por vuestro interés por mis experimentos como si fueran propios. A Álvaro, gracias por tu ayuda desinteresada, por ser tan buen profesor.

A todos los “Mazanares”, ejemplo de trabajo en grupo, gracias por transmitir esa energía y esas ganas por la investigación. A los “Alegre”, a los “Hidalgo”, a Recursos Humanos y a todos los miembros del CNIC que a lo largo de estos años siempre han estado dispuestos a echar una mano, gracias.

To Eric and Kate, thanks for your patience and for teaching me about patch and hiPSC-CMs culture. For those hours spent beside me measuring sodium currents and counting cardiomyocytes. To my Ann Arbor friends -Erik, Roberto, Abuelito, Mary and mis dos Juanes- thanks for turning those months in USA into one of the best experiences I will ever have in my life and make me feel at home. For demonstrating that dancing does not understand about borders. To Ejona, amiga, for taking care of me like a sister, for being such a good friend.

A mi segunda familia, la familia que se elige. A ellas, espejo donde buscarme, mujeres todoterreno, gracias por vuestra valentía y fuerza. A María, Mer y Ángela, mis psicólogas durante estos años. Gracias por caminar junto a mi cada día y alentarme a luchar. Por ser un ejemplo a seguir. A ellos, gracias por vuestra fraternidad y por recargarme siempre de energía positiva. A tod@s, gracias por demostrar que la amistad no entiende de kilómetros y que hay cosas que si son para siempre.

A todos mis ti@s y prim@s. Gracias por formar una familia tan maravillosa. Por ser un matriarcado ejemplar y luchar porque todas tuviéramos las oportunidades que a vosotras os negaron. A mi tío Manu (el Dr. Macías), por motivarme a hacer el doctorado.

A mis abuel@s, gracias por inculcarme tanto, por cuidarme siempre desde allí arriba y desde aquí abajo. A mi segunda madre, mi fan numero uno, gracias.

A mi hermano, mi persona favorita en este mundo. Gracias por aguantarme, perdonarme siempre y hacerme reír como nadie. Por esa maravillosa inteligencia.

A mis padres, la palabra gracias se queda muy corta. Por habérmelo dado TODO. Por haberme apoyado en mis decisiones por locas que os pudieran parecer. Por dejar que me equivoque y que acierte. Por haberme enseñado a ser responsable y persistente. A mi madre, gracias por estar pendiente de todo y ver siempre más allá, por dejarme partir aunque duela, por las croquetas que han recorrido medio mundo. A mi padre, gracias por tu serenidad y tu optimismo, por ser mi chofer sin importar la hora. Gracias por quererlos tanto y ser un gran equipo. Soy muy afortunada.

SUMMARY

SUMMARY

Ventricular arrhythmias (VA) appear during the concealed phase of arrhythmogenic cardiomyopathy (AC). This VA can lead to sudden cardiac death, being in many cases, the first symptom of the disease. Mutations on the desmosomal gene *Plakophilin-2 (PKP2)* have been described as the most prevalent genetic causes of AC. However, the molecular mechanism underlying these early electrical changes during AC development has not been elucidated. PKP2 integrates into the connexome protein network and may lead to changes in its components. In this thesis project we have demonstrated that R735X (a PKP2 truncation associated to AC phenotype) leads to a decrease of the voltage-gated sodium channel $Na_v1.5$ at the plasma membrane of HEK293T and HL-1 cells. In order to study the effect of R735X on a human context, we have developed an AC model based on human induced pluripotent stem cell-derived cardiomyocytes (hiPSC-CM). We have study the role of R735X in hiPSC-CM electrophysiology by comparing electrical features of AC hiPSC-CMs (expressing R735X) with its hiPSC-CM isogenic control. Patch-clamp measurements indicate that R735X leads to a decrease in the fast depolarizing sodium current generated by $Na_v1.5$ channel in hiPSC-CMs. Optical mapping showed an elongation of the action potential duration (APD) and a slowdown in the conduction velocity (CV) of the electrical impulse in mutant 2D hiPSC-CM monolayers, inducing arrhythmogenic events. These results highlight the arrhythmogenic character of R735X protein and could explain the electrical abnormalities reported in AC patients at early stages of the disease.

RESUMEN

RESUMEN

Los pacientes con Cardiomiopatía Arritmogénica (siglas en inglés, AC) pueden sufrir arritmias ventriculares durante la fase subclínica de la enfermedad. Estas arritmias ventriculares pueden provocar la muerte súbita del paciente, siendo en muchos casos, el primer síntoma de la enfermedad. Se ha descrito que la causa genética más prevalente de la AC son mutaciones en el gen desmosomal *Placofilina-2* (siglas en inglés, *PKP2*). Sin embargo, el mecanismo molecular por el que se producen cambios eléctricos en el corazón en fases tempranas durante el desarrollo de la AC no se conoce. PKP2 forma parte de la red proteica conocida como “*connexome*” y puede provocar cambios en sus componentes. En esta tesis, hemos demostrado que R735X (una versión truncada de PKP2 que aparece en pacientes con AC) hace que disminuya la cantidad de canal de sodio ($\text{Na}_v1.5$) en la membrana plasmática de células HEK293T y HL-1. Con el fin de estudiar el efecto de R735X en un contexto humano, hemos generado un modelo de AC basado en cardiomiocitos derivados de células madre pluripotentes inducidas (siglas en inglés, hiPSC-CMs). Hemos estudiado el papel de R735X en la electrofisiología de hiPSC-CMs comparando las características eléctricas de los hiPSC-CMs que expresan la mutación R735X con su control isogénico. Los experimentos de *patch-clamp* demostraron que R735X provoca la reducción en la corriente rápida de sodio que despolariza los cardiomiocitos. Además, el mapeo óptico de monocapas de hiPSC-CMs demostró que R735X provoca un alargamiento de la duración del potencial de acción y enlentece la velocidad de conducción del impulso eléctrico, provocando la aparición de arritmias. Estos resultados subrayan el carácter arritmogénico de la proteína mutante R735X y podría explicar las anomalías eléctricas que se dan en pacientes con AC en fases tempranas de la enfermedad.

INDEX

AGRADECIMIENTOS-ACKNOWLEDGEMENTS.....	9
SUMMARY	15
RESUMEN.....	19
INDEX.....	21
ABBREVIATIONS	25
INTRODUCTION.....	29
1. Cardiac electrophysiology	29
2. Inherited cardiac arrhythmias	31
3. AC: a complex and challenging disease.....	32
3.1. Anatomopathological features.....	33
3.2. Electrocardiogram features.....	34
3.3. AC therapies	34
3.4. Genetics of AC	34
4. AC and the desmosome.....	35
5. PKP2 and the arrhythmogenic phenotype	37
6. PKP2 stop-gain mutations: R735X	38
7. hiPSC-CM as a model of AC	40
7.1. Generation of PKP2 hiPS cell lines.....	40
OBJECTIVES	45
.....	47
MATERIALS AND METHODS.....	49
1. DNA constructs	49
2. Molecular biology	49
3. Cell culture.....	53
4. hiPSCs and hiPSC-CM culture.....	54
5. Electrophysiology.....	60
6. Confocal live imaging	62
7. Statistics	64

RESULTS	69
1. R735X characterization	69
1.1. Subcellular distribution of R735X	69
1.2. Mobility of R735X	72
2. Effect of R735X on Na_v1.5	76
2.1. Subcellular localization of Na _v 1.5 in R735X cells	76
2.1.1. Subcellular localization of Na _v 1.5 in R735X HEK293T cells	76
2.1.2. Subcellular localization of Na _v 1.5 in R735X HL-1 cells	77
2.2. R735X and Na _v 1.5 co-immunoprecipitation	81
2.3. R735X and Na _v 1.5 co-localization	81
2.4. Mobility of Na _v 1.5	83
3. Arrhythmogenic effect of R735X on hiPSC-CM.....	83
3.1. Somatic cell reprogramming and hiPSCs characterization	83
3.1.1. Alkaline phosphatase test.....	84
3.1.2. Karyotype.....	85
3.1.4. <i>In vitro</i> differentiation test	87
3.2. Generation of PKP2 and R735X transgenic hiPS cell lines	88
3.3. hiPSC-CMs maturation.....	89
3.4. Electrical characterization of single transgenic hiPSC-CMs	90
3.5. Analysis of transgenic hiPSC-CM monolayers.....	93
DISCUSSION	105
Transgenic hiPSC-CMs platform to model arrhythmic diseases	105
R735X arrhythmogenic effect on hiPSC-CMs.....	106
AC and BrS: two different diseases?	107
R735X molecular mechanism?.....	108
CONCLUSIONS	115
CONCLUSIONES	119
BIBLIOGRAPHY	123

ABBREVIATIONS

ABBREVIATIONS

AC	Arrhythmogenic cardiomyopathy
AP	Action potential
APD	Action potential duration
APD _x	Action potential duration at X % of repolarization
ARP	Absolute refractory period
ARVC	Arrhythmogenic right ventricular cardiomyopathy
AV	Atrioventricular
BrS	Brugada syndrome
Ca _v	Voltage-gated calcium channel
CV	Conduction velocity
DSC2	Desmocolin-2
DSG2	Desmoglein-2
DSP	Desmoplakin
EBs	Embryoid bodies
ECG	Electrocardiogram
EGFP	Enhanced Green Fluorescent Protein
FRAP	Fluorescence recovery after photobleaching
HEK293T cells	Human embryonic kidney 293T cells
hiPSC-CMs	Human induced pluripotent stem cells-derived cardiomyocytes
hiPSCs	Human induced pluripotent stem cells
I _{Ca}	Calcium L-type current
ID	Intercalated disc
IF	Immobile fraction
IFs	Intermediate filaments
I _{K1}	Inward rectifier potassium current
I _{Kr}	Rapid delayed rectifying potassium current
I _{Ks}	Slow delayed rectifying potassium current
I _{Na}	Sodium current
K _v	Voltage-gated potassium channel
LV	Left ventricle
MF	Mobile fraction
Na _v	Voltage-gated sodium channel
Na _v 1.5	Voltage-gated sodium channel alpha subunit 5
PB	<i>PiggyBac</i>
PDMS	Polydimethylsiloxane
PG	Plakoglobin
PKP2	Plakophilin-2
R735X	PKP2 truncated mutant
RMP	Resting membrane potential
RRP	Relative refractory period

ABBREVIATIONS

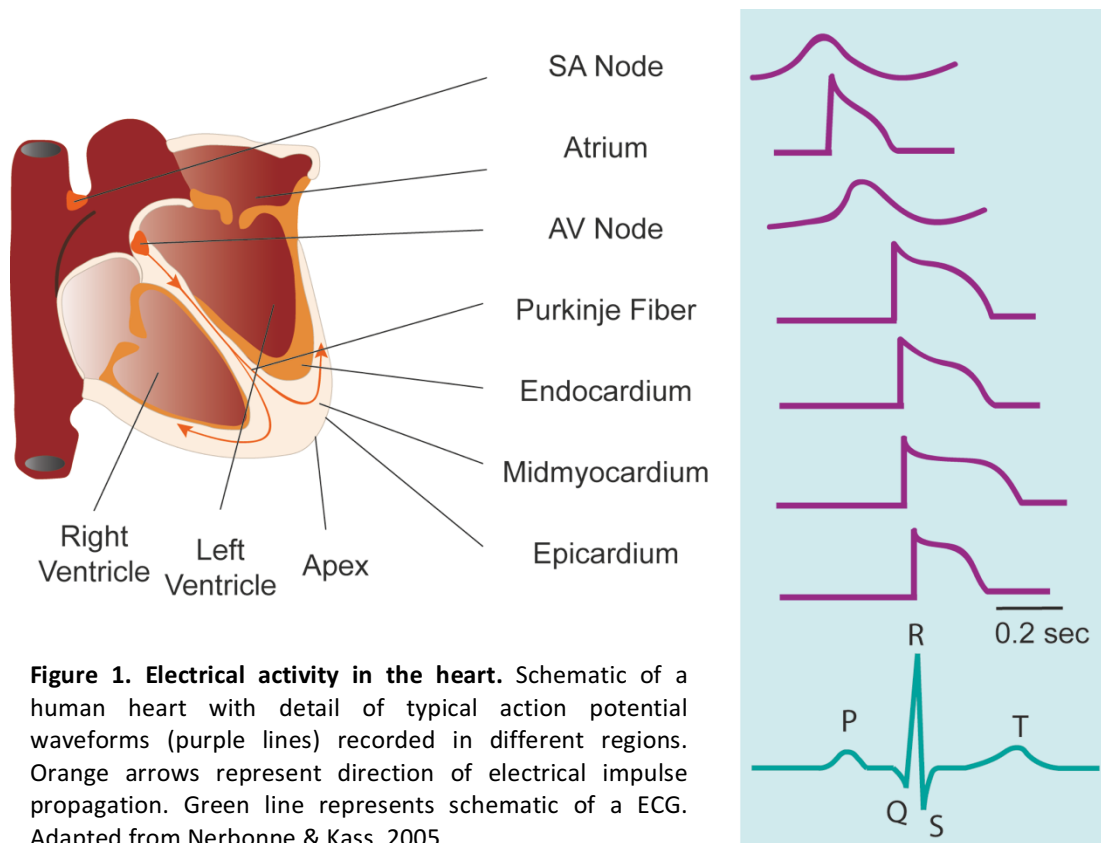
RV	Right ventricle
s.d.	Standard deviation
s.e.m.	Standard error of the mean
SA	Sinoatrial
SCD	Sudden cardiac death
$T_{1/2}$	Half-time of recovery
VA	Ventricular arrhythmias

INTRODUCTION

INTRODUCTION

1. Cardiac electrophysiology

The physiological mechanism whereby the heart pumps blood throughout the body via the circulatory system is a very complex and tightly regulated process. Electrical activity is initiated in the pacemaker cells in the sinoatrial (SA) node and propagated through the atria to the atrioventricular (AV) node. After a brief pause in the AV node, excitation spreads through the Purkinje fibers to the apex of the heart and into the ventricular myocardium (Figure 1). For the cardiomyocytes to contract, an electrical impulse generates an action potential (AP) associated to a contraction event. This event is followed by a relaxation and a refractory period until the next impulse is generated and propagated. An AP is a reversible change in the cell membrane potential that goes from the basal resting membrane potential (RMP, $-85/95\text{mV}$) to approximately $+40/50\text{ mV}$, and returns to the basal RMP. The cardiac AP is the result of the sequential activation and inactivation of ion channels that conduct depolarizing, inward (Na^+ and Ca^{2+}), and repolarizing, outward (K^+) currents. Action potential waveforms are different in each region of the heart, reflecting the heterogeneity of ion channel expression levels in each



cell type. This coordinated electrical activity of the heart can be detected in a surface electrocardiogram (ECG) (Nerbonne and Kass, 2005) (Figure 1).

AP of ventricular cardiomyocytes have four phases (Figure 2) (Grant, 2009) (Nerbonne and Kass, 2005) (Tamargo et al., 2004):

- Phase 0 or fast depolarization: is due to the rapid inward Na^+ current (I_{Na}) through the voltage-gated sodium channel (Na_v). These channels are rapidly opened and closed, becoming inactive.
- Phase 1 or initial rapid repolarization: is consequence of the rapid voltage-dependent inactivation of I_{Na} and the activation of the fast transient voltage-gated outward K^+ current (I_{to}).
- Phase 2 or plateau is the sum of:
 - o inward depolarizing currents of Na^+ (late I_{Na} or I_{NaL}) through the fraction of channels that have not been inactivated completely and Ca^{2+} current (I_{Ca}) through the voltage-gated calcium (Ca_v) L-type channels. Ca^{2+} entry through L-type channels results in Ca^{2+} release from intracellular stores and is the main trigger for excitation-contraction coupling.
 - o the different components of the delayed outward rectifier K^+ current through the voltage-gated K^+ channels (K_v) : rapid (I_{Kr}) and slow (I_{Ks}).
- Phase 3 of repolarization: Na_v and Ca_v channels are inactivated and the outward K^+ currents predominate, resulting in repolarization, bringing the membrane voltage back to the resting potential.
- Phase 4 or diastolic interval: the inward-rectifier K^+ current is activated (I_{K1}) at the end of phase 3. K_1 channels conduct K^+ currents more in the inward direction than in the outward direction, playing an important role in setting the RMP close to the equilibrium potential for K^+ (E_{K} , approximately -90 mV) and in the repolarization of the AP.

During the absolute refractory period (ARP, phase 0-beginning of phase 3) cardiomyocytes are completely unexcitable by a new stimulus. At the relative refractory period (RRP, end of phase 3), cardiomyocytes can be depolarized by a greater than normal stimulus.

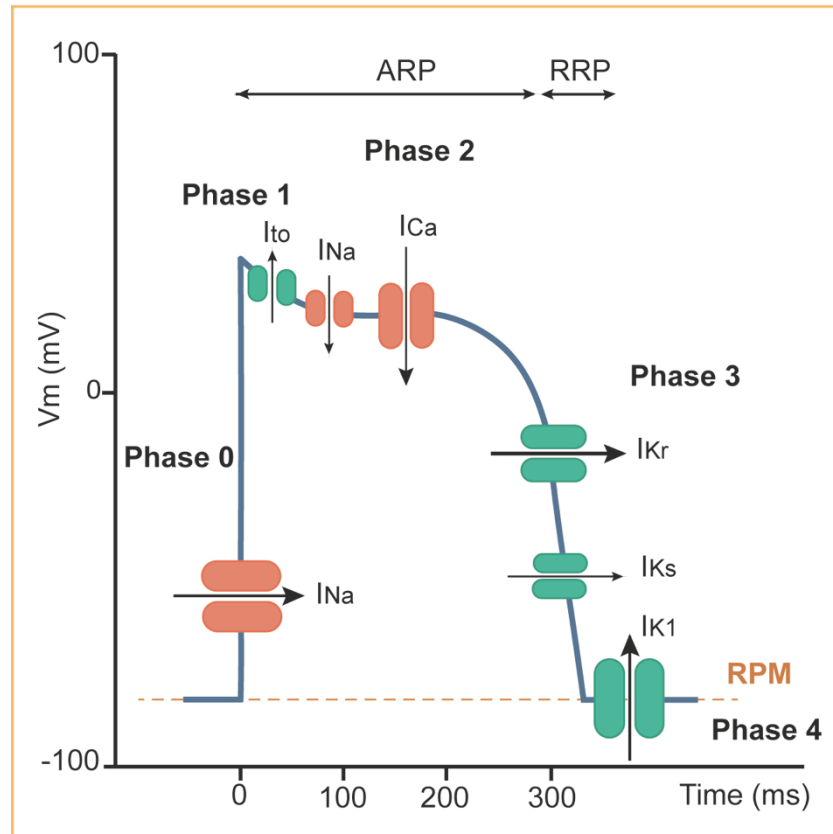


Figure 2. Action potential of a human ventricular cardiomyocyte. Membrane voltage (V_m) in millivolts (y-axis) is plotted against time in milliseconds (x-axis). Resting membrane potential (RMP) is represented at ~ -90 mV. Black arrows represent inwards or outwards ion currents. Red and green ovals represent ion channels. Phase 0-4 of the action potential are indicated. ARP: absolute refractory period. RRP: relative refractory period.

Any factor altering this delicate process would change action potential waveforms, synchronization, and/or propagation, putting the heart at risk of potential life-threatening arrhythmias. Therefore, a thorough understanding of the cardiac electrophysiology and how it might be altered is essential to proper diagnosis and management of cardiac arrhythmias.

2. Inherited cardiac arrhythmias

Inherited cardiac arrhythmias have been classified in two different groups: hereditary arrhythmia syndromes and genetic arrhythmogenic structural heart disease (Beckmann et al., 2011). Hereditary arrhythmia syndromes or channelopathies include several different diseases, such as long QT syndrome (LQTS), Brugada syndrome (BrS), catecholaminergic polymorphic ventricular tachycardia (CPVT), short QT syndrome (SQTS), idiopathic ventricular fibrillation (IVF), and progressive cardiac conduction system disease (PCCD). Ventricular arrhythmias, typical of these syndromes, are caused by mutations of ion channels and their interacting

proteins, mainly involving potassium, sodium, and calcium handling. However, in patients with these diseases, the heart is typically structurally normal without showing macroscopic structural evidence of disease. In fact, patients with channelopathies that suffer sudden cardiac death (SCD) typically show no structural anomalies at the autopsy (Gray and Behr, 2016).

Among the most frequent genetic arrhythmogenic structural heart disease we can find Hypertrophic cardiomyopathy (HCM), Dilated cardiomyopathy (DCM) and Arrhythmogenic cardiomyopathy (AC). Mutations in different sarcomeric, cytoskeletal, desmosomal or nuclear envelope genes mediate structural changes in the cardiac tissue (hypertrophy, dilatation, fibrous infiltration, etc.) which have been related to arrhythmias and SCD (Nishimura Rick A. et al., 2017)(Reichart et al., 2019).

3. AC: a complex and challenging disease

Arrhythmogenic cardiomyopathy (AC), known for many years as arrhythmogenic right ventricular cardiomyopathy (ARVC) (Platonov et al., 2019) is a chronic, progressive and heritable cardiomyopathy. AC is one of the leading causes of **unexpected sudden cardiac death** in young and apparently healthy individuals. It has been classified as a rare cardiac pathology (ORPHA247) (Alcalde et al., 2014) and its estimated prevalence ranges from 1:1000 to 1:5000, sudden death being the first symptom of the disease in many cases (Haugaa et al., 2016).

General AC disease progression has been divided into **three phases** (Haugaa et al., 2016):

1. Early “concealed phase”: in this phase individuals are often asymptomatic, but are at risk of ventricular arrhythmias and sudden cardiac death.
2. Overt “electrical phase”: individuals present with symptomatic arrhythmias. RV morphological abnormalities may still not be detectable by conventional imaging tools.
3. Diffuse, progressive disease resulting in right, left, or biventricular heart failure, often combined with ventricular arrhythmias.

However, it is important to note that 30% of patients with morphological criteria for AC have a so-called ECG-concealed form that does not fulfill the ECG diagnostic criteria.

Diagnosis of AC is one of the most challenging in the field of inherited cardiomyopathies due to two main reasons (Gandjbakhch et al., 2018):

- Its **variable expressivity** and **incomplete penetrance** in relatives.

AC clinical manifestations usually appear during adolescence, but can also manifest later on in adulthood. Disease progression is highly variable. For instance, life-threatening ventricular arrhythmias may present as periodic bursts and “hot phases” instead of manifesting as a steady process. AC progression is strongly determined by environmental factors such as inflammatory processes and exercise. Clinical diagnosis of relatives is particularly difficult in AC because of the low penetrance of mutations. In fact, only one third of relatives fulfill definitive task force criteria diagnosis. Thus, clinical screening is usually not sufficiently accurate to predict their genetic status. Moreover, phenotype and penetrance in AC are age dependent, and phenotypically negative relatives may present with symptoms and cardiomyopathy years after initial screening (Gandjbakhch et al., 2018).

- Absence of specific unique diagnostic criteria.

In 2010, several **combined diagnostic criteria** (task force criteria, TFC) were reviewed and implemented, increasing diagnosis specificity (especially in family members and young athletes). However, AC 2010 TFC still lack sensitivity, in the early stages of the disease (Gandjbakhch et al., 2018). AC task force criteria include: global or regional dysfunction and structural alterations, tissue characterization of the ventricular wall, re- and depolarization or conduction abnormalities, arrhythmias, genetics and family history.

3.1. Anatomopathological features

AC main anatomopathological feature is the loss of cardiomyocytes and its replacement by fibrous or fibroadipose tissue in the RV free wall. LV pathological histology is frequently reported in autopsy cases or explanted hearts, even in the absence of macroscopic LV changes. It should be noted that fatty infiltration by itself is not required as a histological diagnostic criterion. In fact, a systematic study of myocardial biopsies showed the absence of specific RV fat infiltration in contrast to extensive fibrous tissue and cardiomyocyte loss (Gandjbakhch et al., 2018).

3.2. Electrocardiogram features

ECG-based TFC diagnostic criteria include: right precordial T-wave inversions, epsilon waves, and increased duration of the terminal QRS. T-wave inversions in the right precordial leads are present in up to 87% of adult patients with AC and are directly related to RV dilatation, which may extend to the left precordium with time. Tanawuttiwat T. *et al.* (2016) performed a study where they showed the great variety of ECG presentations. It included 35 AC patients with negative precordial T-waves that were studied by epicardial and endocardial mapping, and MRI imaging. They showed the relationship between the QRS and disease localization and extent. For instance, when the QRS appeared normal, the extent of activation after the end of QRS was minimal and mostly subepicardial. On the other hand, the epsilon wave would correspond to epicardial perivalvular activation (Tanawuttiwat et al., 2016). This study reflects the heterogeneity found in electrocardiogram features among patients which is one of the reasons why AC may be easily misdiagnosed.

3.3. AC therapies

At present there is no effective treatment that can prevent the progression of AC. Therapies focus on symptoms treatment such as the prevention of lethal events. Implantable cardioverter defibrillator placement is the only therapy proven to improve mortality in AC patients. The rest of the treatments - medications (beta blockers and antiarrhythmics), radiofrequency ablation, surgery, cardiac transplantation, and lifestyle changes- help to treat symptoms but none of them have proved to decrease mortality (Idris et al., 2018)(Platonov et al., 2019)(Wang et al., 2019).

3.4. Genetics of AC

Molecular genetic reports have revealed AC to be mainly an autosomal dominant inherited disease (Haugaa et al., 2016). To date, up to 16 different genes have been associated with the AC phenotype. Nonetheless, the genetic cause of AC remains unknown for approximately 40% of patients. AC has been mainly associated with mutations in genes encoding the desmosomal proteins: *plakophilin-2 (PKP2)*, *desmoglein-2 (DSG2)*, *desmoplakin (DSP)*, and, more rarely, *desmocollin-2 (DSC2)* and *plakoglobin (JUP)*. In addition, non-desmosomal genes have also been identified as responsible for this pathology: *catenin- α -3 (CTNNA3)*, *cadherin-2 (CDH2)*, *transmembrane protein 43 (TMEM43)*, *lamin A/C (LMNA)*, *desmin (DES)*, *titin (TTN)*, *phospholamban (PLN)*, *ryanodine receptor type 2 (RYR2)*, *sodium voltage-gated channel α*

subunit 5 (SCN5A), tumor protein P63 (TP63) and transforming growth factor-β-3 (TGFB3) (Gandjbakhch et al., 2018). In table 1, all AC associated genes are enlisted together with their frequencies and other associated phenotypes.

Gene	Protein	Frequency in AC ‡	Structure	Phenotype AD
PKP2	Plakophilin-2	20%–45%	Desmosome	ARVC
DSG2	Desmoglein-2	4%–15%	Desmosome	ARVC, BiVCM
DSP	Desmoplakin	1%–13%	Desmosome	ARVC; ALVC, DCM, Cardio-cutaneous Sd, CCD†
DSC2	Desmocollin-2	1%–7%	Desmosome	ARVC, BiVCM cardiomyopathy
JUP	Plakoglobin	0%–1%	Desmosome	ARVC
CTNNA3	α-T-catenin	<1%	Intercalated disc	ARVC
CDH2	N-Cadherin	2%* of patients with negative genetic screening (missense)	Intercalated disc	ARVC
TMEM43	LUMA	<1%	Nuclear envelop, Intercalated disc, sarcolemma	ARVC EDMD
LMNA	Lamin A/C	3%–4%	Nuclear envelop	DCM/BiVCM/ARVC with CCD, AF, VAs _ muscular dystrophy
DES	Desmin	<1%	Intermediate filament	DCM/BiVCM/ARVC with CDD, AF, VAs _ muscular dystrophy
TTN	Titin	18%* of AC patients with negative genetic screening (missense)	Sarcomere	ARVC/BiVCM
PLN	Phospholamban	0%–12% (Netherlands)	Calcium regulatory protein	DCM, BiVCM, ARVC, HCM
RYR2	Ryanodine receptor type 2	9%* of AC patients with negative genetic screening (missense)	Calcium regulatory protein	CPVT _ right ventricular involvement AC
SCN5A	Na _v 1.5	0%–2%*	Cardiac sodium channel	Brugada Sd, Long QT Sd, AF, CDD, DCM, ARVC, MEPPC
TP63	P63	1 case report	Transcription factor	Ectodermic dysplasia. ARVC†, ADULT Sd
TGFB3	TGF-beta 3	2 families	Transforming growth factor	ARVC

*Frequency of rare missense variants. †Unique observation in the literature. ‡Patients with AC phenotype fulfilling task force criteria. AD: autosomal dominant; AF: atrial fibrillation; ALVC: arrhythmogenic left ventricular cardiomyopathy; BiVCM: biventricular cardiomyopathy; CCD: cardiac conduction disease; CPVT: catecholaminergic polymorphic ventricular tachycardia; DCM: dilated cardiomyopathy; EDMD: Emery-Dreifuss muscular dystrophy; HCM: hypertrophic cardiomyopathy; MEPPC: Multifocal ectopic Purkinje-related premature contractions; SCD: sudden cardiac death; Sd: syndrome.

Table 1. List of genes associated with AC. Adapted from Gandjbakhch *et al.* 2018.

4. AC and the desmosome

Desmosomes are membrane protein complexes that play an important role in intercellular adhesion and maintenance of the structural integrity of tissues subjected to mechanical stress, such as the heart and skin. Hemidesmosomes integrate transmembrane proteins: Desmocollin-2 (DSC2) and Desmoglein-2 (DSG2), that attach to their neighbor hemidesmosome

transmembrane proteins; and inner face proteins: Plakophilin-2 (PKP2), Plakoglobin (PG) and Desmoplakin (DSP), that associates with transmembrane proteins and intermediate filaments (IFs) (Figure 3). DSP (member of the Plakin family of cytolinkers) serves as a core constituent of the dense plaque. DSP anchors IF to the plasma membrane by its C-terminus and is tethered indirectly to DSC2 and DSG2 (plasma membrane cadherins) by its N-terminus. N-terminal tethering of DSP is facilitated by PG and PKP2 (armadillo family) (Godsel et al., 2010).

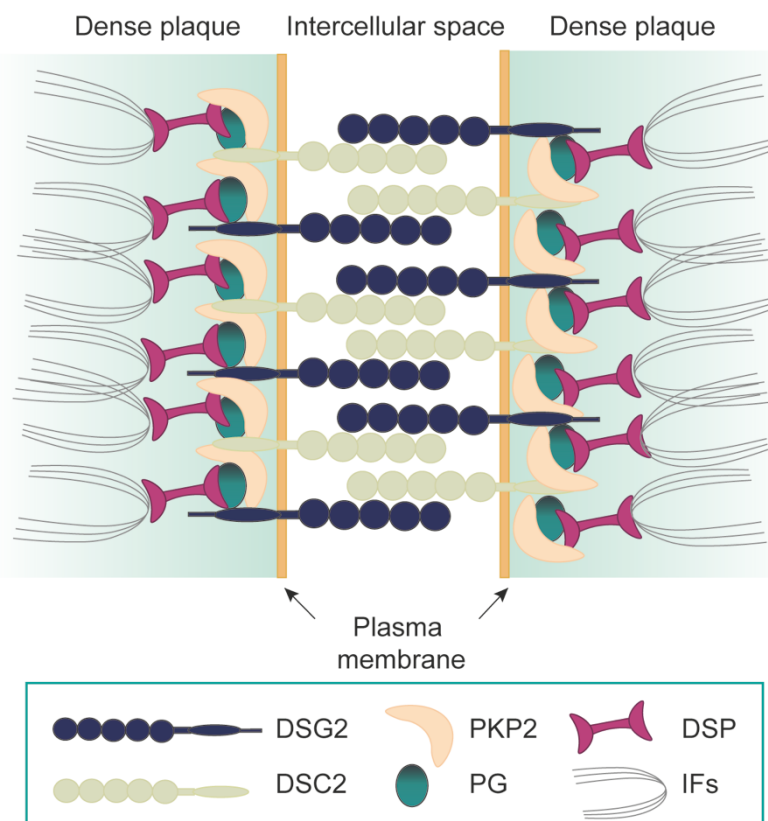


Figure 3. Cardiac desmosome. Organized desmosomal proteins and intermediate filaments (IFs) are represented. DSC2: Desmocollin-2, DSG2: Desmoglein-2, PKP2: Plakophilin-2, PG: Plakoglobin, DSP: Desmoplakin.

Mutations in desmosomal genes have been identified in up to ~60% of AC probands in different patients cohorts. These mutations usually have an autosomal dominant mode of inheritance with incomplete penetrance, leading to an isolated cardiac phenotype. Various types of mutations -missense, stop-gain, splice-site, frameshift, and large deletions- have been reported. PKP2 is the major AC disease-causing gene, accounting for up to ~90% of mutations identified in desmosomal genes (Cox et al., 2011)(Bao Jingru et al., 2013)(Groeneweg et al., 2015)(Fressart et al., 2010). PKP2 mutations are mostly autosomal dominant and are more likely to lead to isolated RV involvement and a conventional phenotype than other desmosomal mutations (te Riele et al., 2013).

5. PKP2 and the arrhythmogenic phenotype

AC patients present an arrhythmogenic phenotype that may exist even from the subclinical or concealed phase of the disease, without being paired with dysfunction and structural alterations. The mechanisms responsible for life-threatening arrhythmias in the concealed phase of AC still remain unclear. There are studies suggesting that, even though most of the AC associated mutated genes do not codify for channel proteins, their proteins would associate with molecules that are crucial for the heart electrical performance. Historically, it has been described that cardiac cells are in direct contact at the site of end-end cell apposition through the intercalated discs (ID). Different separated molecular complexes were defined at the ID: gap junctions, desmosomes, adherens junctions and the voltage-gated sodium channel (Na_v) complex. However, the current experimental data support that instead of being independent, these molecular complexes form a common protein interacting network at the ID, the so-called “connexome”. This protein network will have the role of controlling excitability, electrical coupling and intercellular adhesion. Thus, alterations in one the components of the connexome, could have an effect on the other components (Agullo-Pascual et al., 2014). For instance, an immunohistochemical study (Noorman et al., 2013) performed on human AC patient biopsies (61% of them had PKP2 mutations) revealed that immunoreactive signal of $\text{Na}_v1.5$ (the pore forming α -subunit of Na_v complex) at the intercalated disc was decreased in 65% of AC patients; although immunoreactive signals of the mechanical components appeared generally unaffected. Hence, they propose the decrease of $\text{Na}_v1.5$ at the ID as a possible component of the electrophysiological substrate present in AC patients.

Whole-cell patch-clamp experiments performed on isolated cardiomyocytes from heterozygous null PKP2 mice (PKP2-Hz) revealed that average peak of sodium current density (I_{Na}) in PKP2-Hz cardiomyocytes was significantly reduced when compared with control cells. Same experiment performed on flecainide-treated isolated cardiomyocytes showed a more acute and faster block in PKP2-Hz cells. Electrical epicardial activation mapping of Langendorff-perfused whole heart preparations showed that flecainide caused a most pronounced decrease in longitudinal propagation velocity in PKP2-Hz hearts. Moreover, 50% of PKP2-Hz animals showed flecainide-induced ventricular arrhythmias, while none was observed in any of the wild-type mice tested (Cerrone et al., 2012). Thus, electrophysiological characterization of the PKP2 haploinsufficient mouse indicates that a decrease in normal levels of PKP2 associates with sodium channel dysfunction and increase of susceptibility to ventricular arrhythmias. Moreover, it has been shown that a reduction of PKP2 levels in HL-1 cells (PKP2-KD HL-1 cells) correlates with a

reduction in sodium current density and a decrease of co-localization between $\text{Na}_v1.5$ and N-cadherin at site of cell contact. They also showed how transient transfections of *PKP2* in *PKP2*-KD HL-1 cells was able to restore normal levels of I_{Na} and normal co-localization levels between $\text{Na}_v1.5$ and N-cadherin, while overexpression of different *PKP2* missense mutants were not (Cerrone et al., 2014).

6. *PKP2* stop-gain mutations: R735X

In 2014, Alcalde et al. performed genotype-phenotype correlations of a small AC Spanish cohort (30 patients) to establish the diagnostic value of genetic screening and to assess the role of mutation types in age-related penetrance in AC. After screening the desmosomal genes, they found that stop-gain *PKP2* mutations were the most prevalent desmosome-related gene mutation in AC Spanish patients (Figure 4) (Alcalde et al., 2014).

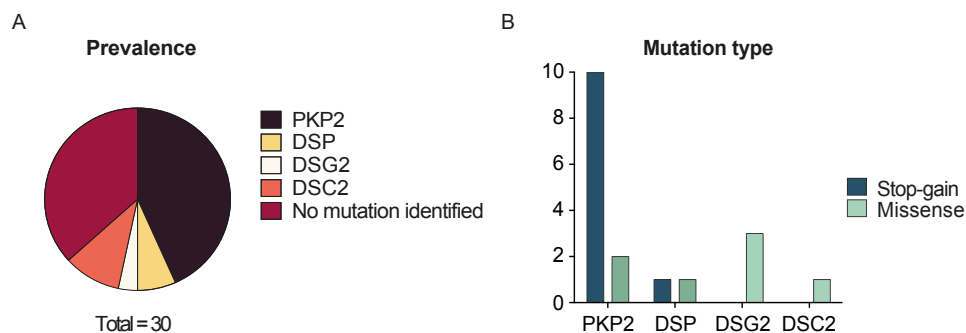


Figure 4. Representation of genetic screening in AC Spanish cohort (30 patients). A. Prevalence of desmosomal gene mutations. B. Prevalence of stop-gain and missense mutations. Adapted from Alcalde et al. 2014

A stop-gain mutation may lead to an haploinsufficiency related phenotype, if the resultant peptide is degraded. However, stop-gain mutations may lead to an actual, “new” protein whose role is to be determined. Thus, we focused on one of the reported *PKP2* truncating mutations to further investigate its molecular mechanism in AC development. Specifically, we chose the mutation c.2203C>T which codifies for an early stop codon in exon 11 (R735X) since this exon is a hot spot of recombination that give raise to several *PKP2* truncations reported in AC patients (Petros et al., 2006)(Gerull et al., 2004)(Tan et al., 2010). The wild-type sequence of *PKP2* has an HR2 domain at its N-terminus and 8 armadillo repeats domains (ARM) and R735X causes the lost of partially ARM6 to C-terminus (Figure 5).

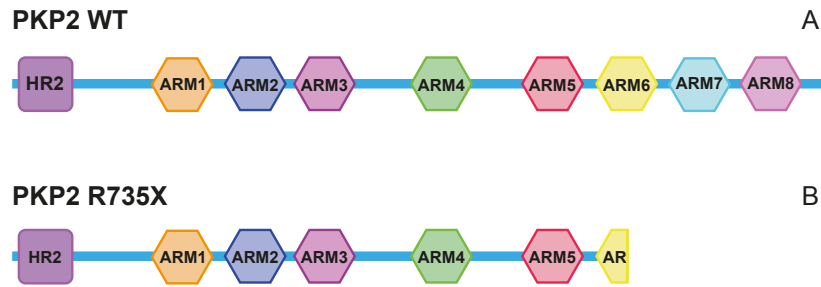


Figure 5. Diagram of PKP2 sequence. A. Representation of PKP2 wild-type sequence: HR2 domain (square) and 8 armadillo (ARM) repeats (hexagons). B. Representation of truncated PKP2. R735X early stop codon mutation causes the loss of partially ARM6 to C-terminus. Adapted from Alcalde et al. 2014.

The AC patient carrying the mutation R735X described by Alcalde et al. (2014) is a 52 years old female that suffered syncope and presents with RV dysfunction and structural alterations, repolarization abnormalities, ventricular arrhythmias and family history of SCD. An example of her ECG can be found in figure 6. R735X mutation has also been found in other patient cohorts that presented with syncope, ventricular tachycardia, right ventricular and in some cases left ventricular involvement and family history (Gerull et al., 2004). The characterization of the wild-type mice injected with adeno-associated virus (AAV) encoding for R735X demonstrated that the truncated PKP2 functions as a dominant-negative protein. R735X mice showed a prolongation of the QRS, reduction in right ventricular ejection fraction and poor contractility when subjected to endurance training (Cruz et al., 2015).

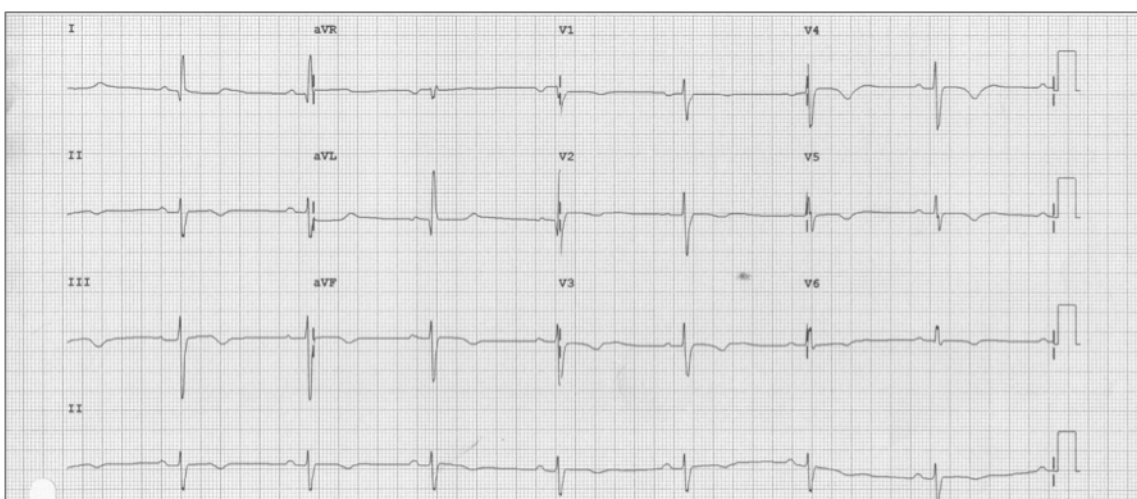


Figure 6. Electrocardiogram of a patient carrying c.2203C>G p.R735X mutation in PKP2 gene. Patient was diagnosed with mayor repolarization abnormalities (T-wave inversion) according to the TFC of the European Society of Cardiology/International Society and Federation of Cardiology criteria for ARVC (Alcalde et al., 2014).

7. hiPSC-CM as a model of AC

Animal models or cell-derived animal models have helped to enlighten the pathogenesis of AC. Indeed, during this thesis project, different cell models (such as HEK293T and HL-1 cells) have been used to characterize the molecular biology of R735X. However, regarding electrophysiological studies, the significant differences between these models and the human electrical features may interpose limits on the interpretation and application of the obtained data. Nonetheless, the study of AC electrical mechanisms in human cardiomyocytes is extremely limited because obtaining cardiac samples from early stages of human AC hearts is not always possible since AC is commonly diagnosed at later stages or post-mortem, and biopsies may result in cardiac perforation. At this point, development of human induced pluripotent stem cell-derived cardiomyocytes (hiPSC-CMs) technology appears as an alternative platform to study the effect of AC-related mutations in the human electrophysiology.

7.1. Generation of PKP2 hiPS cell lines

Since hiPSCs generation technology and optimization of differentiation protocols became popular, many studies have been done comparing hiPS cells derived from patients and hiPSCs from healthy donors. This system is interesting because these hiPSC lines carry the genetic identity of each patient including disease-causing mutations and its genetic context. However, interpretation of its endpoints can be challenging due to differences in their genetic background. On the other hand, using genome-editing technologies, such as CRISPR/Cas9 system, to introduce or correct specific mutations in hiPSCs has become an alternative to overcome this problem (Paul J Tesar, 2018).

Instead, we decided to create a platform that allow us to generate hiPS cell lines that express specific disease-related transgenes over a common, irrespective of patient's genetic background using the *piggyBac* (PB) technology. PB technology allows for the efficient and rapid integration of a DNA sequence of interest into a host genome. The PB system used in this project was composed by two different elements: the PB transposon and the PB transposase. The PB transposon is a mobile genetic element consisting of any sequence flanked by a specific inverted terminal repeats (5'-TRs and 3'TRs). The transposase is an enzyme that recognize the TRs placed on both ends of the transposon sequence and insert the transposon into TTA genome sites through a "cut-and-paste" mechanism in a very efficiently way (Allan Bradley, 2007). This approach has been proved to be a simple and versatile way to stably integrate and express

transgenes in hiPSCs. It is a robust and straightforward method to gene delivery into hiPSCs compared with classical delivery viral or BAC vectors. The cargo capacity of PB is massive compared to virus and does not have the risk of resection or fragmentation seen with random BAC integration (Kim et al., 2016). This method is less time consuming and more efficient than CRISPR/Cas9 system. Moreover, it allows to perform comparative studies between different transgenic lines with isogenic background. As a proof of concept of this approach, we have developed an AC model based on hiPSC-CMs consisting on: a non-modified hiPS cell line generated from reprogrammed somatic cells of a healthy donor (control line), a R735X hiPS cell line generated by integrating the mutant transgene (R735X) into the control line and a PKP2 hiPS cell line generated by integrating the wild-type version of the transgene (PKP2) into the control line (Figure 7).

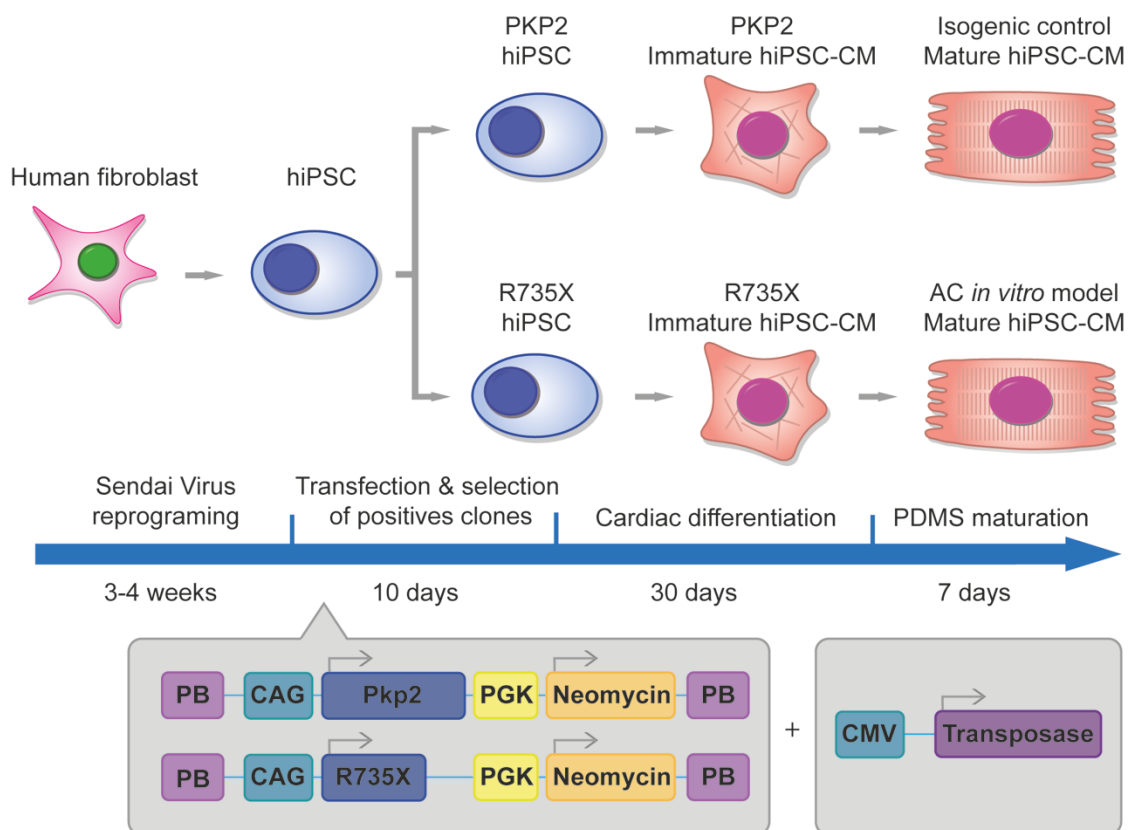


Figure 7. Generation of the AC model based on hiPSC-CMs. Human dermal fibroblast were reprogrammed into hiPS cells. hiPSCs were co-transfected with the constructs *pPB-CAG-PKP2-PGK-Neomycin-PB* or *pPB-CAG-R735X-PGK-Neomycin-PB*, and *pCMV-Transposase*. *CMV*: human cytomegalovirus promoter. *CAG*: CMV enhancer fused to the chicken beta-actin promoter. *Neomycin*: Neomycin resistance gene. *Transposase*: Transposase gene. Positives clones were selected with Neomycin treatment. hiPSC were differentiated into cardiomyocytes using a small molecule based protocol (see Materials and Methods). Resultant hiPSC-CMs were matured for 7 days on PDMS. R735X hiPSC-CMs and its isogenic control (PKP2 hiPSC-CMs) were characterized.

OBJECTIVES

OBJECTIVES

1. To study the impact of the mutation R735X in the localization and mobility of the PKP2 protein.
2. To study the effect of R735X on the voltage-gated sodium channel $\text{Na}_v1.5$.
3. To generate an AC model based on hiPSC-CMs.
4. To characterize the effect of R735X on single hiPSC-CM electrophysiology.
5. To evaluate the potential arrhythmogenic effect of R735X in hiPSC-CMs monolayers.

MATERIALS AND METHODS

MATERIALS AND METHODS

1. DNA constructs

Fluorescent-tagged proteins

The wild-type sequence of *plakophilin-2* (*PKP2*) gene was purchased from Gene Cube. The stop codon in the amino acid 735 was introduced in the wild-type sequence of *PKP2* gene by PCR to generate the truncation R735X. The sequence of the *SCN5A* gene (hH1a isoform) codifying for the sodium voltage-gated channel alpha subunit 5 (Na_v1.5) was kindly provided by Dr. Eva Delpón, Autonomous University of Madrid.

SCN5A was cloned into the plasmid *pEGFP-C1* (Clontech) to generate the plasmid codifying for the fusion protein EGFP-Na_v1.5 (N-terminal EGFP). The same strategy was followed to generate the plasmids codifying for both EGFP-*PKP2* and EGFP-R735X proteins (N-terminal EGFP). Plasmids codifying for tdTomato-*PKP2* and tdTomato-R735X proteins (N-terminal tdTomato) were generated by substitution of the *EGFP* sequence for the *tdTomato* sequence, kindly provided for Dr. Joan Invern (CNIC).

PiggyBac constructs

To generate stable cell lines, both *PKP2* and *R735X* genes were cloned into a *piggyBac* (PB) vector. Both PB vector and PB transposase vector were kindly provided by Dr. Allan Bradley (Sanger Institute).

All the plasmids were cloned and propagated in the Stb13 *E. coli* strain (Invitrogen, C737303).

2. Molecular biology

Western Blot

25 µg of proteins were mixed with loading buffer (60 mM Tris-Cl pH 6.8, 2% SDS, 10% glycerol, 5% β-mercaptoethanol, 0.01% bromophenol blue) and boiled at 95°C during 10 min. Boiled proteins were loaded in home-made 6% acrylamide mini (8.6 x 6.7 cm) SDS-PAGE gel. Gels were run at

30 mA in running buffer (25 mM Tris, 190mM Glycine, 0.1% SDS). When resolving smaller proteins was needed, Novex™ NuPAGE™ 4-12% Bis-Tris Protein Gels (Invitrogen, 10472322) were used. These gels were run on ice at 80 V. Proteins were transferred from the gel to a PVDF membrane (Membrana Immobilon-P, 0.45 µm, Merck, IPVH00010) in a transfer tank filled with transfer buffer (50 mM Tris, 380 mM Glycine, 10% methanol) at 30V during 16 hours at 4°C.

Nonspecific binding sites were blocked with 5% BSA-TBST buffer during 1 hour at room temperature in agitation and subsequently, incubated overnight with primary antibodies (Table 2) diluted in 1% BSA-TBST buffer in agitation at 4°C. Membranes were washed with TBST buffer and incubated for 1 hour with secondary antibodies (Table 2) diluted in 1% BSA-TBST buffer in agitation at room temperature. Membranes were washed again and we proceeded to analyze them either using the Odyssey imaging system (Li-Cor) for secondary antibodies conjugated to a fluorophore or using Amersham ECL Western Blotting Detection Reagent (GE Healthcare, RPN2209) for secondary antibodies conjugated to a HRP (horseradish peroxidase). Densities of proteins were measured using Image J software.

Antibody	Reference	Source	Dilution
Na _v 1.5	Alomone, ASC-005	Rabbit	1:1000
PKP2	Everest Biotech, EB10841	Goat	1:1000
GAPDH	Santa Cruz Biotechnology, sc-32233	Mouse	1:1000
N-Cadherin	Santa Cruz Biotechnology,	Mouse	1:1000
Na ⁺ /K ⁺ ATPase	Abcam, ab7671	Mouse	1:1000
Vinculin	Sigma, V4139	Rabbit	1:1000
Anti-Mouse Immunoglobulins/HRP	Dako, P0447	Goat	1:5000
Anti-Rabbit Immunoglobulins/HRP	Dako, P0448	Goat	1:5000
Anti-Goat Immunoglobulins/HRP	Dako, P0449	Rabbit	1:5000
Alexa Fluor 680 Anti-Mouse IgG (H+L)	Invitrogen, A-21158	Goat	1:5000
Alexa Fluor 680 Anti-Rabbit IgG (H+L)	Invitrogen, A-21109	Goat	1:5000

Table 2. Primary and secondary antibodies used for Western Blot.

Total protein extraction

Cells were washed twice with PBS and resuspended in total protein extraction buffer (10% SDS, 0.2 M Tris pH6.8) supplemented with Protease Inhibitor Cocktail (Merck, 535140). Total protein was extracted by constant agitation at 4°C during 30 minutes. To remove cell debris, samples were centrifuged at 16,000xg during 15 minutes and the pellet was discarded. Proteins were quantified using the colorimetric assay DC Protein Assay (Biorad, 5000111).

Total membrane protein extraction

To purify integral membrane proteins and membrane-associated proteins, we used the kit MemPERTM Plus Kit (Thermo Scientific, 89842Y). One p100 plate of HEK293T cells at 70% of confluence was co-transfected with *pEGFP-Na_v1.5*, and *pEGFP-PKP2* or *pEGFP-R735X*. After 48 hours of transfection, cells were collected with a scraper and washed with 3 ml of Cell Wash Solution buffer. Cells were resuspended in 0.75 ml of Permeabilization buffer and incubated 10 minutes at 4°C with constant mixing. Permeabilized cells were centrifuged for 15 minutes at 16,000×g. Pellet was resuspended in 0.5 ml of Solubilization Buffer and incubated at 4°C for 30 minutes with constant mixing. Samples were centrifuged at 16,000×g for 15 minutes. Supernatant containing solubilized membrane and membrane-associated proteins was saved for later analysis by Western Blot.

Plasma membrane protein extraction

To separate plasma membrane proteins from the rest of cell proteins, we used the kit Plasma Membrane Protein Extraction Kit (Abcam, ab65400). Six p150 plates of HEK293T cells at 70% of confluence were co-transfected with *pEGFP-Na_v1.5*, and *pEGFP-PKP2* or *pEGFP-R735X*. After 48 hours of transfection, cells were washed with ice-cold PBS, collected with a scraper and washed again with ice-cold PBS. Cells were resuspended in 2 ml of Homogenize Buffer supplemented with Protease Inhibitor Cocktail and homogenized using a Dounce homogenizer 50 times on ice. Cytosolic and plasma membrane proteins were obtained from different density gradient centrifugations. Cell protein fractions (cytosolic and plasma membrane proteins) were analyzed by Western Blot.

Cell surface biotinylation assay

To isolate plasma membrane proteins, HL-1 cells were labeled with EZ-Link™ Sulfo-NHS-SS-Biotin (Thermo Scientific, 21331). This is a biotinylation reagent that reacts with primary amines (-NH₂) of the proteins present in the cell surface, since it is a reagent negatively charged and is not able to penetrate the plasma membrane. Cells were plated at 80% of confluence in supplemented Claycomb medium. Cells were washed twice with ice-cold PBS pH8.0 and incubated with diluted EZ-Link™ Sulfo-NHS-SS-Biotin (0.5 mg/ml) in ice-cold PBS pH8.0 during 1 hour at 4°C in agitation. Cells were washed twice with PBS pH8.0. To quench the rest of reactive biotin, cells were incubated with Glycine 100 mM (nzytech, MB01401) during 10 minutes at 4°C

in agitation. Cells were washed twice with PBS pH8.0 and lysated using a protein extraction buffer (25 mM Tris HCl pH7.5, 150 mM NaCl, 1 mM EDTA, 1% Triton X-100).

Proteins were quantified, and 300 µg of protein were incubated with 180 µl of Pierce™ Streptavidin Magnetic Beads (Thermo Scientific, 88816) overnight at 4°C in agitation. Before the incubation, magnetic beads were washed 3 times with protein extraction buffer. After overnight incubation, magnetic beads were pulled down with a DynaMag™-2 Magnet (Invitrogen, 12321D), supernatant was collected and saved for analysis, and beads were washed 3 times with protein extraction buffer. Proteins labeled with EZ-Link™ Sulfo-NHS-SS-Biotin were separated from the Streptavidin Magnetic Beads by incubating the complex with a 10% SDS buffer (10% SDS, 0.2M Tris pH6.8) at 60°C during 1 hour in agitation. Precipitated proteins were analysed by Western Blot. In this case, proteins were mixed with a loading buffer that do not contain β-mercaptoethanol and samples were not boiled to avoid cleavage of the link between proteins and biotin.

Genomic DNA extraction

Cells were lysate with 400 µl of buffer lysis (0.1 M TrisHCl pH8.5, 5 mM EDTA, 0.2% SDS, 200 mM NaCl) supplemented with proteinase K (100 µg/ml) and incubated overnight at 37°C. DNA was precipitated with 2-propanol/sodium acetate and 70% ethanol.

RNA extraction and cDNA synthesis

RNA was extracted with the kit Direct-zol™ RNAMiniPrep kit (Zymo, R2051) according to manufacturer's instructions and reverse transcription was performed with the kit High-Capacity cDNA Reverse Transcription (ThermoFisher, 4368814).

PCR

PCR was performed according to the protocol of AccuPrime™ Pfx DNA Polymerase (ThermoFisher, 12344024). Primers are enlisted in table 3.

Primers	Sequence	Length
PKP2-F	AACCTCACGGCCGGAAGTGGACCAATGCCGACATC	PKP2-652pb
PKP2-R	GGTTGTGCCGCCTTTGCAGGTGTATCTTATACACG	R735X-209pb
Neo-F	AGGATCTCCTGTCTATCTCACCTTGCTCGTG	485 bp
Neo-R	AAGAACTCGTCAAGAAGGCGATAGAAGGCG	
hc-Myc-F	CGCCAGCGAGGATATCTGGAAG	224 bp
hc-Myc-R	CCGGGTCGCAGATGAAACTCTGG	
hKlf4-F	AGATCGTTGAACTCCTCGGTCTC	251 bp
hKlf4-R	ATCTTTCTCCACGTTTCGCGTCTG	
hOct4-F	CGGGACACCTGGCTTCGGATTC	284 bp
hOct4-R	CCTCAGGCTGAGAGGTCTCCAAG	
hSox2-F	AGATGCAGCCCATGCACCGCTAC	207 bp
hSox2-R	CTGGAGTGGGAGGAAGAGGTAAC	
SV-F	GGATCACTAGGTGATATCGAGC	181pb
SV-R	ACCAGACAAGAGTTTAAGAGATATGTATC	

Table 3. List of primers used to assess the expression of pluripotency markers to genotype hiPSCs. F: Forward. R: Reverse. Length of the PCR product is indicated in the third column.

3. Cell culture

HEK293T cell line culture and transfection

HEK293T cell line is a cell line derived from human embryonic kidney cells. HEK293T cells were maintained in DMEM medium supplemented with 10% fetal bovine serum (FBS), 4 mM L-glutamine and 1% penicillin-streptomycin. Cells were maintained as a monolayer and passaged twice a week when reached 90-100% of confluence. Plates were kept in an incubator at 37°C, 5% CO₂.

To perform transient transfections, HEK293T cells were plated at 70% of confluence in supplemented DMEM medium and were incubated overnight with a mix of DNA and PEI 25K (Polyethylenimine, Linear, MW 25000, Transfection Grade, Polysciences, 23966-1) in a ratio 1:3 (w/v).

HL-1 cell line culture and transfection

HL-1 cell line is a cardiac muscle cell line, derived from the AT-1 mouse atrial cardiomyocyte tumor lineage. These cells maintain the ability to contract and retain differentiated cardiac morphological, biochemical and electrophysiological properties. HL-1 cells were cultured in Claycomb medium supplemented with 100 μM norepinephrine, 10% FBS, 4 mM L-glutamine and 1% penicillin-streptomycin and plated in 0.02% gelatin/fibronectin (Sigma Aldrich)-coated

plates. HL-1 cells were maintained as a monolayer and passaged every other day when reached the 90-100% of confluence. Plates were kept in an incubator at 37°C, 5% CO₂.

To achieve a 30-40% of transfected HL-1 cells, we used the transfection reagent jetPRIME[®] (Polyplus transfection, 114-07). Cells were plated at 70% of confluence in supplemented Claycomb medium, and they were incubated overnight with a mix of DNA, JetPRIME[®] and jetPRIME[®] buffer. The optimized ratio DNA-jetPRIME[®] was 1:3 (w/v).

HL-1 stable cell lines

To generate HL-1 cell lines stables for the expression of a gene of interest, we used the *piggyBac* (PB) transposon system. This technology allows the efficient insertion of a DNA sequence into a host genome in a one-step transfection. Cells were transfected with JetPRIME[®] and a mix of DNA containing the constructs *pPB-CAG-PKP2-PGK-Neomycin-PB* or *pPB-CAG-PKP2-PGK-Neomycin-PB*, and *pCMV-Transposase* in a ratio of 1:5 (w/w). PB transposase will mediate the integration of the PB cassette into the genome. Forty-eight hours after transfection, we started the selection of the stably transfected cells by adding 300 ng/μl G418 (Neomycin, Merck, G8168) to the culture media. Cells were treated with G418 during at least 10 days (Figure 8).

4. hiPSCs and hiPSC-CM culture

Human dermal fibroblast reprogramming

hiPSCs were generated from human dermal fibroblasts (HDFa, ScienCell Research Laboratory, 2320). HDFa were reprogrammed using the non-integrative method CytoTune iPS 2.0 Sendai Reprogramming Kit (Invitrogen, A16517). HDF were transduced with CytoTune™ 2.0 Sendai reprogramming vectors codifying for the reprogramming factors: hOct3/4, hSox2, hKlf4 and hc-Myc.

Twenty-four hours after transduction, fibroblast medium was refreshed. Cells were cultured during 6 days with media changes every other day. Seven days after transduction, fibroblast cells were transferred to MEF-coated culture dishes. Twenty-four hours later, fibroblast media was changed to iPSC medium. During the next days, cells were monitored under a microscope for the emergence of cell clumps indicative of reprogrammed cells. 3-4 weeks after transfection, colonies were manually picked and transferred to MEF-coated plates. hiPS colonies were expanded and tested for pluripotency and stemness.

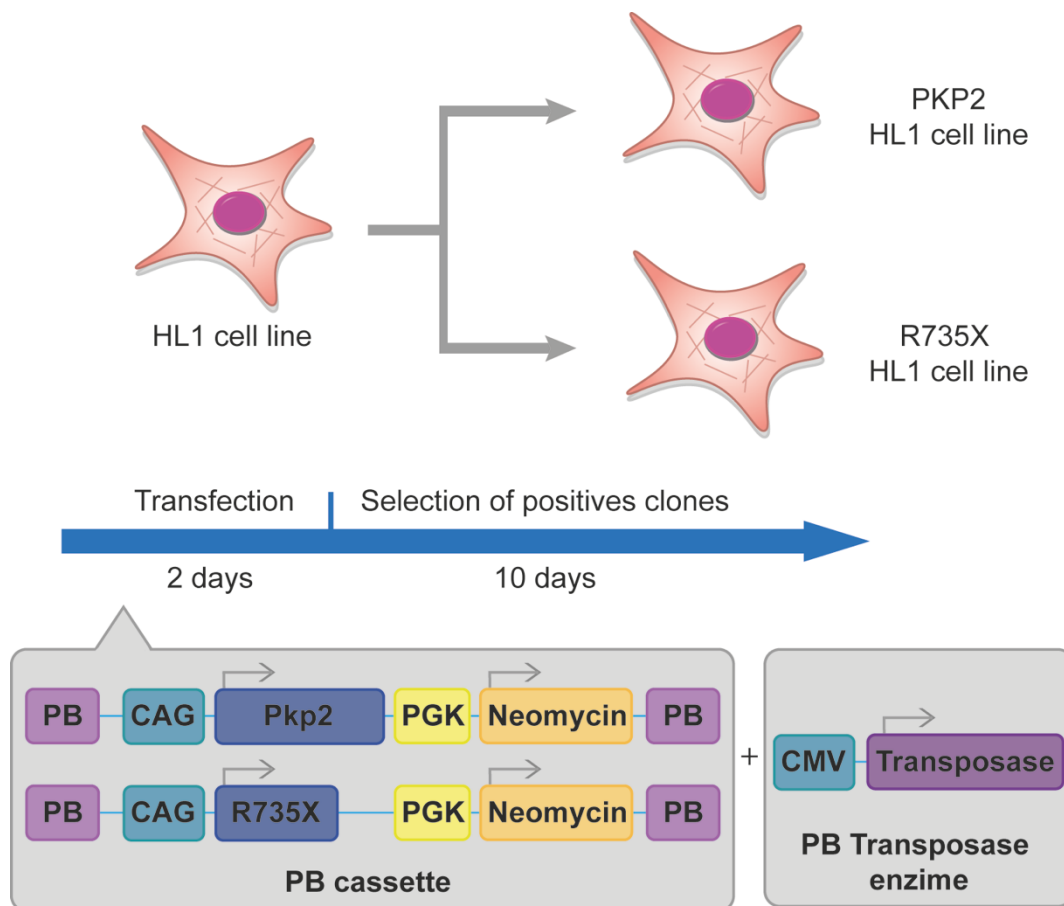


Figure 8. Generation of HL-1 stable cell line. HL-1 cells were co-transfected with the constructs *pPB-CAG-PKP2-PGK-Neomycin-PB* or *pPB-CAG-R735X-PGK-Neomycin-PB*, and *pCMV-Transposase*. CMV: human cytomegalovirus promoter. CAG: CMV enhancer fused to the chicken beta-actin promoter. Neomycin: Neomycin resistance gene. Transposase: Transposase gene. Positives cells were selected with Neomycin treatment during 10 days. R735X HL-1 and its isogenic control (PKP2 HL-1) were characterized.

hiPSCs culture

Human induced pluripotent stem cells (hiPSCs) were cultured using the commercial culture media StemMACS iPS-Brew XF (Miltenyi Biotec, 130-104-368). hiPSCs were maintained as colonies and passaged every 7 days on plastic plates coated with 500 $\mu\text{g}/\text{ml}$ matrigel (BD Biosciences). Every day, the cells that differentiate spontaneously were marked and removed manually before the media change. Plates were kept in an incubator at 37°C, 5% CO₂.

hiPSCs stably transfected cell lines

hiPSCs were cultured in StemMACS iPS-Brew XF supplemented with 10 μM Rock Inhibitor for 24 hours. Cells were washed with HBSS (Thermofisher, 14025092) and treated with Accutase (Thermofisher, 00-4555-56) for 5 minutes at 37°C. Single cells were transferred to a 15 ml

conical tube and centrifuged at 200xg during 5 minutes. Approximately 10^6 cells were resuspended in the transfection mix (82 μ l of P3, 18 μ l of supplement, 1 μ g of PB cassette vector and 250 μ g of PB transposase plasmid) and transferred to a cuvette. Cells were electroporated with 4D-Nucleofector System (Lonza) using the program H9. Cells were re-plated in a p100 plate with StemMACS iPS-Brew XF supplemented with 10 μ M Rock Inhibitor. Forty-eight hours after transfection, we started the selection of the stably transfected cells by adding 50 μ g/ml G418 (Neomycin, Merck, G8168) to the culture media. Cells were treated with G418 during at least 10 days. After that, independent colonies were picked and transferred to separate wells to establish different clonal cell lines.

Alkaline phosphatase staining

Alkaline phosphatase activity was detected in hiPSC cultures using the alkaline phosphatase detection kit (Sigma, SCR004) according to the manufacturer's instructions.

Karyotype

Karyotype analysis was performed using standard G-banding chromosome technique. Samples were analyzed by the Cytogenetics Unit at CNIO according to standard procedures.

Embryoid bodies (EBs) generation and three germ layer *in vitro* differentiation

hiPSC colonies plated on matrigel-coated wells were washed with PBS and treated with 200 U/ml Collagenase type IV (Thermofisher, 17104019) in KO DMEM/F-12 (Thermofisher, 12660012) for 20 minutes at 37°C. Cells were detached in big pieces and transferred to a low attachment well with StemMACS iPS-Brew XF during 3-4 days until EBs have formed. For endoderm and mesoderm differentiation, EBs were transferred into a matrigel-coated chamber slides in differentiation medium. Differentiation medium was changed after 1-2 days when EBs were attached, and they were kept in culture for 3 weeks with medium change every other day. For ectoderm differentiation, EBs were kept in suspension with ectoderm differentiation medium with 100 ng/ml FGF for 10 days. After that, EBs were plated on matrigel-coated chamber slides and cultured for 3 weeks with ectoderm differentiation media without FGF.

Endoderm differentiation medium: 10% FBS, 1% Glutamax, 1% NEAA, 1% penicilin-streptomycin, 0.1% β -mercaptoethanol in KO DMEM (Thermofisher, 10829018). Mesoderm differentiation

medium: endoderm differentiation medium supplemented with 0.5 mM Ascorbic acid (fisher scientifique, AC352680050). Ectoderm differentiation medium: 50% Neurobasal medium (Thermofisher, 21103049), 50% DMEM/F-12 (Thermofisher, 11320033), 1% Glutamax, N2 supplement (Thermofisher, 17502001), B27 supplement (Thermofisher, A3582801), 1% NEAA, 1% penicilin-streptomycin, 0.1% β -mercaptoethanol

Cardiac differentiation protocol

Cardiac differentiation was achieved using a protocol based in small molecules, commonly known as the GiWi protocol (Lian et al., 2012)(Lian et al., 2013). hiPSCs were separated with Versene Solution (EDTA 48 mM in PBS, Gibco, LS15040066), plated in monolayers in 6 well plates (10^6 hiPSCs/ well aprox.) and maintained in StemMACS iPS-Brew XF (Miltenyi Biotec, 130-104-368) culture media during 1 or 2 days until the cells cover completely the surface of the well (90-100% of confluence). On day 0 of the protocol, hiPSCs monolayers were washed with HBSS and cultured in RPMI 1640 media (Thermofisher, 31870082) supplemented with B27 without insulin (RPMI/B27-insulin, Thermofisher, A1895601) and the glycogen synthase kinase-3 inhibitor, CHIR99021 (12 μ M, Miltenyi Biotec, 130-103-926). After 24 hours, CHIR99021 was removed and fresh RPMI/B27-insulin was added. On day 3, we added a mix composed of half of the volume of used media and half of fresh media (RPMI/B27-insulin) and the inhibitor of Wnt production-4, IWP4 (5 μ M, Stemgent, 686772-17-8). On day 5, IWP4 was removed and fresh RPMI/B27-insulin was added. On day 7, cells were cultured in RPMI/B27+insulin (Thermofisher, A3582801). On day 8, we could start seeing some cells beating as a signal of success in the cardiac differentiation process. Human induced pluripotent stem cells derived cardiomyocytes (hiPSC-CMs) were cultured in RPMI/B27+insulin during 30 days with media changes every two days.

Purification of hiPSC-CM

The cardiac differentiation protocol is not 100% efficient and not all the hiPSCs differentiate into cardiomyocytes, obtaining mixed cultures. At day 30 of differentiation, cells were trypsinized and incubated with a cocktail of antibodies that recognize epitopes of non-cardiomyocytes cells (Miltenyi Biotec, PSC-derived cardiomyocyte isolation kit-human, 130-110-188). Then, these cells were incubated with a secondary antibody conjugated with magnetic beads. Magnetically labeled cells were retained in LS columns (Miltenyi Biotec, 130-042-401) inserted into a magnetic field. LS columns matrix is composed by ferromagnetic spheres, which amplifies the

magnetic field. This magnetic-activated cell sorting targets and depletes non-cardiomyocytes from the whole cell population, enriching the sample in cardiomyocytes up to 98%.

Maturation of hiPSC-CM

Purified hiPSC-CMs were plated in wells covered with PDMS (transparent sheets of vulcanized silicon of polydimethylsiloxane) that improves the maturation of these cells. PDMS sheets (40D, Durometer ≈ 1000 kPa) were obtained from Specialty Manufacturing, Inc. PDMS coverslips with a diameter of 15 mm were cut manually and placed in 24 well plates. Each plate was sterilized using ethylene oxide. To promote cell adhesion, PDMS coverslips were coated with matrigel for 1 hour prior to plate the cells. hiPSC-CMs were maintained in culture on matrigel-PDMS coated plates during 7 days, with RPMI/B27 + insulin before any experiment.

PDMS micropatterns

For experiments requiring isolated single cells, such as patch-clamp experiments, hiPSC-CMs were plated in PDMS micropatterns. We used PDMS stamps printed with a micropattern composed by lines of a single cell size and squares where small monolayers (around 100-300 cells) can be seeded. These small monolayers will be around the single cells and will support their survival. PDMS stamps were cleaned with scotch tape followed by sonication in 70% ethanol for 20 minutes. In the hood, they were air dried and incubated with 250 μ l matrigel diluted in water (100 μ g/ml) at room temperature for 1 hour. After that, the matrigel solution from the PDMS stamps was aspirated.

In parallel, 18 mm PDMS circles were sonicated in 70% ethanol for 20 minutes and transferred, under the hood, to a 6-well plate where ethanol was air dried. The culture dish was UVO treated for 10 minutes. Before the re-plating of the cells, plates were cleaned with penicillin-streptomycin antibiotic for 1 hour and exposed to UV light during 15 minutes. Once PDMS stamp and PDMS circles were ready, dried stamps were inverted onto each PDMS circle and removed one by one after ~ 2 minutes. The micropatterned PDMS plates were incubated with pluronic-F27 overnight at room temperature.

Single cell re-plating

hiPSC-CMs monolayers that have been plated 7 days on PDMS were dissociated by using trypsin 0.025% with EDTA for 8-10 minutes. Dissociation was stopped by adding RPMI/B27+insulin supplemented with 10% FBS. Cells were filtered using a 70 μm filter to removed non-dissociated cells and were centrifuged at 100xg for 3 minutes. Then, cells were resuspended in warm re-plating media (RPMI/B27+insulin supplemented with 2% FBS and 5 μM Rock Inhibitor). Approximately, 60K cells resuspended in 350 μL of media were placed in the center of the micropatterned area. After 5 hours, 2 ml of re-plating media was added very gently. Media change was performed at day 1 and 3 after re-plating the cells. Cells must be on micropatterns (Figure 9) at least 4 days before patch-clamp experiments.

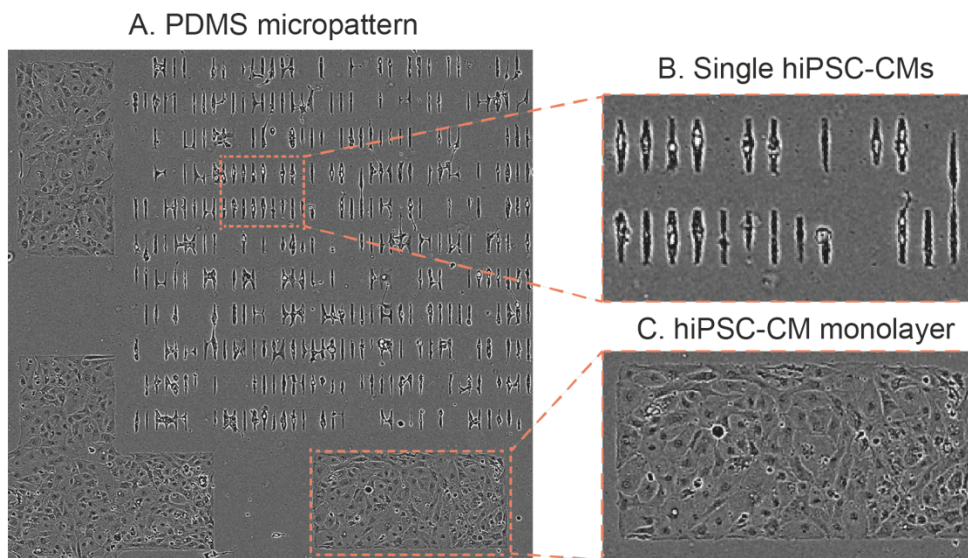


Figure 9. hiPSC-CMs plated on a PDMS micropattern. A. hiPSC-CMs are plated in PDMS micropatterns as single cells. Small monolayers of hiPSC-CM are plated surrounding single hiPSC-CMs to improve single cell survival. Image obtained under bright field microscope, objective 20x. B. Digital magnification of single hiPSC-CMs. C. Digital magnification of small hiPSC-CM monolayers.

Immunofluorescence

hiPSC-CMs were washed with PBS and then fixed with 3% paraformaldehyde for 10 minutes and rinsed twice before adding blocking-permeabilization solution (10% normal goat serum, 0.1% Triton X-100 in PBS) for 40 minutes at room temperature. Primary antibodies (Table 4) were diluted in 5% normal goat serum and 0.05% Triton X-100 in PBS and incubated overnight at 4°C. Subsequently, cells were washed three times with 10% normal goat serum and 0.1% Triton X-

100 in PBS. The secondary antibodies (Table 4), diluted in the same solution as the primary antibodies, were applied to cells and incubated at room temperature in the dark for 2 hours. After incubation, cells were washed three times with 10% normal goat serum and 0.1% Triton X-100 in PBS and once with PBS only. Then, nuclei were stained with DAPI (1:1000, Invitrogen) for 10 minutes in the dark at room temperature. Coverslips were mounted on slides for confocal imaging. Slides were analyzed under a Confocal System Nikon A1R coupled to an Eclipse Ti microscope (Nikon Corp., Japan) using a Plan Apo VC 60x/1,4 Oil objective, with the command of NIS Elements AR 4.30.02. Build 1053 LO software.

Antibody	Reference	Source	Dilution
α -actinin	Sigma, A7732	Mouse	1:250
SMA-Cy3	Dako, M0851	Mouse	1:400
AFP	Dako, A0008	Rabbit	1:400
Tuj1	Covance, MMS-435P	Mouse	1:500
GFAP	Dako, Z0334	Rabbit	1:1000
MHC (MF20)	DSHB	Chicken	1:250
Cx43	Sigma, C6219	Rabbit	1:100
Alexa Fluor 488 Anti-Mouse IgG (H+L)	Invitrogen, A-11001	Goat	1:400
Alexa Fluor 488 Anti-Rabbit IgG (H+L)	Invitrogen, A-21109	Goat	1:400
Alexa Fluor 568 Anti-Mouse IgG (H+L)	Invitrogen, A-11004	Goat	1:400
Alexa Fluor 488 Anti-Chicken IgG (H+L)	Invitrogen, A-11039	Goat	1:250
Alexa Fluor 668 Anti-Rabbit IgG (H+L)	Invitrogen, A-11011	Goat	1:250

Table 4. Primary and secondary antibodies used for immunofluorescence.

5. Electrophysiology

Patch-clamp recordings in hiPSC-CM

Standard patch-clamp recording techniques were used to measure I_{Na} , I_{Ca} , and I_{K1} . All the experiments were performed at room temperature (22°C–25°C).

Voltage-clamp experiments were controlled with a Multiclamp 700B amplifier and pClamp 10.2/Digidata 1440A acquisition system (Molecular Devices). Data were filtered at 5 kHz and sampled at 5–20 kHz. Activation curve data were fitted to a Boltzmann equation, with the form $G = G_{max}/(1 + \exp((V_{1/2} - V_m)/k))$, where G is the conductance, G_{max} the maximum conductance, V_m is the membrane potential, $V_{1/2}$ is the voltage at which half of the channels are activated and k is the slope factor.

Pipettes were made of aluminosilicate glass (Science Products, AF150-100-10), pulled with a P-97 horizontal puller (Sutter Instruments), reaching resistances between 2 and 3 M Ω for patch-clamp experiments when filled with the respective pipette solutions (described below).

For I_{Na} , a pulse protocol from -80 mV to +55 mV with a holding potential of -160 mV was used. Recordings were made in a bath solution containing 10 mM NaCl, 1 mM MgCl₂, 0.1 mM CdCl₂, 20mM HEPES, 11 mM Glucose, 60 mM CsCl, and 72.5 mM Choline chloride, pH = 7.35 adjusted with CsOH. The pipette solution contained 60 mM CsF, 5 mM NaCl, 10 mM EGTA, 5 mM HEPES, 5 mM MgATP, and 75 mM Choline chloride, pH = 7.2 adjusted with CsOH. Chemicals were purchased from Sigma.

I_{K1} was elicited from a holding potential of -50 mV by 500-ms steps from -120 to +40 mV. The external recording solution contained 148 mM NaCl, 0.4 NaH₂PO₄, 1 mM MgCl₂, 5.5 mM Glucose, 1.8 mM CaCl₂, 5.4 mM KCl, 15 mM Hepes, and 5 μ M Nifedipine, pH = 7.4 adjusted with NaOH. 1 mM BaCl₂ was used to isolate I_{K1} from other background currents (subtract solution). The internal solution contained 1 mM MgCl₂, 5 mM EGTA, 140 mM KCl, 5 mM HEPES, 5 mM Phosphocreatine, 4.4 mM K₂ATP, and 2 mM Hydroxybutyric acid, pH = 7.2 adjusted with KOH.

I_{Ca} was evoked applying a voltage-step protocol from -50 mV to +70 mV with a holding potential of -50 mV. The cells were bathed in 137 mM TEA-Cl, 5.4 mM CsCl, 1 mM MgCl₂, 1.8 mM CaCl₂, 4 mM Aminipyridine, 10 mM HEPES, 30 mM TTX, and 11 mM Glucose, pH=7.4 adjusted with CsOH. The pipette solution contained 20 mM TEA-Cl, 120 mM CsCl, 1 mM MgCl₂·6H₂O, 5.2 mM Mg-ATP, 10 mM HEPES, 10 mM EGTA, pH=7.2 adjusted with CsOH.

Data analysis was performed using Clampfit 10.2 (Axon Instruments), OriginPro 9 (OriginLab Corporation), and GraphPad Prism 7 (San Diego) software.

Optical mapping of hiPSC-CM monolayers

hiPSC-CMs were plated on PDMS-matrigel coated wells in 2D monolayers during 1 week (2×10^5 cells / p24 well). hiPSC-CM monolayers were loaded with FluoVolt (Life Technologies, F10488), a voltage sensitive fluorescent probe that responds to changes in membrane potential. After 30 minutes of incubation, cells were washed with HBSS. Cells were positioned on a heating block to keep them at physiological temperature (37 °C) and below a high speed CCD camera (200 fps, 80 \times 80 pixels). Blue LED illumination with the CCD camera via appropriate emission filter (515 nm, green light, Chroma) was used to record spontaneous or electrically paced action

potentials. Electrical pacing was done using a custom made frame of point stimulation electrodes to enable electrical pacing of 6 x 6 array of wells. Recorded data was analyzed using Scroll, custom software developed by Dr. Jalife's laboratory, University of Michigan, Ann Arbor (USA). Scroll allowed us to calculate action potential duration at different percentage of repolarization and conduction velocity of the electrical impulse.

6. Confocal live imaging

For all the experiments involving confocal live imaging, HL-1 cells were plated in p35 glass-bottomed plates (MatTek, P35G-1.5-14-C). Before imaging, growth media was replaced with phenol-red free medium (Leibovitz's L-15 Medium, no phenol red, 21083027).

For EGFP-PKP2 and tdTomato-PKP2 imaging, HL-1 were transfected 24h before the experiment. Confocal live imaging was performed using a Confocal System Nikon A1R coupled to an Eclipse Ti microscope (Nikon Corp., Japan) using a Plan Apo VC 60x/1,4 Oil objective. Microscope was equipped with an incubator chamber to provide controlled temperature (37°C) and humidity, all under the command of NIS Elements AR 4.30.02. Build 1053 LO software. Images were acquired as a z-stack with step size of 0.2 μm to give a total of 75 slices. Images were saved as ND2 files and z-stack projection images were obtained using Image J software (NIH, USA).

For EGFP-Na_v1.5 imaging, HL-1 were transfected 48 hours before the experiment. Confocal live imaging was performed using a Confocal TCS Leica SP8 coupled to a DMI8 microscope (Leica Microsystems GmbH, Germany) using a HC PL Apo CS2 63x/1.4 OIL objective. Microscope was equipped with an incubator chamber to provide controlled temperature (37°C) and humidity, all under the command of LAS X 3.1.1. 15751 software. Images were acquired as a z-stack with step size of 0.17 μm to give a total of 8 slices. Pixel size was set following Nyquist sampling theorem to apply deconvolution on the acquired images later on.

Deconvolution

Deconvolution process is a combination of optical and computational techniques aimed to increase resolution, gain a better contrast and improved signal-to-noise ratio when imaging a biological specimen. Optical microscopes have inherent limitations that cause out-of-focus light, forming images that are not a true representation of the biological specimen. Deconvolution uses mathematical models to predict the distribution of this out-of-focus light and apply

computer algorithms to compensate it (Biggs, 2010).

The quality of EGFP-Nav1.5 images was low and deconvolution process was necessary to improve the resolution and the signal-to-noise ratio. Z-stack projections were deconvoluted with Huygens Software (Scientific Volume Imaging B.V., The Netherlands), using the GMLE algorithm, with SNR:5 and 10 iterations. After deconvolution, we measured the intensity of the plasma membrane and the cytoplasm regions. To do so, we drew regions of interest (ROIs) defining the plasma membrane and the cytoplasm, and excluding the nucleus and big vacuoles on each cell. Then, we calculated the ratio plasma membrane-cytoplasm intensity as a way to normalize the intensity of the plasma membrane to the level of transfection on each single cell.

To study the co-localization of EGFP-Nav1.5 and tdTomato-PKP2, we performed the same deconvolution process described above. Using the Huygens Software, we drew a 3 μm line on the plasma membrane area and analyzed profiles of intensity on both EGFP and tdTomato signal. We identified peaks matching with the plasma membrane and we measured the distance between green and red peaks as an indirect way to study the co-localization of Nav1.5 and PKP2 proteins in HL-1 cells.

Fluorescence recovery after photobleaching (FRAP)

FRAP experiments were performed on a Confocal System Nikon A1R coupled to an Eclipse Ti microscope (Nikon Corp.) using a Plan Apo VC 60x/1,4 Oil objective. Microscope was equipped with an incubator chamber to provide controlled temperature (37°C) and humidity, all under the command of NIS Elements AR 4.30.02. Build 1053 LO software.

In cells transfected with EGFP-Nav1.5, EGFP was bleached by radiating a circular region of interest (ROI) of 1.5 μm of diameter, using 488 nm laser at 100% of power during 4s (one lighting iteration). Pinhole was set to 35 μm . In cells transfected with EGFP-PKP2 or EGFP-R735X, EGFP was bleached by radiating a circular regions of interest (ROIs) of 1.5 μm of diameter, using 488 nm laser at 100% of power during 7.77s (four lighting iterations). In both cases, for prebleach and postbleach periods, images were captured every 2 s. Postbleaching captures continued for 120 seconds. Data were normalized to the initial fluorescence intensity (value=1) and to after bleaching intensity (value=0), after background subtraction. Half-time of recovery ($T_{1/2}$) and mobile fraction (MF) were calculated with nonlinear regression software, GraphPad Prism 7, using the one-phase association equation.

7. Statistics

Statistical analyses were performed with GraphPad Prism 7. Data are presented as means \pm s.e.m (standar error of the mean) or means \pm s.d (standar deviation) as indicated. Differences were considered statistically significant at p-value < 0.05 . In each figure p-value is represented as follows: * $p < 0.05$, ** $p < 0.01$, *** $p < 0.001$, **** $p < 0.0001$ y ns $p > 0.05$. Test used to calculate p-value are detailed in figure legends. Student's t-test was used to compare two groups. One-way o two-way ANOVA with Tukey's multiple comparison post-test was used to compare several groups.

RESULTS

RESULTS

1. R735X characterization

1.1. Subcellular distribution of R735X

It has been previously shown that some PKP2 mutants fail to localize at the plasma membrane and are found in the intracellular space (Joshi-Mukherjee et al., 2008). These results led us to question whether the truncated PKP2 protein R735X would be mislocalized. The study of the subcellular distribution of PKP2 by immunofluorescence was limited since endogenous PKP2, and both exogenous PKP2 and R735X proteins are recognized by the same antibody. Therefore, we tagged PKP2 proteins with EGFP to be able to track them by confocal microscopy. The tag was placed at the N-terminal of PKP2 proteins since it has been described that N-terminal EGFP tag does not alter PKP2 localization (Godsel et al., 2010). We transiently transfected *pEGFP-PKP2* and *pEGFP-R735X* constructs in HL-1 cells to study the subcellular distribution of PKP2 and R735X proteins in a cardiac cell context. HL-1 is a mouse cardiac muscle derived cell line that has differentiated cardiac features (morphological, biochemical and electrophysiological) and maintains the ability to contract (Claycomb et al., 1998). We observed that EGFP-PKP2 localized mainly at the border of the cells, following a continuous linear pattern surrounding the perimeter of the cell. In contrast, most of the EGFP-R735X signal was found in the cytoplasm and not at cell borders (Figure 10). This result would indicate that R735X is mislocalized from the inner face of the plasma membrane to the intracellular space, away from junctional complexes.

To test whether R735X might alter the localization of PKP2 protein and *vice versa*, we performed co-transfections of PKP2 and R735X in HL-1 cells. We tagged both PKP2 and mutant R735X proteins with the fluorescent protein tdTomato and co-transfected them with PKP2 or its mutant counterpart tagged with EGFP to track both proteins in the same cell by confocal microscopy. We observed that cells expressing EGFP-PKP2 and tdTomato-R735X presented a green signal at the cell border and a red cytoplasm. On the other hand, cells expressing tdTomato-PKP2 and EGFP-R735X showed a cell border stained in red and a green cytoplasm (Figure 11). Thus, data showed in figure 10 and 11 indicates that R735X fails to localize at the inner face of the plasma membrane and is mainly found at the cytoplasm, independently of the tag. It also shows that R735X does not disrupt the proper localization of PKP2.

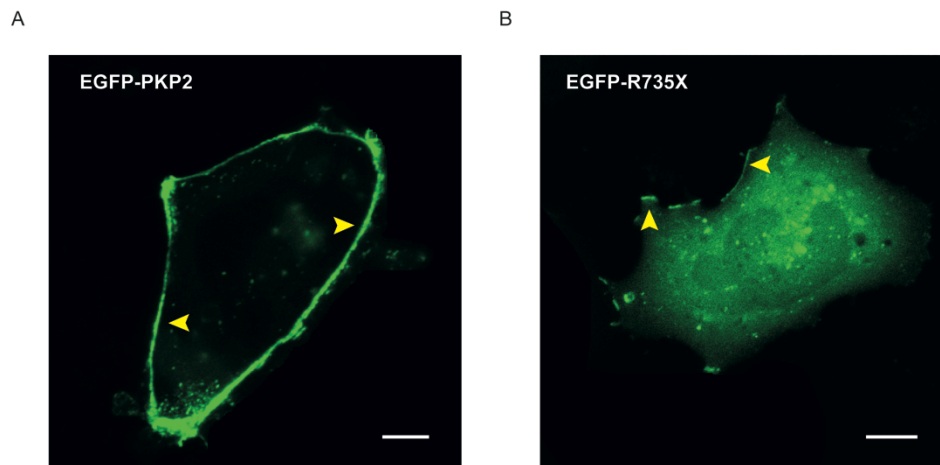


Figure 10. PKP2 C-terminal deletion alters the subcellular localization of the protein. A. Z-stack projection of a HL-1 cell transiently expressing EGFP-PKP2. B. Z-stack projection of a HL-1 cell transiently expressing EGFP-R735X. Yellow arrowheads indicate, respectively, EGFP-PKP2 and EGFP-R735X localization at cell borders. Scale bar =10 μ m.

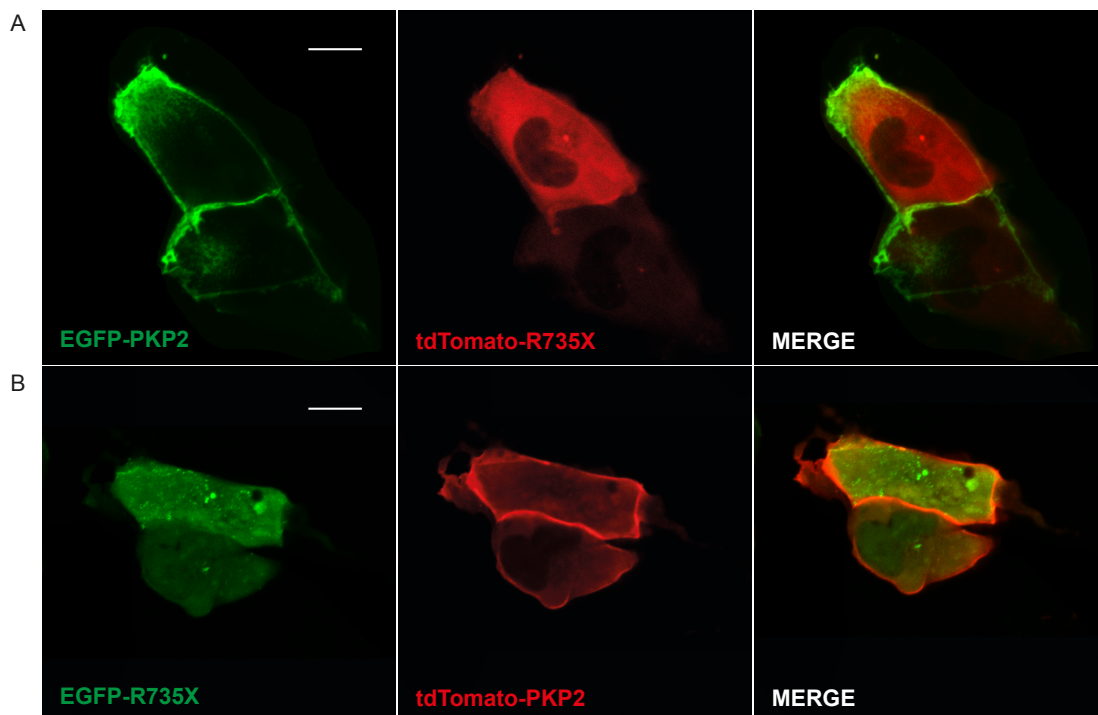


Figure 11. R735X does not alter PKP2 localization. A. Z-stacks projections of HL-1 cells co-transfected with *pEGFP-PKP2* (left panel) and *ptdTomato-R735X* (central panel). Merge is showed at right panel. B. Z-stack projections of HL-1 cells co-transfected with *pEGFP-R735X* (left panel) and *ptdTomato-PKP2* (central panel). Merge is showed at right panel. Scale bar = 10 μ m.

To confirm that the tag is not affecting the subcellular distribution of PKP2 proteins, we transfected HEK293T cells with *pCAG-PKP2* and *pCAG-R735X* without tags and we isolated proteins from cytoplasmic and plasma membrane fractions. The amount of R735X in the cytoplasmic fraction was approximately 1.5 times the amount of PKP2 found in the same fraction (Figure 12A&C). In contrast, R735X was only detectable in the plasma membrane fraction when overexposing the membrane (Figure 12B). Subcellular fractionation in HEK293T cells corroborates the results obtained by microscopy analysis of fluorescent-tagged PKP2 and R735X proteins in HL-1 cells, indicating altogether that R735X is mislocalized from the desmosome in the inner face of the plasma membrane to the cytoplasm.

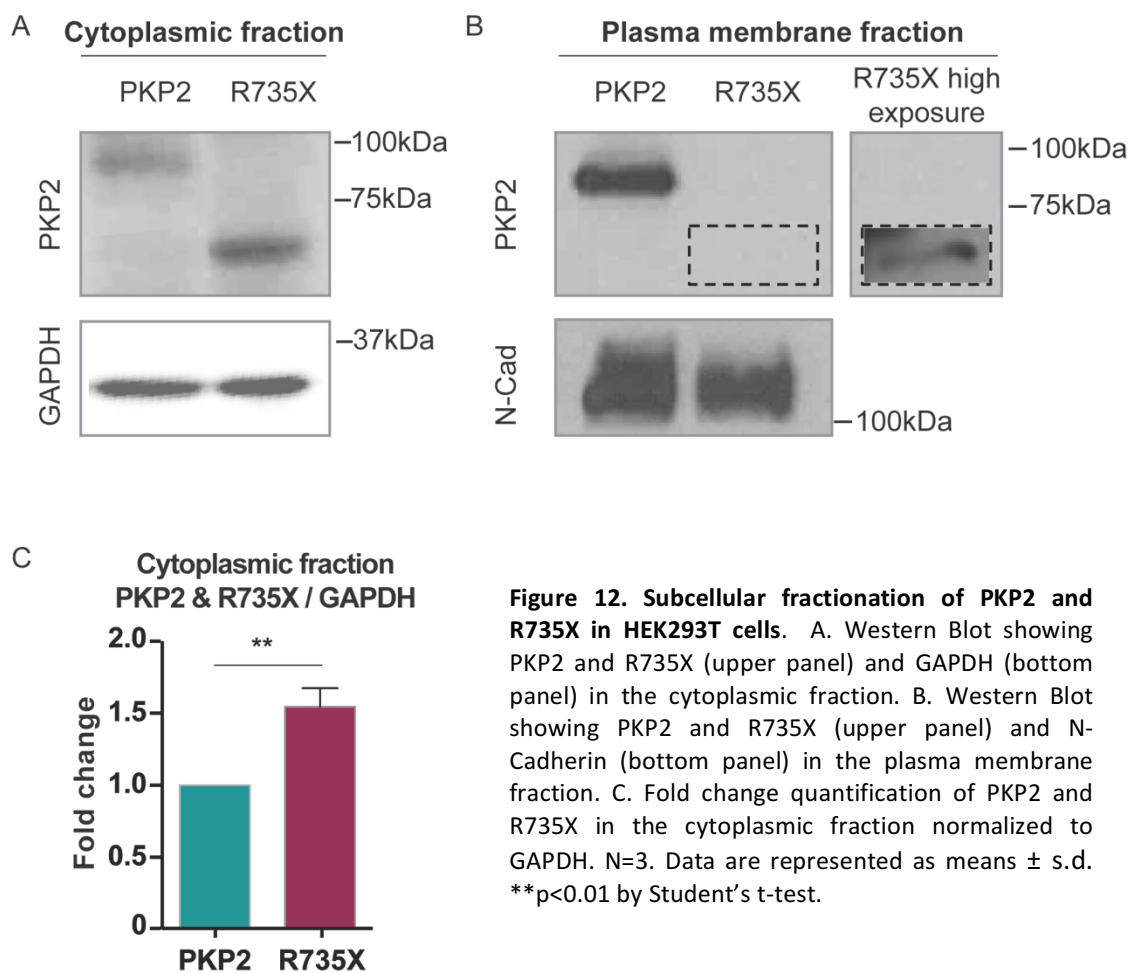


Figure 12. Subcellular fractionation of PKP2 and R735X in HEK293T cells. A. Western Blot showing PKP2 and R735X (upper panel) and GAPDH (bottom panel) in the cytoplasmic fraction. B. Western Blot showing PKP2 and R735X (upper panel) and N-Cadherin (bottom panel) in the plasma membrane fraction. C. Fold change quantification of PKP2 and R735X in the cytoplasmic fraction normalized to GAPDH. N=3. Data are represented as means \pm s.d. ** $p < 0.01$ by Student's t-test.

1.2. Mobility of R735X

We have shown that the amount of R735X located at the plasma membrane is decreased in comparison with PKP2. Thus, we hypothesized that the mobility of R735X along the membrane could also be affected. To study the mobility of PKP2 proteins, we transfected HL-1 cells with *pEGFP-PKP2* and *pEGFP-R735X*, and performed a Fluorescence Recovery After Photobleaching (FRAP) experiment. After photobleaching a region of interest (ROI, diameter = 1.5 μm) at the plasma membrane with a high level light, we measured the rate of fluorescence recovery during 120 seconds (Figure 13).

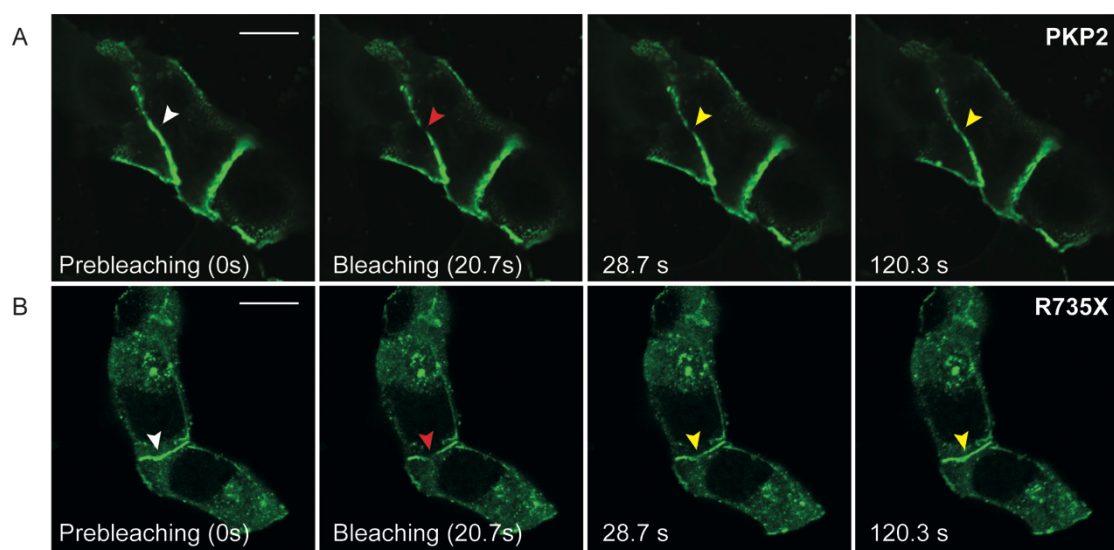


Figure 13. Representative images from FRAP experiments of EGFP-PKP2 and EGFP-R735X in HL-1 cells. A. Still frames from FRAP movies of HL-1 cells transfected with *pEGFP-PKP2*. B. Still frames from FRAP movies of HL-1 cells transfected with *pEGFP-R735X*. Arrowheads indicate regions of interest (ROIs). White arrowheads indicate prebleaching ROI. Red arrowheads indicate bleaching ROI. Yellow arrowheads indicate recovery after bleaching ROI at different times. Time of recording is indicated in each panel. Scale bar = 10 μm .

Levels of initial fluorescence in areas selected for bleaching were not significantly different between the two groups (PKP2 = 937.9 ± 230.0 AU and R735X = 519.0 ± 89.33 AU) (Figure 14A). After bleaching a region of the cell-cell contact, both EGFP-PKP2 and EGFP-R735X proteins were able to recover approximately 60% of the initial fluorescence after 120 seconds (Figure 14B). This indicates that EGFP-PKP2 protein population is composed by 60% of mobile proteins (mobile fraction, MF) and 40% of immobile proteins (immobile fraction, IF). This would mean that 40% of the initial signal is coming from proteins that are stably anchored to the membrane to not be moving during the recording time. On the other hand, 60% of the initial signal is coming

from proteins that are able to move during the time of measurement. Despite representing the same percentage, EGFP-PKP2 and EGFP-R735X mobile fraction showed a different recovery curve. Indeed, half-time of recovery (time necessary to achieve half of the final fluorescence, $T_{1/2}$) was 2.5 times shorter for EGFP-R735X (EGFP-PKP2 $T_{1/2} = 24.29 \pm 2.33$ s and EGFP-R735X $T_{1/2} = 9.31 \pm 2.40$ s) (Figure 14C). Moreover, the percentage of bleaching that we were able to achieve in the mutant was lower than in PKP2 (PKP2 = $78.95 \pm 3.61\%$ and R735X = $47.72 \pm 3.56\%$) (Figure 14D). This would agree with the observed differences in the mobility of both proteins; the percentage of bleaching of the mutant might be masked by the rapid diffusion of the protein. Thus, FRAP results would indicate that EGFP-R735X moves 2.5 times faster along the plasma membrane than EGFP-PKP2 protein.

To check if R735X might alter the mobility of PKP2, we performed FRAP on HL-1 cells co-transfected with *pEGFP-PKP2* and *ptdTomato-R735X*. EGFP-PKP2 alone or co-expressed with tdTomato-R735X showed a similar kinetics of fluorescence recovery after photobleaching (Figure 15C). Initial fluorescence and percentage of bleaching achieved in EGFP-PKP2 were similar regardless of the co-expression of tdTomato-R735X (data not shown). In both situations, EGFP-PKP2 showed a similar half-time of recovery (PKP2 $T_{1/2} = 33.28 \pm 5.84$ s and PKP2 (R735X) $T_{1/2} = 36.49 \pm 7.47$ s) (Figure 15A) and a similar mobile fraction (~60%) (Figure 15B). These results would indicate that the mobility of EGFP-PKP2 is not affected by the co-expression of tdTomato-R735X.

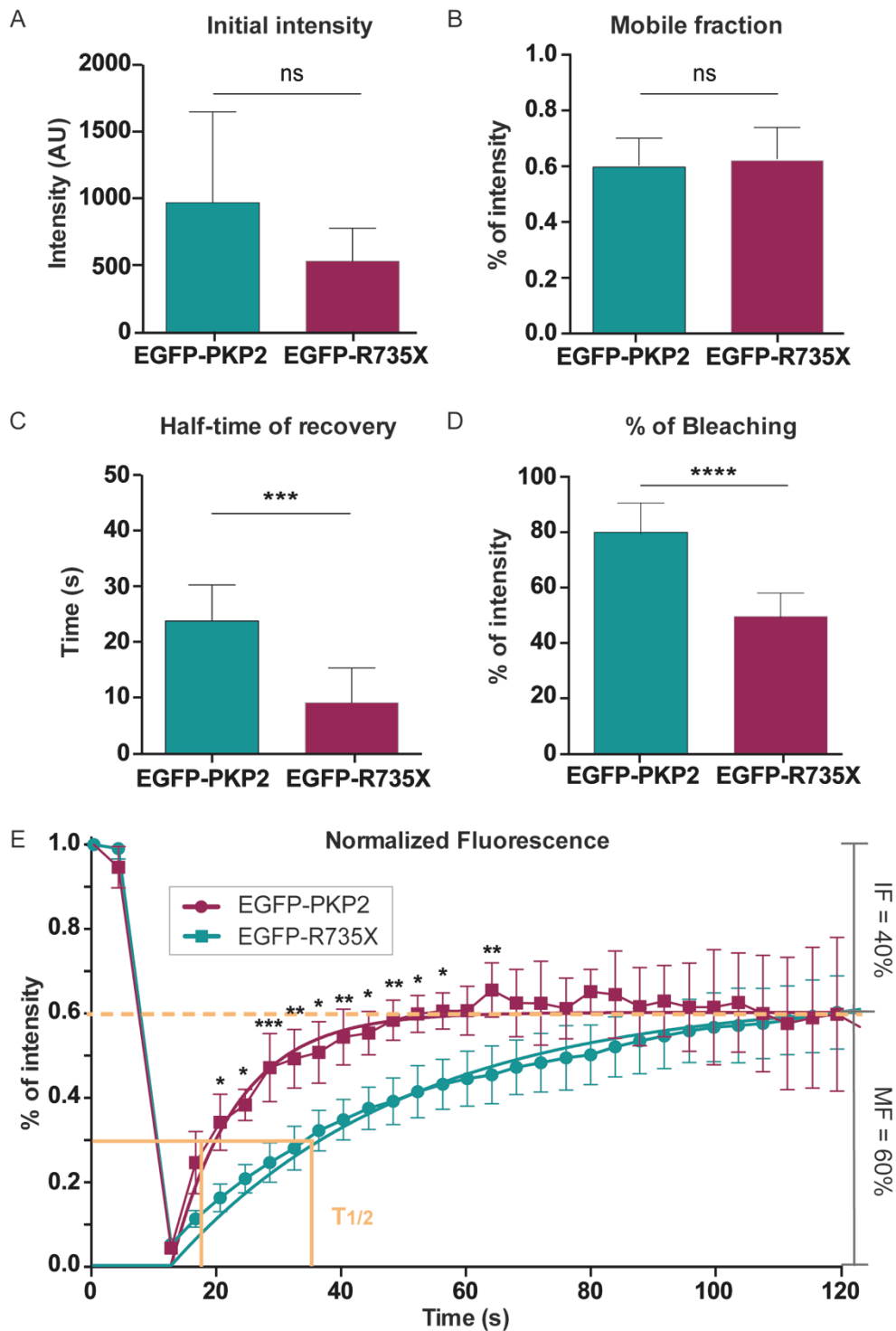


Figure 14. PKP2 C-terminal deletion alters plasma membrane mobility. FRAP of EGFP-PKP2 and EGFP-R735X in HL-1 cells. A. Intensity of the stimulation ROI at 0 seconds. ns $p > 0.05$ by Student's t-test. B. Quantification of the Mobile fraction (MF). ns $p > 0.05$ by Student's t-test. C. Quantification of the half-time of recovery after photobleaching ($T_{1/2}$). *** $p < 0.001$ by Student's t-test. D. Percentage of bleaching achieved after laser stimulation. **** $p < 0.0001$ by Student's t-test. E. Normalized fluorescence intensity plotted (y-axis) against time (x-axis), fitted to a single component exponential (solid lines). Mobile fraction (MF) and Immobile fraction (IF) are delimited by orange dashed line. Half-time of recovery is indicated with solid orange lines. * $p < 0.05$ in Time = 20.7, 24.8, 36.8, 44.9, 52.9 and 57.0 s; ** $p < 0.01$ in Time = 32.8, 40.8, 48.9, 65.0 s; *** $p < 0.001$ in Time = 28.8s by two-way ANOVA. Data are represented as mean \pm s.d. EGFP-PKP2 $n = 8$ and EGFP-R735X $n = 7$.

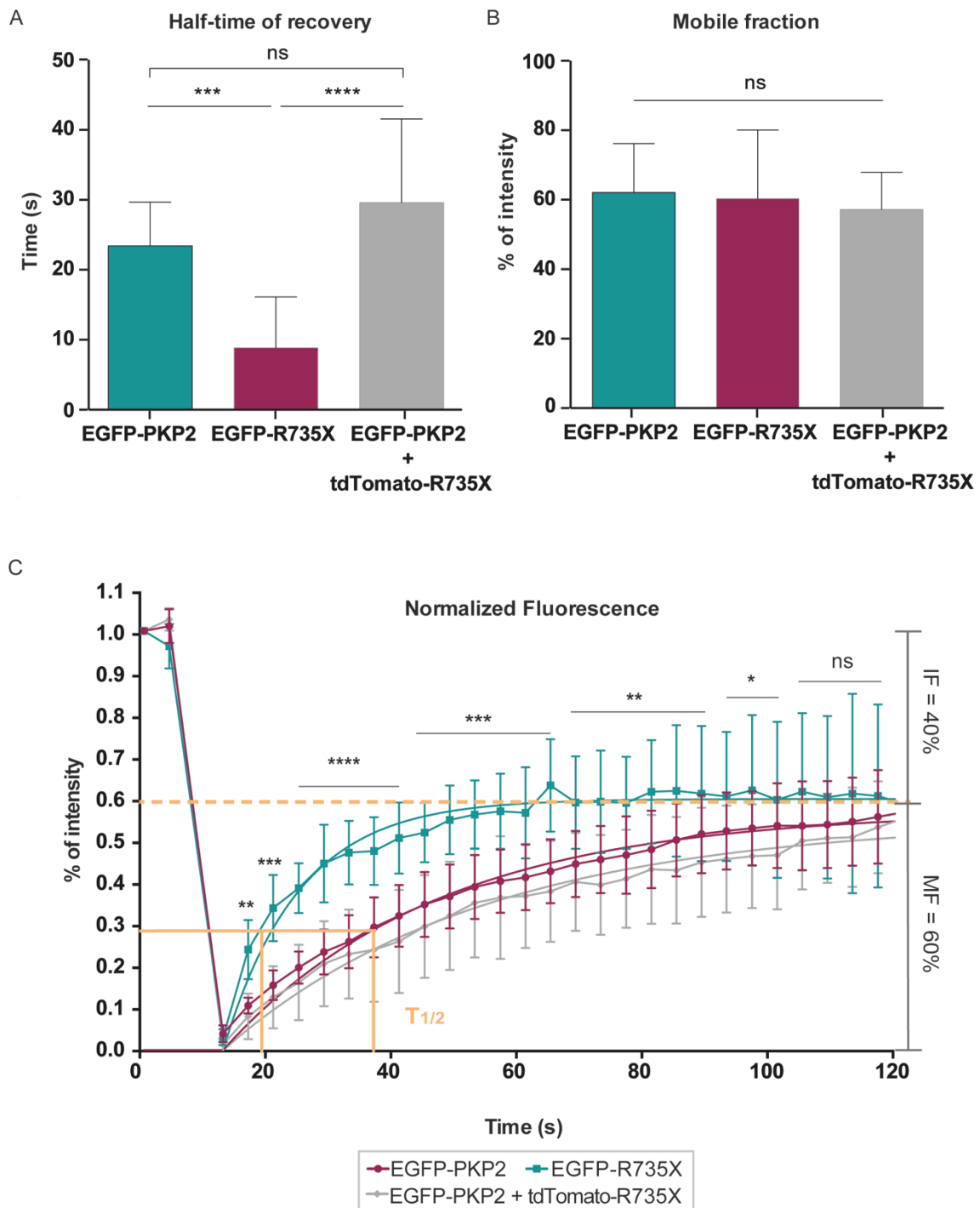


Figure 15. R735X does not alter PKP2 plasma membrane mobility. FRAP of EGFP-PKP2 in control HL-1 cells, EGFP-R735X in control HL-1 cells and EGFP-PKP2 in HL-1 cells co-transfected with tdTomato-R735X. A. Quantification of the half-time of recovery after photobleaching ($T_{1/2}$). *** $p < 0.001$, **** $p < 0.0001$ by one-way ANOVA. B. Quantification of the Mobile fraction (MF). ns $p > 0.05$ by one-way ANOVA. C. Normalized fluorescence intensity plotted (y-axis) against time (x-axis), fitted to a single component exponential (solid lines). Mobile fraction (MF) and Immobile fraction (IF) are delimited by orange dashed line. Half-time of recovery is indicated with solid orange lines. * $p < 0.05$, ** $p < 0.01$, *** $p < 0.001$, **** $p < 0.0001$ by two-way ANOVA. Data are represented as means \pm s.d. EGFP-PKP2 $n = 12$, EGFP-R735X $n = 13$ and EGFP-PKP2 + tdTomato-R735X $n = 6$.

2. Effect of R735X on Na_v1.5

AC patients at early stages of the disease (the so-called “concealed phase”) are normally asymptomatic, but risk suffering ventricular arrhythmias and sudden cardiac death. The mechanism leading to these ventricular arrhythmias is not well understood. Several studies have demonstrated that PKP2 mutations might alter proteins from the intercalated disc, such as Na_v1.5, and have proposed that this could contribute to ventricular arrhythmias during the concealed phase. Thus, we tested whether R735X affects Na_v1.5.

2.1. Subcellular localization of Na_v1.5 in R735X cells

2.1.1. Subcellular localization of Na_v1.5 in R735X HEK293T cells

It has been reported that protein levels of Na_v1.5 channel decrease at the plasma membrane in PKP2 mutant cells (Cerrone et al., 2014). To study whether R735X has an effect on the amount of Na_v1.5 that localizes at the plasma membrane, we co-transfected HEK293T cells with *pEGFP-Na_v1.5* and *pCAG-PKP2* or *pCAG-R735X*, and we analyzed the amount of Na_v1.5 at the total membrane (Figure 16A) and the plasma membrane fractions (Figure 16B). We found that Na_v1.5 protein levels were similar in both PKP2 and R735X total membrane fractions (Figure 16C) while the amount of Na_v1.5 detected at the plasma membrane of cells overexpressing R735X was almost five times smaller than the amount of Na_v1.5 detected in cells overexpressing PKP2 (Figure 16D). This result would indicate that R735X leads to a decrease in the amount of Na_v1.5 located at the plasma membrane in HEK293T cells.

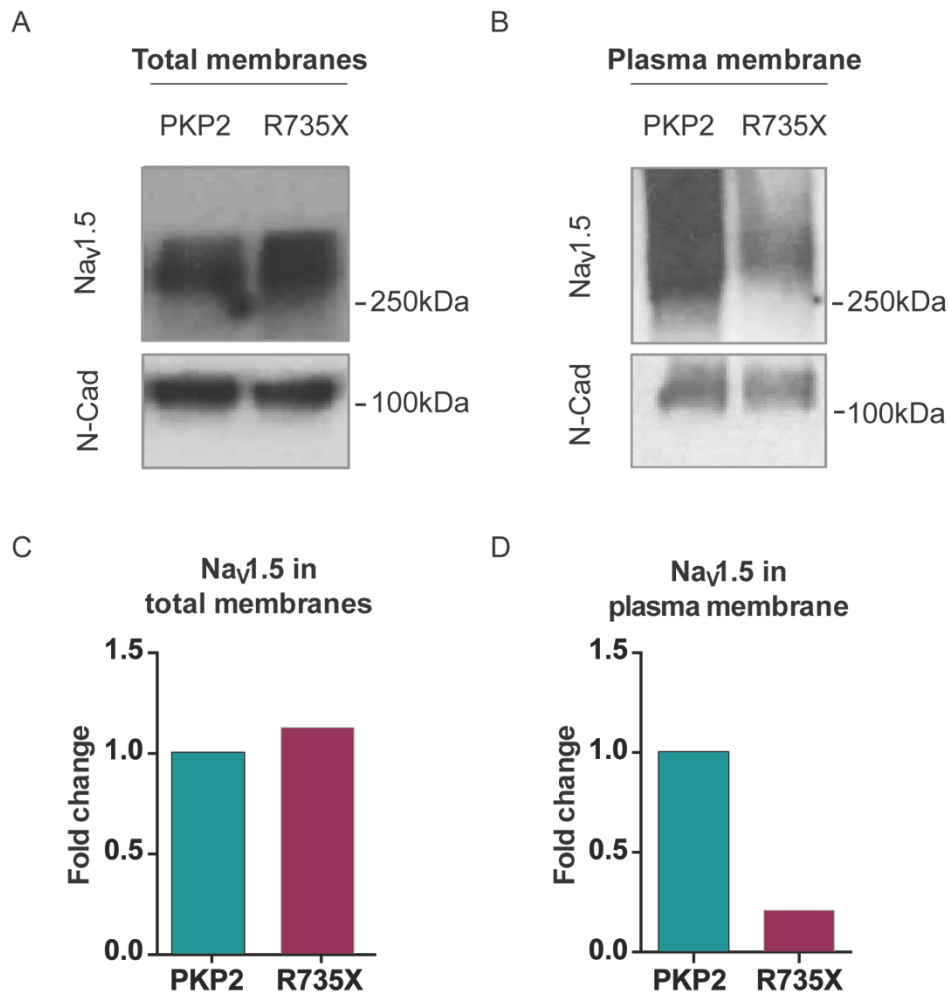


Figure 16. R735X leads to a decrease of Nav_v1.5 at the plasma membrane in HEK293T cells. Subcellular fractionation of Nav_v1.5 in HEK293T cells transiently expressing PKP2 and R735X proteins. A. Immunoblot of total membrane protein fraction incubated with anti-Nav_v1.5 and anti-N-Cadherin antibody. B. Immunoblot of plasma membrane protein fraction incubated with anti-Nav_v1.5 and anti-N-Cadherin antibody. C & D. Quantification of Nav_v1.5 in total and plasma membrane protein fractions normalized to N-Cadherin.

2.1.2. Subcellular localization of Nav_v1.5 in R735X HL-1 cells

We have shown that R735X leads to a decrease in the amount of Nav_v1.5 located at the plasma membrane using transient transfections in HEK293T cells. To check whether R735X have the same effect on Nav_v1.5 in the mouse cardiac derived HL-1 cells, we generated HL-1 cell lines stable for the expression of PKP2 and R735X. These cell lines will also allow us to validate the effect of R735X on Nav_v1.5 independently of PKP2 and R735X transient transfections. We transfected PKP2 and R735X HL-1 stable cell lines with *pEGFP-Nav_v1.5*. EGFP tag was placed at the N-terminal region of Nav_v1.5 since it has been described that it does not affect densities of

currents generated by the channel (Clatot et al., 2012). Overexpression of Nav_v1.5 channels is toxic in HL-1 cells (data not shown) (Moriya, 2015). Therefore, we selected cells with fluorescence intensity level below 500 AU and did not show any apoptotic features (Figure 17A). To increase resolution, to get a better contrast, and to improve signal-to-noise ratio, we took z-stack pictures and we deconvoluted the images. Analysis of deconvoluted z-projections (Figure 17B) showed that the ratio membrane-cytoplasm intensity was 1.769 ± 0.16 in PKP2 HL-1 cells and 0.8799 ± 0.08 in R735X HL-1 cells (Figure 17C). This data would suggest that R735X decrease the amount of EGFP-Nav_v1.5 protein found in the plasma membrane of HL-1 cells.

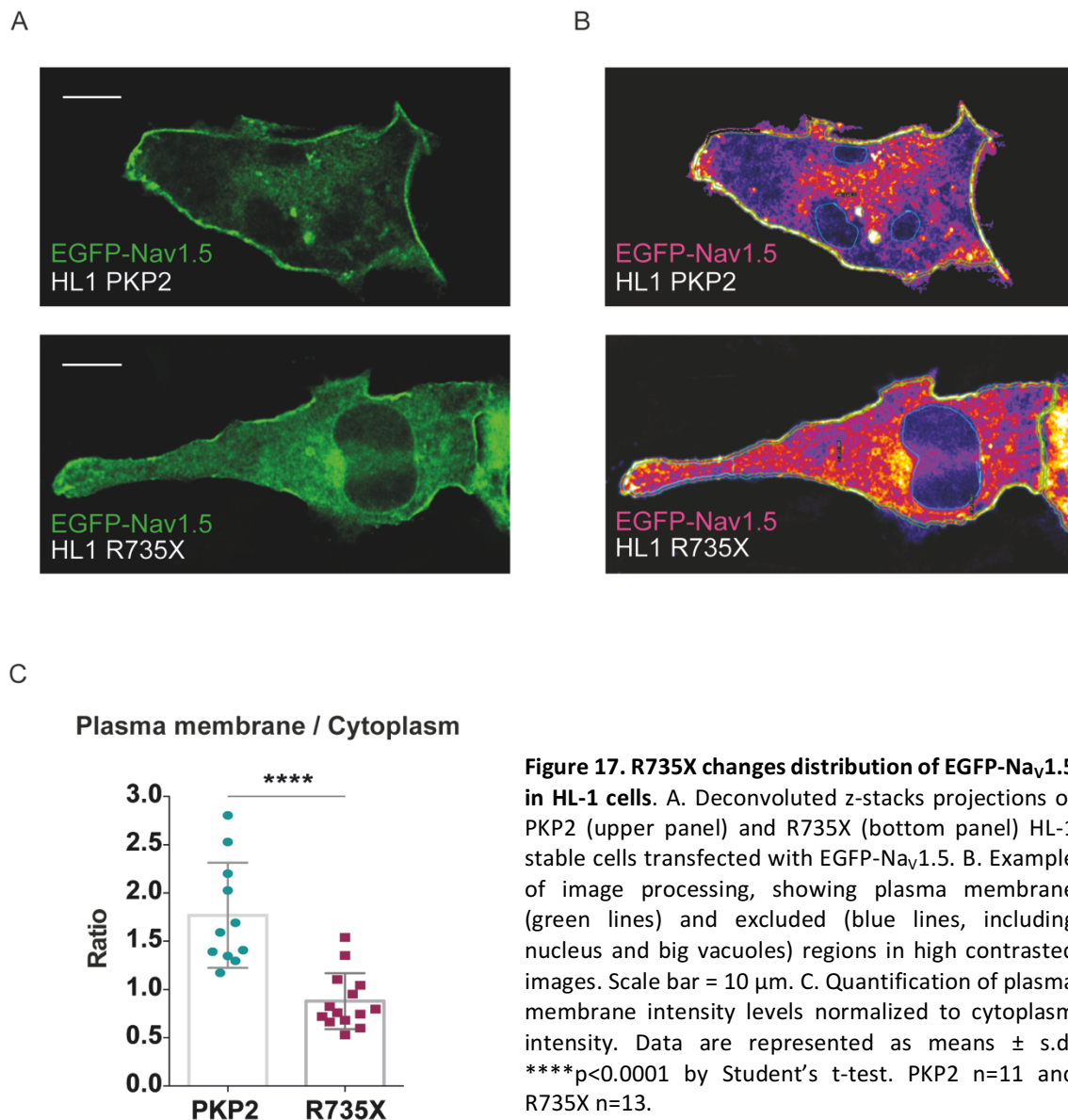


Figure 17. R735X changes distribution of EGFP-Nav_v1.5 in HL-1 cells. A. Deconvoluted z-stacks projections of PKP2 (upper panel) and R735X (bottom panel) HL-1 stable cells transfected with EGFP-Nav_v1.5. B. Example of image processing, showing plasma membrane (green lines) and excluded (blue lines, including nucleus and big vacuoles) regions in high contrasted images. Scale bar = 10 μ m. C. Quantification of plasma membrane intensity levels normalized to cytoplasm intensity. Data are represented as means \pm s.d. **** $p < 0.0001$ by Student's t-test. PKP2 $n=11$ and R735X $n=13$.

To check whether R735X has an effect on endogenous Na_v1.5 levels in the plasma membrane, we performed a cell surface protein biotinylation assay. In parallel, we analyzed by Western Blot total protein samples obtained from Control, PKP2 and R735X HL-1 stable cell lines (Figure 18A). Quantification of these samples showed no differences between groups (Figure 18B). To quantify the endogenous Na_v1.5 levels in the plasma membrane, we incubated HL-1 monolayers with a biotinylation reagent that labels proteins on the outer face of the plasma membrane (Figure 18C). Biotin labeled proteins were pulled down and analyzed by Western Blot (Figure 18D). In an attempt to normalize for the amount of surface Na_v1.5 with respect to total surface proteins, each biotin labeled fraction of the Na_v1.5 band was compared to the Streptavidin intensity of the same lane. Since the Streptavidin intensity correlates with the total amount of surface protein that was pulled down, we were able to calculate relative Na_v1.5 amount for each group. Na_v1.5-Streptavidin ratio in R735X cells was ~0.5 times lower than in the case of PKP2 cells (PKP2 = 0.95 ± 0.02 and R735X = 0.42 ± 0.13). It is also important to note that Control cells (non-modified cells) showed a similar Na_v1.5-Streptavidin ratio to PKP2 cells (Figure 18E).

This result agrees with the distribution of the exogenous EGFP-Na_v1.5 in the cell, and altogether, this data indicates that R735X leads to a decrease in the amount of sodium channel Na_v1.5 located at the plasma membrane in HL-1 cells. Moreover, we did not observe an effect on Na_v1.5 plasma membrane levels on PKP2 HL-1 cells when compared with Control cells. This means that the level of PKP2 overexpression in HL-1 stable cell lines do not have an effect on Na_v1.5. In addition, this data indicates that R735X does not lead to a decrease in the total amount of Na_v1.5 protein.

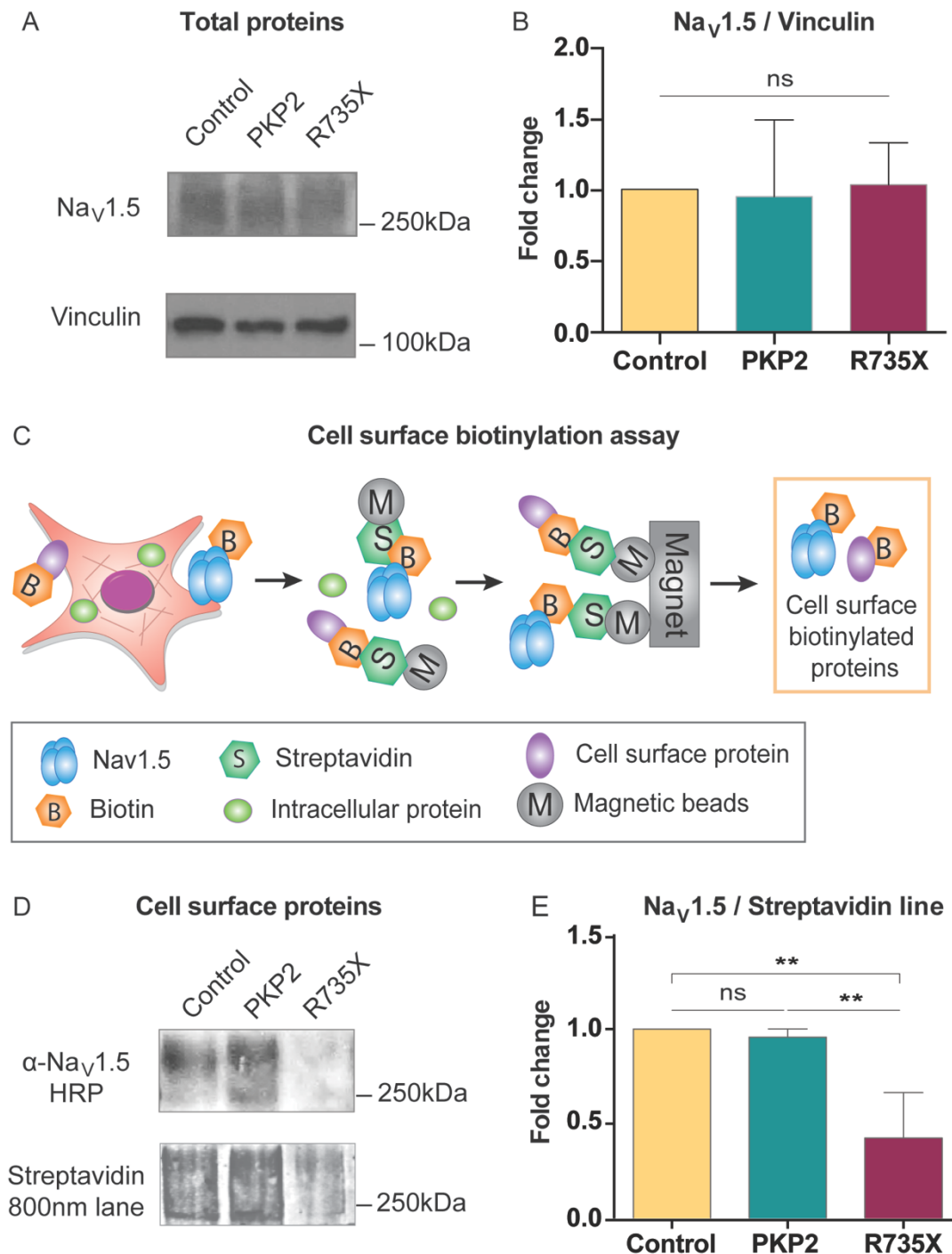


Figure 18. R735X drives to a decrease in plasma membrane Na_v1.5 in HL-1 stable cell lines. A. Immunoblot of total protein samples from HL-1 cells incubated with anti-Na_v1.5 (upper panel) and anti-Vinculin (bottom panel) antibodies. B. Quantification of total Na_v1.5 normalized to Vinculin. Data are represented as means ± s.d. ns p>0.05 by one-way ANOVA. N=3 for each group. C. Diagram illustrating cell surface protein labeling with Biotin method (see Materials and Methods). D. Immunoblot of protein samples precipitated with streptavidin-coated magnetic beads. The immunoblot is incubated with anti-Na_v1.5 antibody (upper panel) and streptavidin-800nm (bottom panel). E. Quantification of precipitated Na_v1.5 normalized to Streptavidin signal in each lane. Data are represented as means ± s.d. **p<0.01 by one-way ANOVA. N=3 for each group.

2.2. R735X and Na_v1.5 co-immunoprecipitation

It has been reported that the N-terminal region of PKP2 (amino acids 1-335) interacts with Na_v1.5 channels in adult heart lysate (Sato et al., 2009). To further investigate the role of the C-terminal region in the interaction with the channels, we performed an immunoprecipitation assay of Na_v1.5 and PKP2 or R735X. Briefly, HEK293T cells were co-transfected with *pEGFP-Na_v1.5* and *pCAG-PKP2* or *pCAG-R735X* constructs, and protein samples were precipitated with an α -GFP antibody-coated Protein A beads complex.

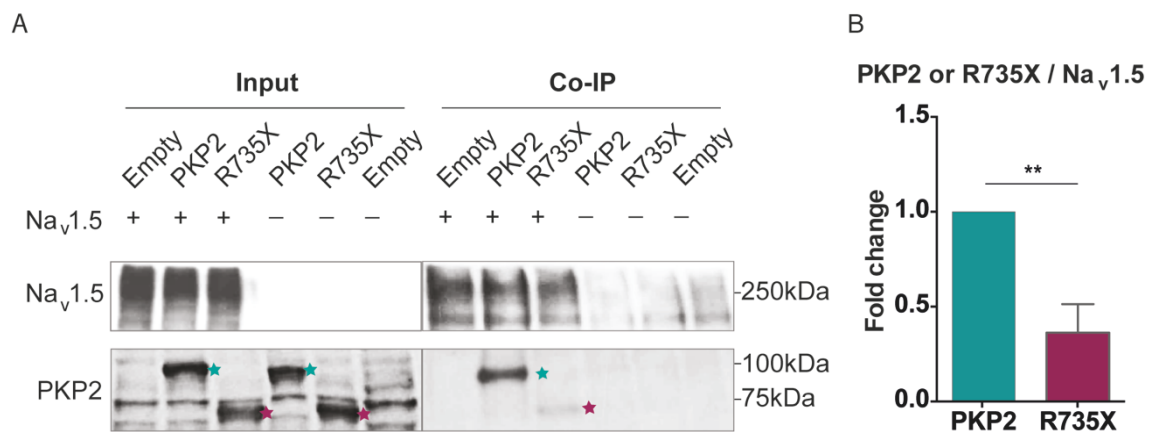


Figure 19. R735X co-immunoprecipitates with Na_v1.5. A. Symbols + and - indicate transfection or not with EGFP-Na_v1.5. Left panels: immunoblot for Na_v1.5 (top) and PKP2 (bottom) from input samples. Right panels: Immunoblot for Na_v1.5 (top) and PKP2 (bottom) from samples exposed to α -GFP antibody-coated Protein A beads. Samples not transfected with *pEGFP-Na_v1.5* run as negative control. Green stars indicate PKP2 protein (98kDa) and pink stars indicate R735X protein (~65kDa). B. Quantification of PKP2 and R735X proteins precipitated with EGFP-Na_v1.5, normalized to precipitated EGFP-Na_v1.5 levels. Data are means \pm s.d. **p<0.01 by Student's t-test. N=3 for each group.

Both PKP2 and R735X were able to precipitate with EGFP-Na_v1.5 (Figure 19A). However, R735X co-immunoprecipitation with EGFP-Na_v1.5 was reduced in a 60% (0.3629 ± 0.09) when compared with PKP2 (Figure 19B). The fact that EGFP-Na_v1.5 was able to precipitate with R735X agrees with what has been described: the common region between PKP2 and R735X is enough to establish an interaction with the channel. However, the lack of PKP2 C-terminal region leads to a decrease in the level of interaction between R735X and Na_v1.5.

2.3. R735X and Na_v1.5 co-localization

It has been reported that PKP2 and Nav1.5 co-localize at the intercalated disc of cardiomyocytes (Sato et al., 2009). To determine whether R735X and Na_v1.5 interact at the cell membrane in a cardiac context, we co-transfected HL-1 cells with *pEGFP-Na_v1.5* and *ptdTomato-PKP2* or *ptdTomato-R73X* and analyzed z-stack projections by confocal microscopy. Z-projections were

deconvoluted to improve EGFP signal quality (Figure 20A). We identified peaks of fluorescence intensity at the plasma membrane and quantified the distances between red and green peaks (Figure 20B). We observed that in cells expressing tdTomato-PKP2, most of red and green peaks were aligned while in cells expressing tdTomato-R735X, red and green peaks were separated. (PKP2 = $0.03978 \pm 0.005 \mu\text{m}$ and R735X = $0.2022 \pm 0.021 \mu\text{m}$) (Figure 20C). This result would suggest that the co-localization between R735X and $\text{Na}_v1.5$ is impaired at the plasma membrane in HL-1 cells.

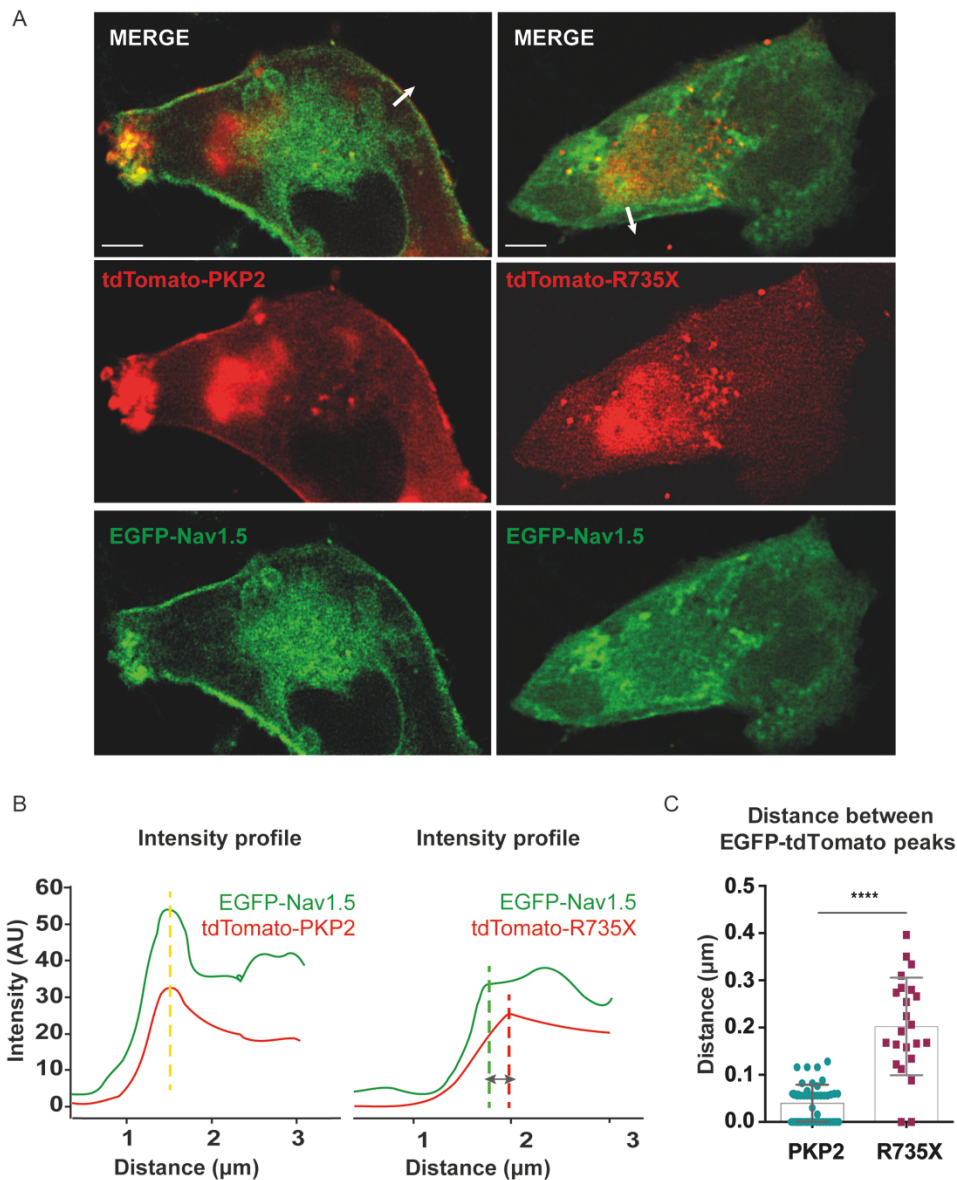


Figure 20. R735X and $\text{Na}_v1.5$ do not co-localize in HL-1 cells plasma membrane. A. HL-1 cells co-transfected with *pEGFP-Nav1.5* and *ptdTomato-PKP2* (right panels) or *ptdTomato-R735X* (left panels). White arrows (3 μm) indicate where the intensity profile of EGFP and tdTomato signal has been analyzed. Scale bar = 5 μm . B. EGFP and tdTomato intensity profiles along a 3 μm line (white arrows in A upper panels). Left panel: EGFP- $\text{Na}_v1.5$ and tdTomato-PKP2 peaks. Yellow dashed line indicating peaks alignment. Right panel: EGFP- $\text{Na}_v1.5$ and tdTomato-R735X peaks. Green and red dashed lines indicating separation between peaks. C. Quantification of the distance between EGFP and tdTomato peaks at the plasma membrane. Data are means \pm s.d. **** $p < 0.0001$ by Student's t-test. N=23 for each group.

2.4. Mobility of Na_v1.5

As demonstrated previously, R735X shows a different pattern of mobility than PKP2 at the cell borders and is able to co-precipitate with Na_v1.5. We questioned whether R735X could lead to a decrease in Na_v1.5 at the plasma membrane by altering the channel mobility. To study Na_v1.5 mobility at the plasma membrane, we transfected PKP2 and R735X HL-1 stable cell lines with *pEGFP-Na_v1.5* and performed FRAP on 1.5 μm diameter ROIs at the plasma membrane. Curves of normalized fluorescence recovery after photobleaching were similar between cell lines (Figure 21A). EGFP-Na_v1.5 mobile fraction was approximately 70% in all groups analyzed (Control = 67.72 ± 5.87% , PKP2 = 69.46 ± 4.36% and R735X = 73.52 ± 5.03%) (Figure 21B) and T_{1/2} was not statistically different (Control = 10.65 ± 1.71 s, PKP2 = 11.23 ± 1.63 s and R735X = 13.34 ± 2.28 s) (Figure 21C). Therefore, this data indicates that R735X does not alter EGFP-Na_v1.5 mobility at the plasma membrane.

3. Arrhythmogenic effect of R735X on hiPSC-CM

Several studies have been done in mice or cell derived from mice to study the effect of PKP2 mutations on cardiac electrophysiology. However, it has been shown that human and murine cardiac electrophysiology differ in many aspects, and some mechanisms of arrhythmias in mice may differ from those in humans (Kaese and Verheule, 2012). Therefore, to further investigate the effect of the mutant R735X on a human cardiac context, we generated an AC model based on human induced pluripotent stem cell-derived cardiomyocytes (hiPSC-CMs).

3.1. Somatic cell reprogramming and hiPSCs characterization

Available commercial human dermal fibroblasts (HDF) were reprogramed using CytoTune-iPS 2.0 Sendai Reprogramming technology. CytoTune system is a footprint-free reprogramming technology based on the transduction of somatic cells with Sendai virus derived RNA vectors codifying for reprogramming factors (hOct3/4, hSox2, hKlf4 and hc-Myc). Colonies with hiPSC morphology were expanded and tested for the expression of endogenous pluripotency markers and the ability to differentiate into different lineages *in vitro*.

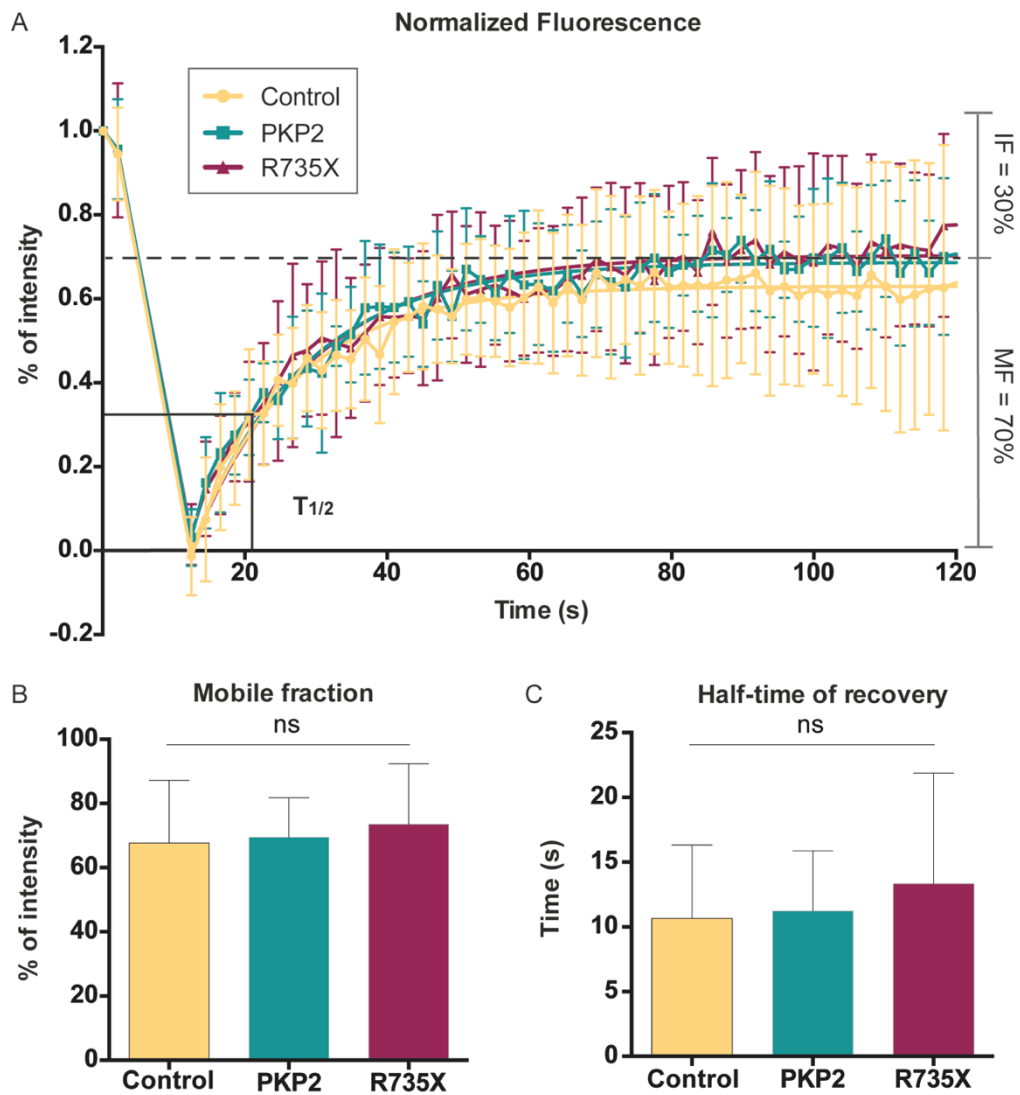


Figure 21. R735X does not affect Na_v1.5 mobility at the plasma membrane. FRAP of EGFP-Na_v1.5 in PKP2 and R735X stable HL-1 cells. A. Normalized fluorescence intensity plotted (y-axis) against time (x-axis), fitted to a single component exponential (solid lines). Mobile fraction (MF) and Immobile fraction (IF) are delimited by black dashed line. Half-time of recovery is indicated with solid black lines. No significant differences were observed in normalized fluorescence intensity by two-way ANOVA analysis. B. Quantification of the Mobile fraction (MF). ns $p > 0.05$ by one-way ANOVA. C. Quantification of the half-time of recovery after photobleaching ($T_{1/2}$). ns $p > 0.05$ by one-way ANOVA. Data are means \pm s.d. Control $n = 12$, PKP2 $n = 9$ and R735X $n = 14$.

3.1.1. Alkaline phosphatase test

Alkaline phosphatase (ALP) activity has been shown to be up-regulated in pluripotent stem cells (Štefková et al., 2015). After reprogramming, emerging colonies were tested for ALP activity. We selected hiPSC colonies positive for ALP staining to be expanded as clonal cell lines (Figure 22A).

3.1.2. Karyotype

The selected hiPS cell line was karyotyped using high resolution Giemsa banding. The Giemsa staining of chromosomes showed a normal diploid chromosomal content of the hiPS cell line. In this case, hiPS cell line was derived from fibroblasts of a female donor (Figure 22B).

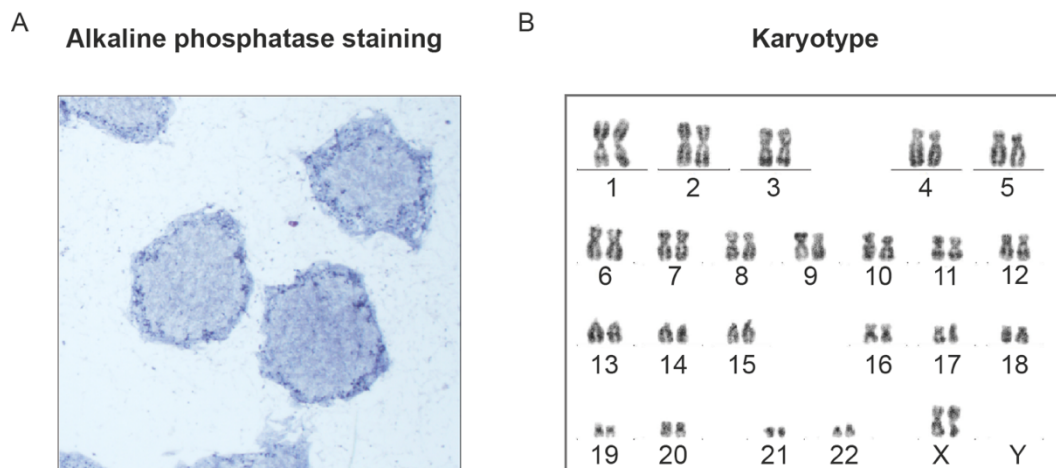


Figure 22. Alkaline phosphatase staining and karyotype in hiPSCs. A. Alkaline phosphatase staining in hiPSCs colonies reprogrammed from HDFs. B. Karyotype of the selected hiPSC cell line.

3.1.3. Detection of pluripotency markers by semiquantitative PCR

hiPSC cell line was examined for the expression of pluripotency markers, such as *OCT4*, *SOX2*, *KLF4*, and *c-MYC*. We extracted RNA from hiPSCs and performed a reverse transcription PCR to detect the expression of these pluripotency markers. Human embryonic stem cell line (ES4 cell line, accession number CVCL_C771) samples were used as a positive control. We observed that hiPSCs and ES4 cells showed similar expression of *OCT4*, *SOX2*, *KLF4*, and *c-MYC*. (Figure 23).

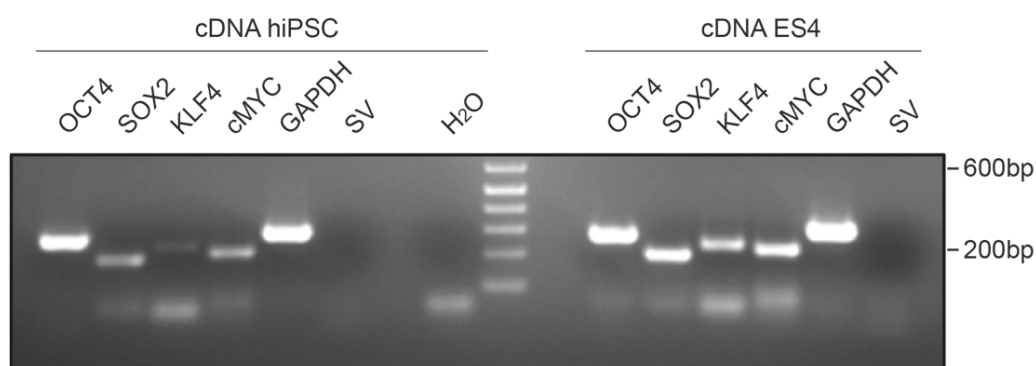


Figure 23. Expression of pluripotency markers (*OCT4*, *SOX2*, *KLF4*, and *c-MYC*) in hiPSCs. ES4 cDNA was used as a positive control of the expression of pluripotency markers. SV indicates a PCR product using primers that anneals at the Sendai Virus genome sequence. It indicates that the genome of Sendai Virus has been eliminated.

3.1.4. Detection of pluripotency markers by immunofluorescence

To double check the expression of pluripotency markers, we performed immunofluorescence of OCT4, NANOG, SSEA4 and TRA1-80 in hiPSC colonies. hiPS cell line showed expression of all tested pluripotency markers (Figure 24).

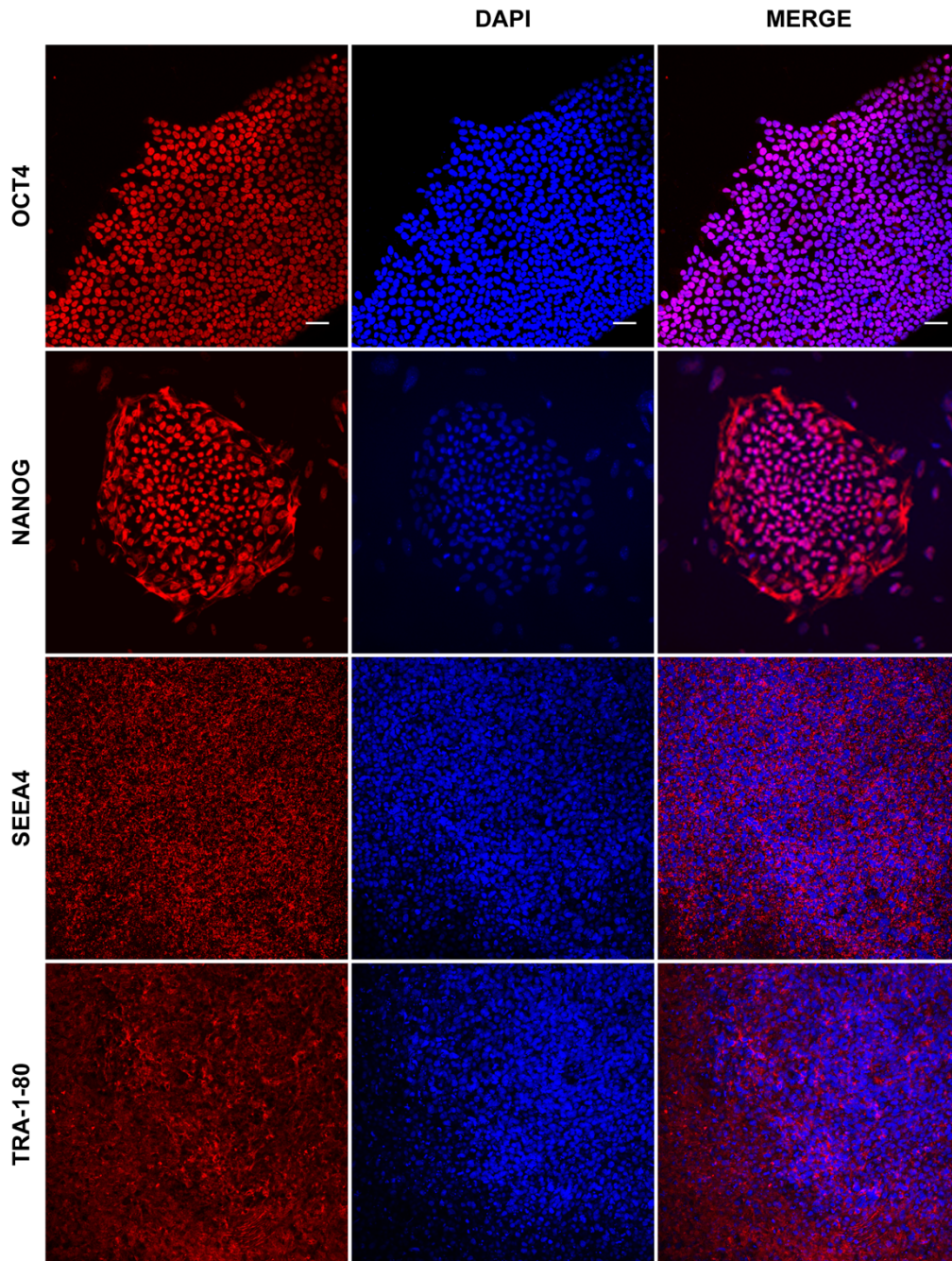


Figure 24. Immunofluorescence of OCT4, NANOG, SSEA4 and TRA 1-80 in hiPSC colonies. Scale bar = 50 μ m.

3.1.4. *In vitro* differentiation test

We evaluated the capacity of the hiPS cell line to differentiate into the three germ layers: mesoderm, endoderm, and ectoderm. hiPSCs were cultured as embryoid bodies (EBs) and expression markers of each germ layer were detected by immunofluorescence. hiPS cell line showed expression for the markers smooth muscle actin (SMA) for mesoderm layer, α -fetoprotein (AFP) for endoderm layer, Glial Fibrillary Acidic Protein (GFAP) and neuron-specific class III beta-tubulin (Tuj1) for ectoderm layer (Figure 25).

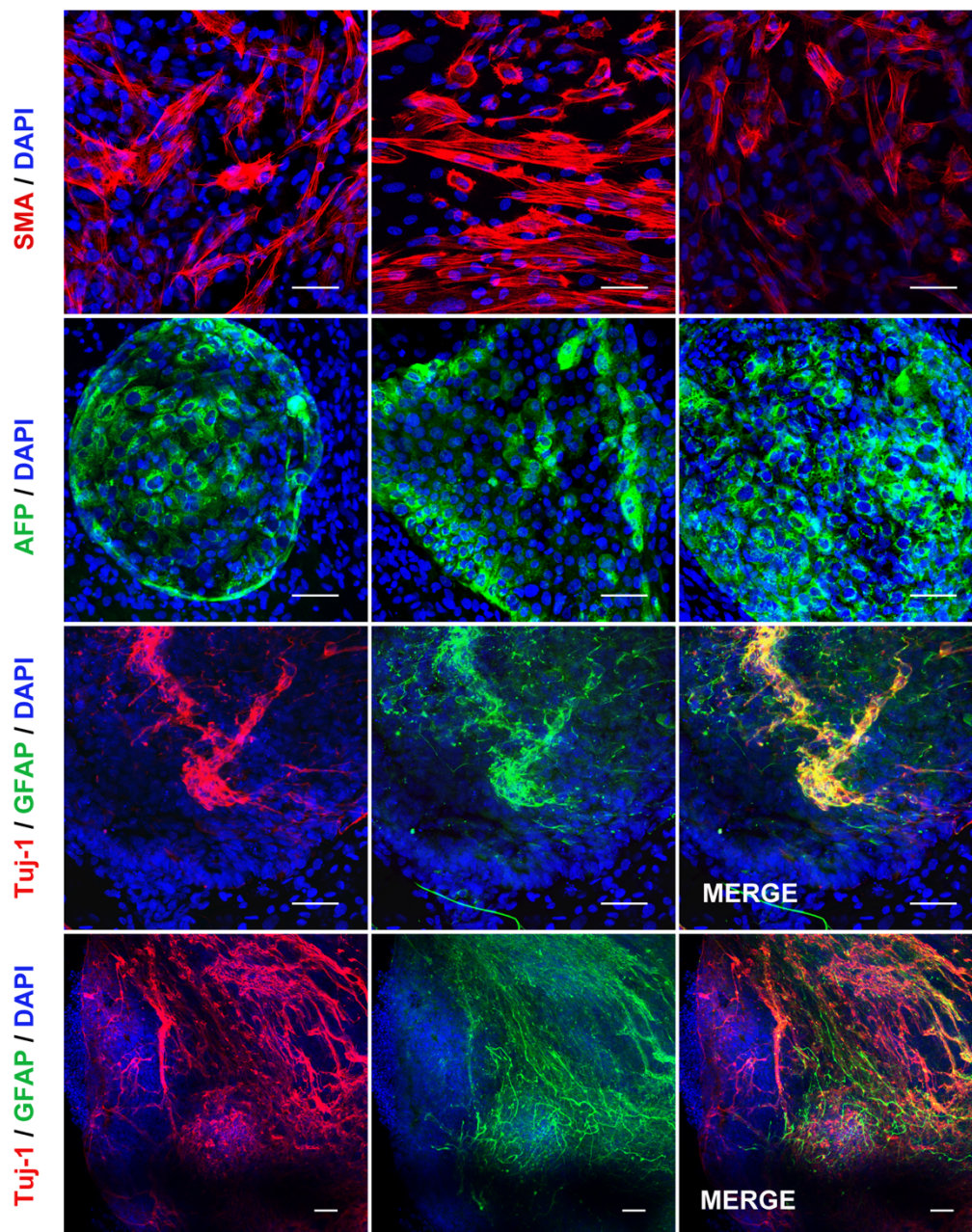


Figure 25. *In vitro* differentiation test of hiPSCs into the three germ layers. Immunofluorescence of smooth muscle actin (SMA) (mesoderm layer), α -fetoprotein (AFP) (endoderm layer), Glial Fibrillary Acidic Protein (GFAP) and neuron-specific class III beta-tubulin (Tuj1) (ectoderm layer). Scale bar = 50 μ m.

3.2. Generation of PKP2 and R735X transgenic hiPS cell lines

Once the hiPS cell line was characterized and established, we generated hiPS cell lines that stably expressed PKP2 or R735X. We transfected hiPSCs by electroporation with two plasmids containing the PB cassette (*pPB-CAG-PKP2* or *pPB-CAG-R735X*) and the PB transposase (*pCMV-Transposase*). After 10 days of treatment with Neomycin, individual colonies of resistant hiPSCs were picked and propagated as different clonal cell lines. Each clonal cell line will have a variable number of insertions (between 1-7 insertions) and these insertions will be in a random site of the genome. To confirm that the fragment of interest has been inserted into the genome, we genotyped different clones by extracting genomic DNA and running a PCR using primers that anneal in *PKP2* or *R735X* (Figure 26A) and *Neomycin resistance* gene (Figure 26B).

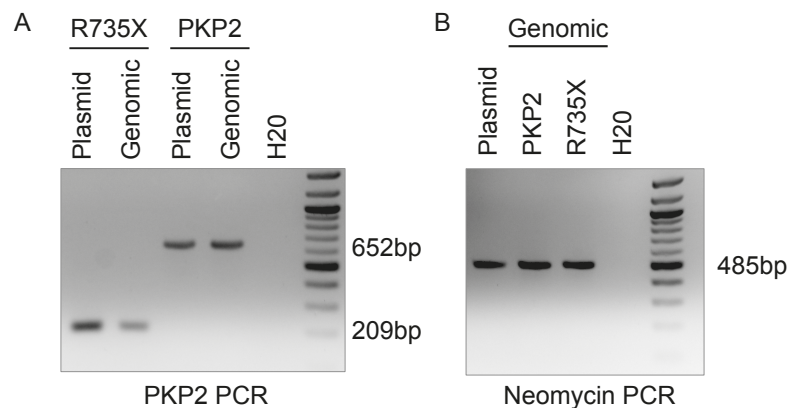


Figure 26. Transgenic hiPSCs genotyping. A. PCR on PKP2 or R735X sequence. PCR product was 652bp long for hiPSCs transfected with the construct *pPB-CAG-PKP2-PGK-Neo-PB* and 209bp long in cells transfected with the construct *pPB-CAG-R735X-PGK-Neo-PB*. B. PCR on Neomycin resistance gene. PCR product was 485bp long for cells transfected with both constructs.

Since the number of insertions in hiPSCs does not necessarily correlate with the final amount of exogenous protein present in hiPSC-CMs, we measured the actual PKP2 and R735X proteins levels on cardiomyocytes derived from hiPSC cell lines by Western Blot (Figure 27A). We observed a mild overexpression of PKP2 (98kDa band) in the PKP2 cell line compared to Control cell line (1.238 ± 0.072). However, PKP2 levels in mutant cell line (1.134 ± 0.087) were not significantly different when compared to PKP2 or Control cells. On the other hand, R735X protein (~65 kDa band) is 63% fewer than the amount of PKP2 protein (98kDa band) in the mutant cell line (Figure 27B).

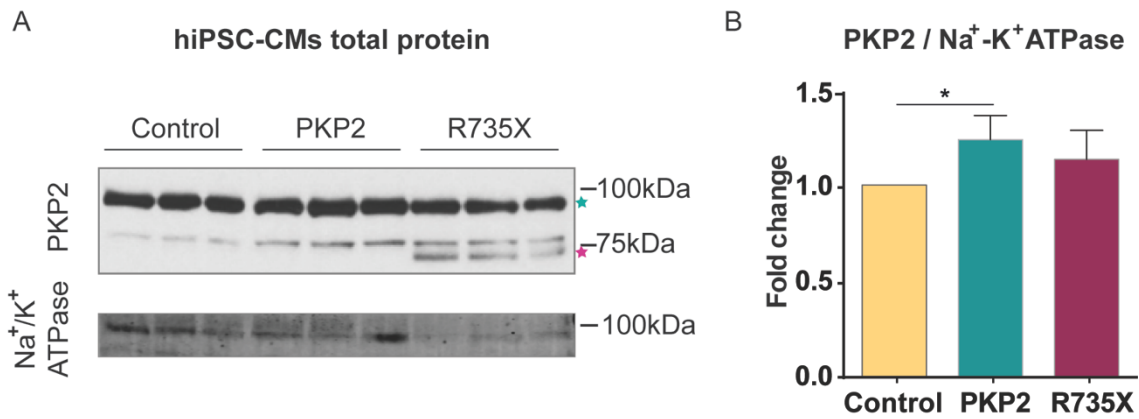


Figure 27. PKP2 and R735X protein expression in hiPSC-CM lines. Western Blot from hiPSC-CM total protein samples. A. Immunoblot incubated with anti-PKP2 antibody (upper panel) and immunoblot incubated with anti-Na⁺/K⁺ ATPase (bottom panel). Green star indicates PKP2 protein (98kDa) and pink star indicates R735X protein (~65 kDa). B. Quantification of the expression of PKP2 protein normalized to the expression of Na⁺/K⁺ ATPase. Data are means \pm s.d. ns $p > 0.05$, * $p < 0.05$ by One-way ANOVA. N=3 for each group.

3.3. hiPSC-CMs maturation

Using hiPSC-CMs to model human cardiac disease has extraordinary and unique advantages. However, it is widely recognized that hiPSC-CMs remain immature in terms of structure and function, showing fetal gene expression, disorganized morphology, and electrophysiological properties that differ from those of adult cardiomyocytes. As such, using these cells to model adult human cardiac disease may be limited (Machiraju and Greenway, 2019). It has been described that hiPSC-CMs showed more mature features (increase of I_{Na} and I_{K1} levels, overexpression of Cx43, increase in cell size, etc.) after being plated over a matrigel-PDMS coated plate for 1 week (Herron et al., 2016). For this reason, in this thesis project, transgenic hiPSC-CMs were routinely matured before performing any experiment by implementing the above-described protocol. Transgenic hiPSC-CMs were immunostained with α -actinin, revealing that PKP2 and R735X hiPSC-CMs did not show any evident abnormality (Figure 28).

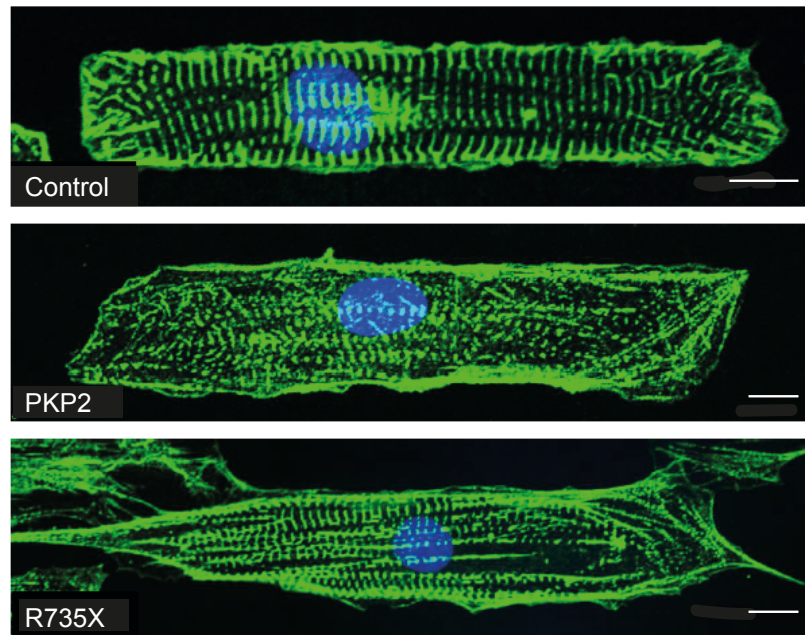


Figure 28. α -actinin immunostaining in transgenic hiPSC-CMs after one week of PDMS maturation. Scale bar = 10 μ m.

3.4. Electrical characterization of single transgenic hiPSC-CMs

To study the electrical changes that hiPSC-CMs overexpressing PKP2 or R735X could undergo, we measured the density of the main independent ion currents of single hiPSC-CMs by whole-cell patch-clamp recordings under the same ionic conditions. Before each experiment, purified hiPSC-CMs were plated as a monolayer over matrigel-PDMS coated plates for 7 days and subsequently, re-plated on matrigel-PDMS micropatterns for at least 4 days. Control, PKP2 and R735X cells presented the same I_{Ca} current density (Control = -10.09 ± 1.6 pA/pF, PKP2 = -8.669 ± 1.2 pA/pF, R735X = -9.01 ± 1.35 pA/pF at $V_m = 5$ mV) along a range of voltage pulses from -50 mV up to +70 mV (Figure 29A-B). Also, three hiPSC-CM lines showed no significant differences in I_{K1} density (Control = -2.22 ± 0.35 pA/pF, PKP2 = -2.77 ± 0.63 pA/pF, R735X = -2.81 ± 0.50 pA/pF at $V_m = -120$ mV) (Figure 29C-D).

However, R735X cells showed a strong and substantial reduction in the mean sodium current density by $\sim 70\%$ when compared with Control and PKP2 cells (Figure 30A-C). Reduction in the sodium current density was accompanied by a lower conductance without changes in the electrophysiological properties of the sodium channel, since the $V_{1/2}$ and the slope was not statistically different between groups (Figure 30D). Reproducible data from three independent

differentiations experiments where collected. Figure 30E shows sodium current density at -20 mV obtained from Figure 33C and conductance parameters ($V_{1/2}$ and slope) calculated from Figure 33D. Thus, patch-clamp experiments indicate that I_{K1} and I_{Ca} are not affected by PKP2 and R735X transgenes in hiPSC-CM. They also revealed that R735X expression in hiPSC-CM leads to a decrease of total cell I_{Na} density without altering the electrical features of $Na_v1.5$.

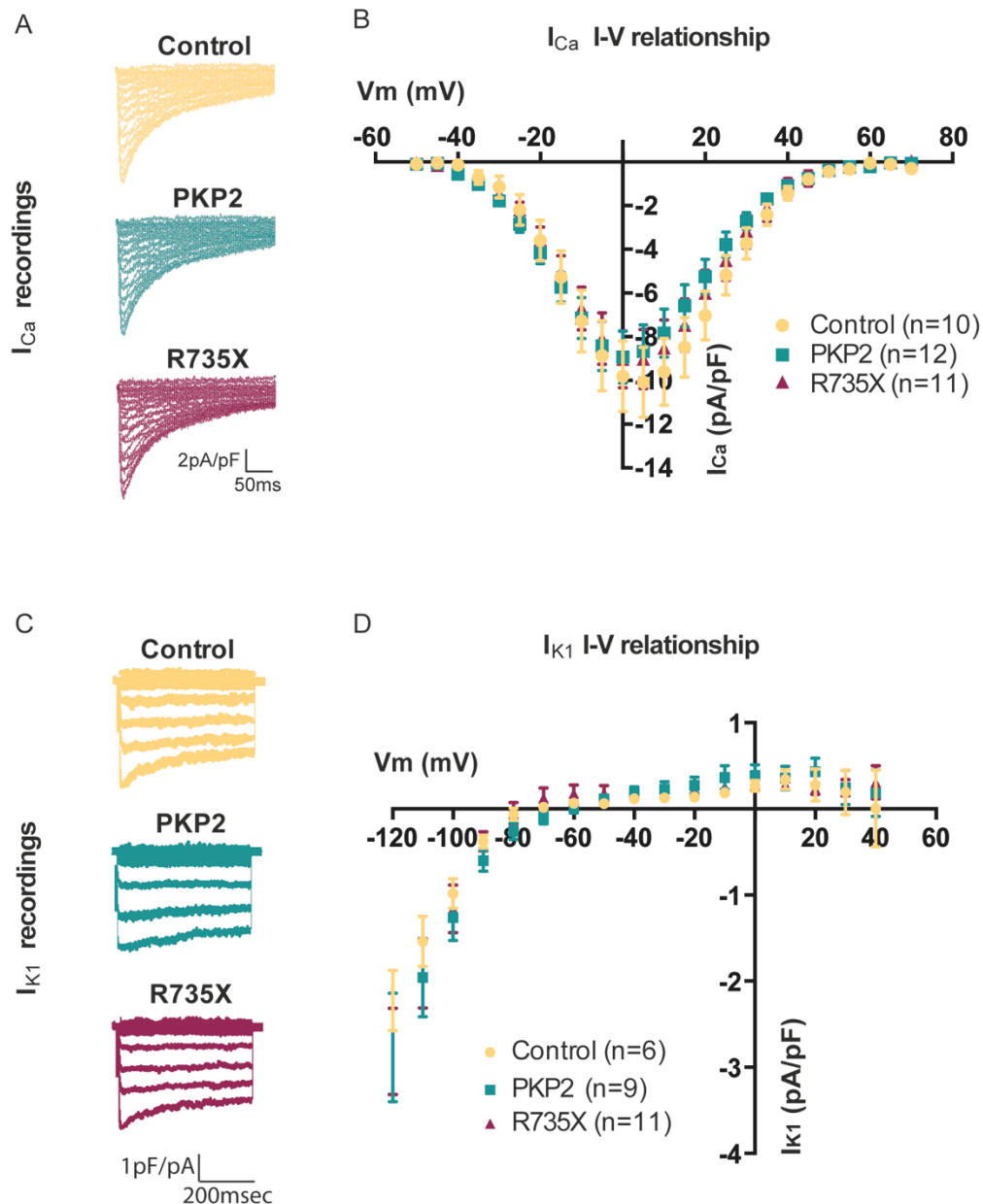


Figure 29. R735X does not have an effect on I_{Ca} and I_{K1} currents. Whole-cell patch-clamp measurements of Ca^{2+} current (I_{Ca}) and inward-rectifier K^+ current (I_{K1}) in Control, PKP2 and R735X hiPSC-CMs. A. I_{Ca} traces. B. I_{Ca} current-voltage relationship. C. I_{K1} traces. D. I_{K1} current-voltage relationship. Data are means \pm s.e.m. hiPSC-CMs showed no significant differences in I_{Ca} and I_{K1} between groups (Two-way ANOVA). Number of observations are indicated in the figure.

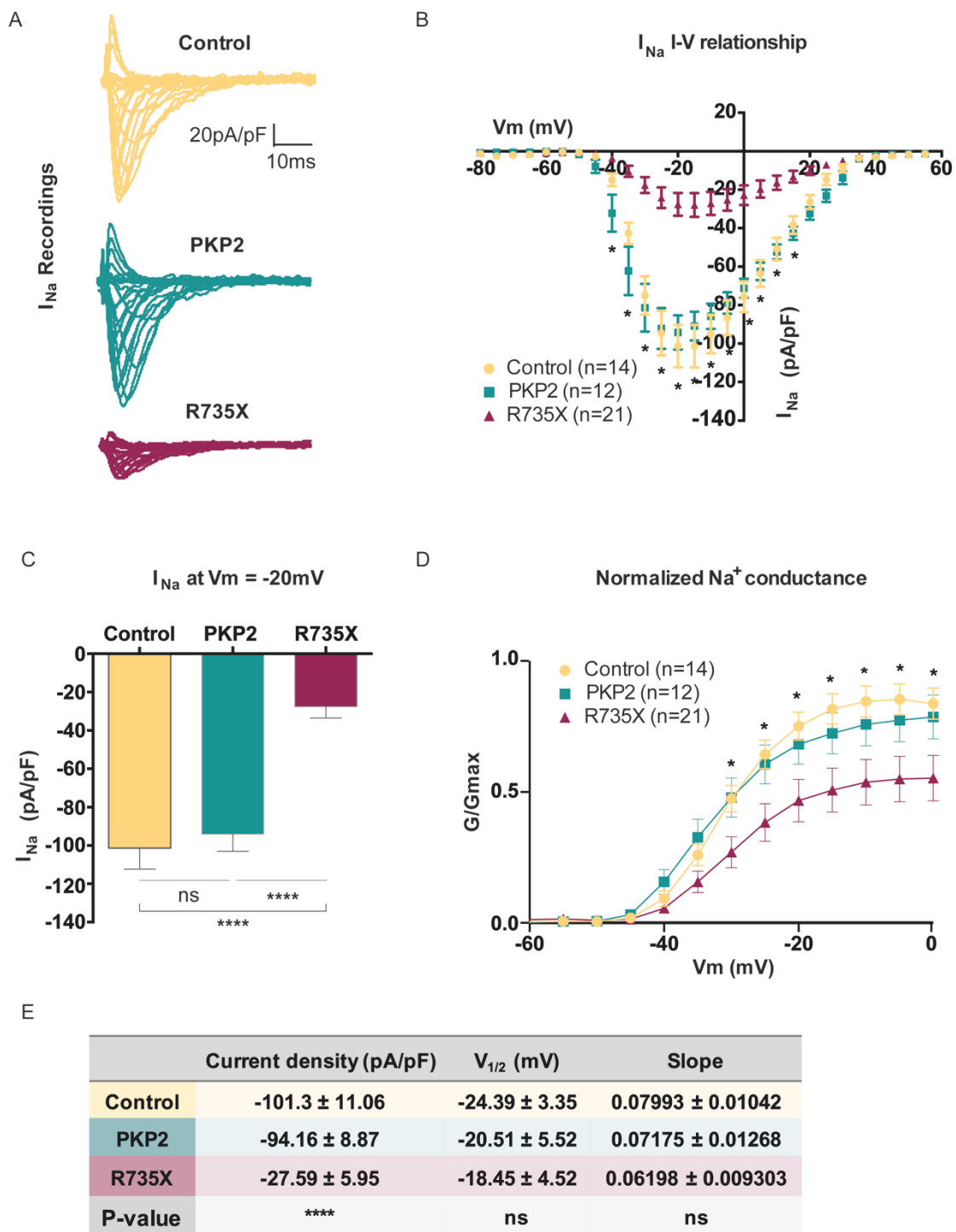


Figure 30. R735X leads to a decrease in I_{Na} current. Whole-cell patch-clamp measurements of Na^+ current (I_{Na}) in Control, PKP2 and R735X hiPSC-CMs. A. I_{Na} traces. B. I_{Na} current-voltage relationship. R735X cells showed significant reduction in I_{Na} amplitude (from -40 to +15 mV, no significant differences between Control and PKP2 cells, **** $p < 0.0001$ between Control and R735X cells by Two-way ANOVA). V_m , membrane voltage. C. Detail of maximum I_{Na} at -20 mV (**** $p < 0.0001$ by One-way ANOVA). D. Voltage dependence of channel activation or channel conductance (G), estimated by dividing I_{Na} at each test potential by the electrochemical driving force for Na^+ , normalized to the maximum Na^+ conductance (G_{max}). R735X cells showed significant reduction in Na^+ conductance (from -20 to 0 mV, no significant differences between Control and PKP2 cells, *** $p < 0.001$ between Control and R735X cells by Two-way ANOVA). E. Values of sodium current density, $V_{1/2}$ and Slope of all groups. **** $p < 0.0001$ and ns $p > 0.05$ by One-way ANOVA. Data are means \pm s.e.m. Number of observations are indicated in the figure.

3.5. Analysis of transgenic hiPSC-CM monolayers

Since we have demonstrated that R735X leads to a 4 times decrease in sodium current density, we questioned whether this sodium current reduction could have arrhythmogenic effects. In order to study the arrhythmogenic effect of R735X mutation, we performed optical mapping on hiPSC-CM monolayers. We cultured the transgenic hiPSC-CMs in circular monolayers and let them mature for 7 days on PDMS. Two or three days after being plated in monolayers, hiPSC-CMs reestablished intercellular attachments and some of them took the role of pacemaker. In physiological situations, electrical impulse originated at the pacemaker propagates through the surrounding cells towards the well edges; generating a spontaneous, rhythmic beating activity.

Transgenic hiPSC-CM monolayers were loaded with a voltage sensitive fluorescent probe that responds to changes in membrane potential (FluoVolt), and we recorded their electrical activity with a high speed CCD camera. Analysis of spontaneous activity revealed that the amplitude of action potentials in PKP2 monolayers was higher than in R735X monolayers (PKP2 amplitude = 205.0 ± 20.62 AU and R735X amplitude = 110.0 ± 6.32 AU) (Figure 31A). Spontaneous frequency in PKP2 monolayers was faster than in R735X monolayers (PKP2 frequency = 0.7250 ± 0.09 Hz and R735X frequency = 0.3200 ± 0.03 Hz) (Figure 31C). Moreover, it is remarkable the irregularly timed peaks seen in all R735X monolayers. Meanwhile, all PKP2 monolayers presented a regular activity, showing consistent intervals between peaks during the same recorded time (Figure 31C-D). This data indicates that the decrease of the sodium currents in mutant cells leads to a reduction in the excitability of cells. As a consequence, some of the spontaneous stimulus would not be able to elicit an AP and that would drive to a lower spontaneous frequency and an arrhythmic activity.

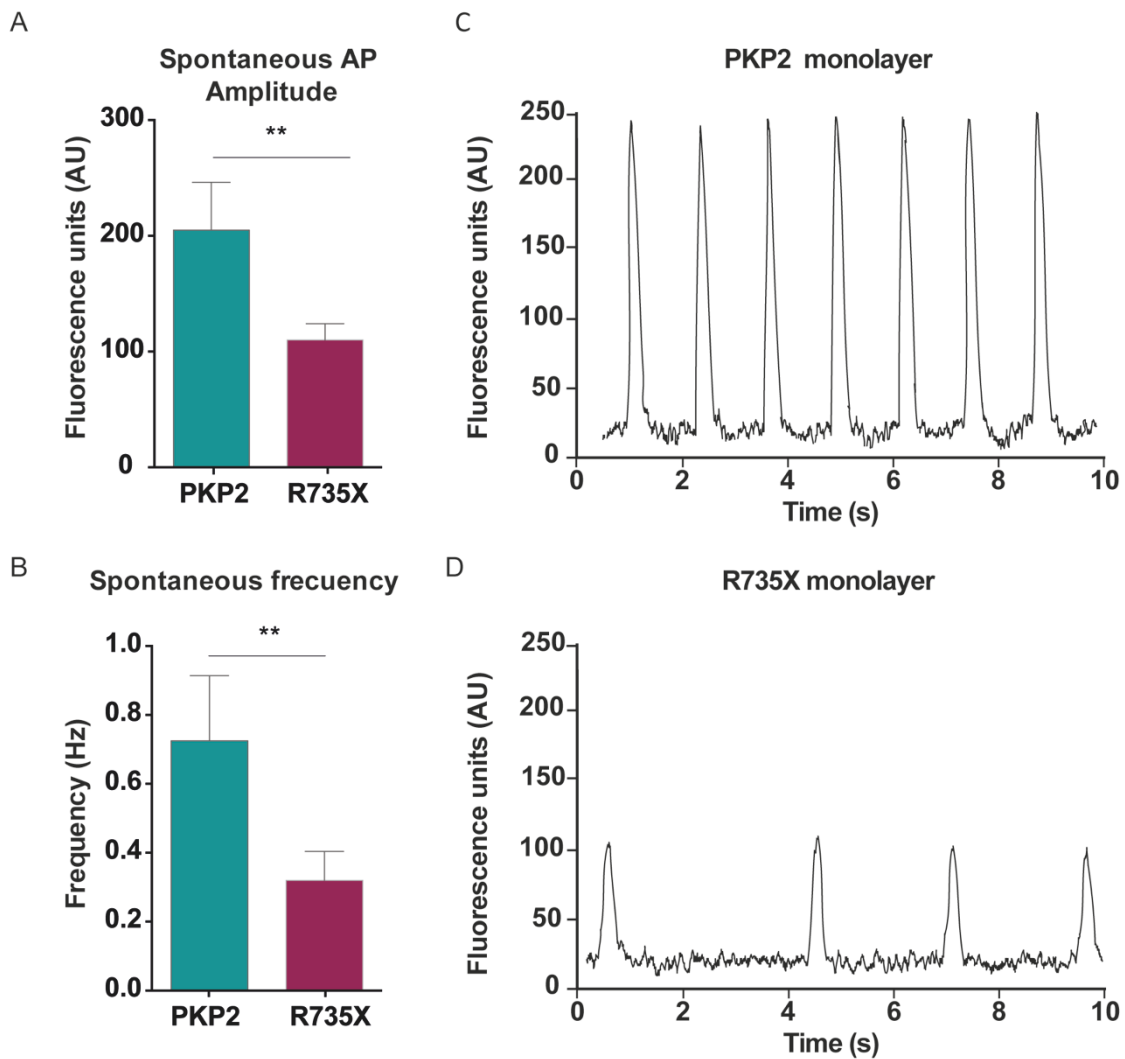


Figure 31. R735X monolayers exhibit arrhythmic activity. Spontaneous activity of PKP2 and R735X hiPSC-CMs recorded by optical mapping. A. Spontaneous AP amplitude. B. Spontaneous beating frequency. Data are represented as means \pm s.d. ****** $p < 0.01$ by Student's t-test. $N = 5$ for each group. C. Single pixel recordings from spontaneous activity of a PKP2 monolayer (upper panel) and a R735X monolayer (bottom panel).

Optical mapping allowed us to quantify the duration of the action potential that occurs in an image pixel (where several cells can be found) and the conduction velocity (CV) of the electrical impulse along the well. To compare these parameters between monolayers, we synchronized them by applying point stimulation in each monolayer using a custom made electrical pacing frame. PKP2 monolayers were able to follow a wider range of frequencies than R735X monolayers (Figure 32A). The amplitude of the action potential was higher in PKP2 monolayers than in mutant monolayers (PKP2 amplitude = 140.0 ± 7.07 AU and R735X amplitude = 100.0 ± 4.08 AU) (Figure 32B-D).

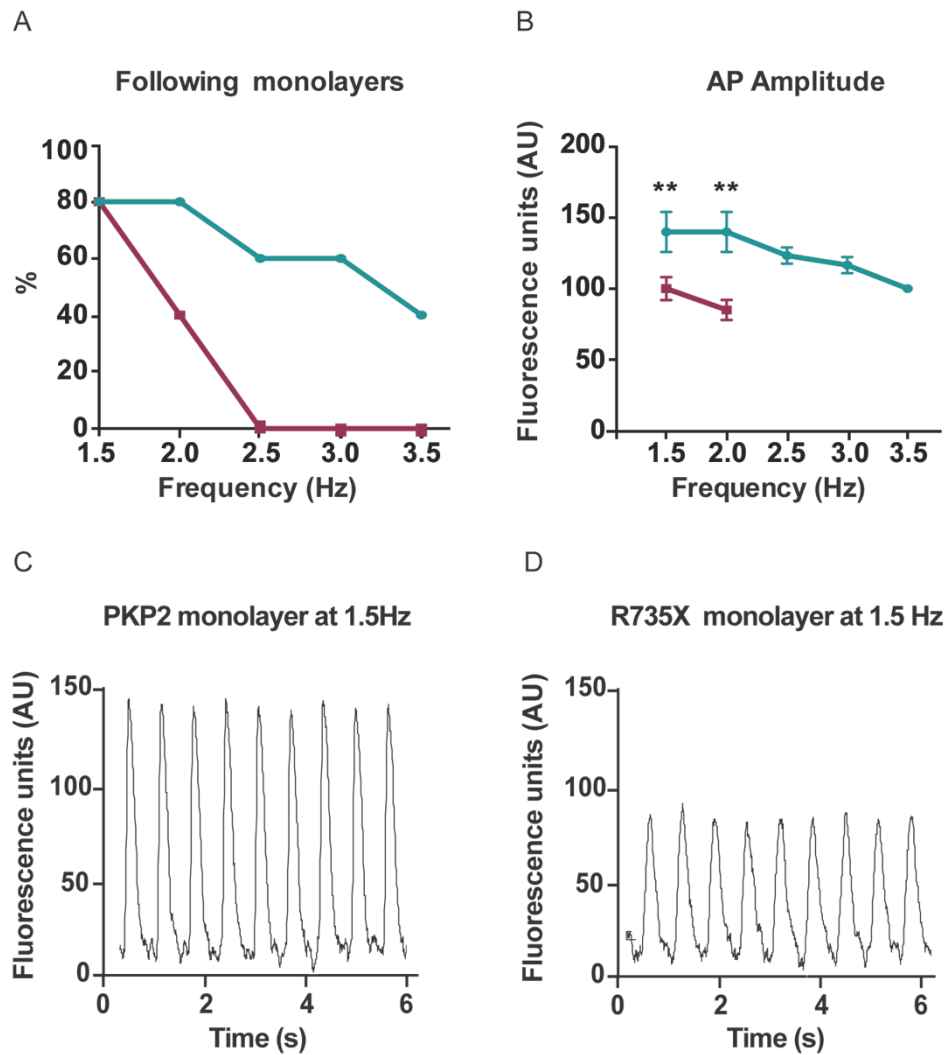


Figure 32. PKP2 monolayer follow a wider range of pacing frequencies. Optical mapping of PKP2 and R735X hiPSC-CMs paced at different frequencies. A. Percentage of monolayers that were able to follow the pacing at different frequencies. B. Quantification of AP amplitude at different frequencies. $**p < 0.01$ by Student's t-test. Data are represented as means \pm s.d. $N=4$ for each group at pacing=1.5Hz. $N=3$ for each group at pacing=2Hz. No R735X monolayer followed the pacing beyond 2Hz. C & D. Single pixel recordings from a PKP2 monolayer (right panel) and R735X monolayer (left panel) paced at 1.5Hz.

APD_{80} (action potential duration at 80% of repolarization) was 1.5 times longer in R735X monolayers than in PKP2 monolayers (PKP2 $APD_{80} = 267.5 \pm 4.78$ ms and R735X $APD_{80} = 407.5 \pm 4.78$ ms, monolayers paced at 1.5Hz) (Figure 33A). Pixel action potentials obtained from optical mapping have to predominant phases: depolarization and repolarization (Figure 33B). The ratio APD_{20}/APD_{90} (ratio between the APD at 20% of repolarization and the APD at 90% of repolarization) is an indirect measurement of the repolarization time. Quantification of APD_{20}/APD_{90} showed no differences between PKP2 and R735X monolayers (Figure 33C). However, quantification of the slope of the depolarization phase revealed that PKP2 monolayers depolarized two times faster than R735X monolayers (PKP2 slope= 3.44 ± 0.18 AU and R735X

slope = 6.18 ± 0.82 AU, monolayers paced at 1.5Hz) (Figure 33D). To measure the depolarization slope we normalized the amplitude of the AP of both groups. These results indicate that R735X leads to a prolongation of the action potential duration due to a slower depolarization phase. Thus, the observed decrease in the inward sodium current density is leading to a slow depolarization phase and, as a consequence, to a prolongation of the APD in paced R735X monolayers.

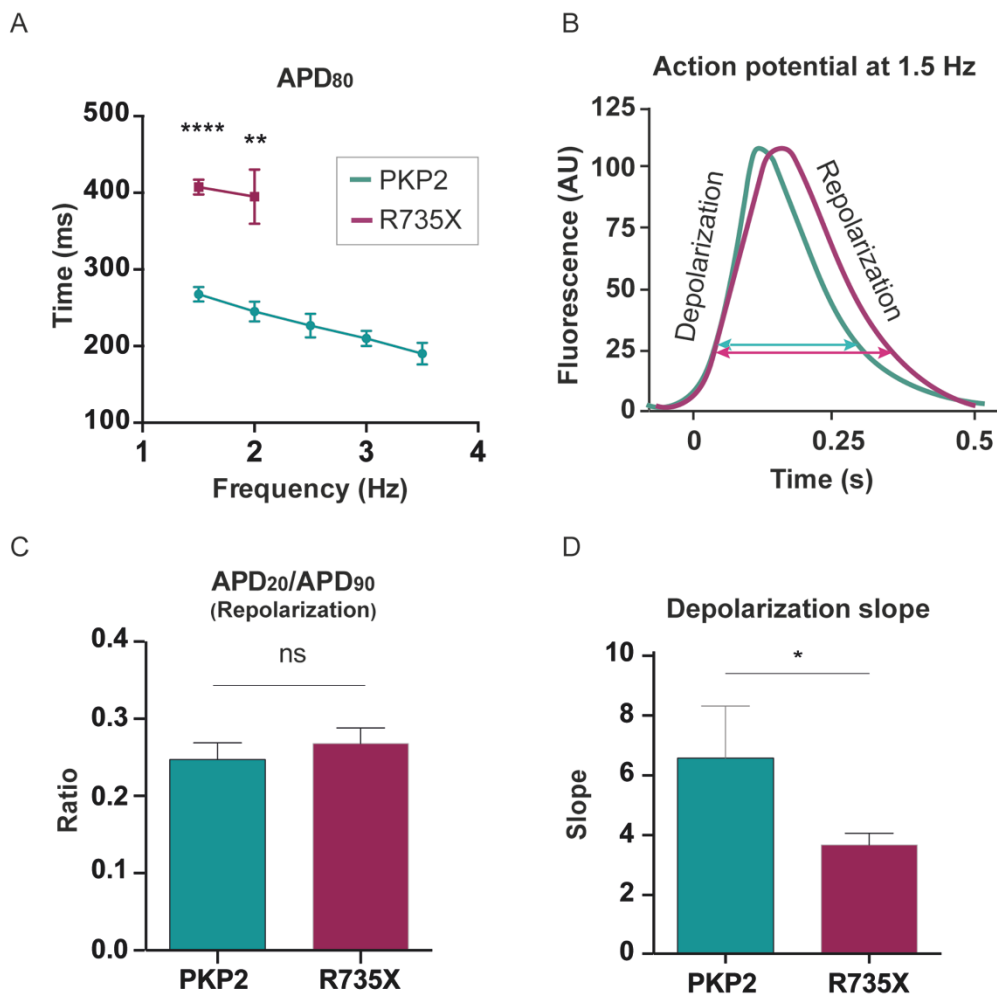


Figure 33. R735X monolayers showed an elongated APD. A. Quantification of action potential duration at 80% of repolarization (APD₈₀) at different frequencies. N=4 for each group at pacing = 1.5 Hz. N=3 for each group at pacing = 2 Hz. No R735X monolayer followed the pacing beyond 2Hz. B. Detail of an action potential of a PKP2 and R735X monolayer paced at 1.5Hz. Action potential lines have been escalated up to the same amplitude. Green (PKP2) and pink (R735X) solid arrows indicate AP width. Grey solid arrow indicates depolarization phase and grey dashed arrow indicates repolarization phase. C. Ratio between action potential duration at 20% of repolarization (APD₂₀) and action potential duration at 90% of repolarization (APD₉₀) at 1.5 Hz. N=4 for each group. D. Quantification of the depolarization slope at 1.5 Hz. N=4 for each group. Data are represented as means \pm s.d. ns $p > 0.05$, * $p < 0.05$, ** $p < 0.01$ and *** $p < 0.001$ by Student's t-test.

Analysis of the activation maps revealed how the impulse propagation is slower in R735X monolayers than in PKP2 monolayers (Figure 34A). In fact, conduction velocity (CV) was 3.6 times slower in R735X monolayers when compared with PKP2 monolayers (PKP2 CV = 9.25 ± 0.52 cm/s and R735X CV = 2.57 ± 0.09 cm/s, monolayers paced at 1.5Hz) (Figure 34B).

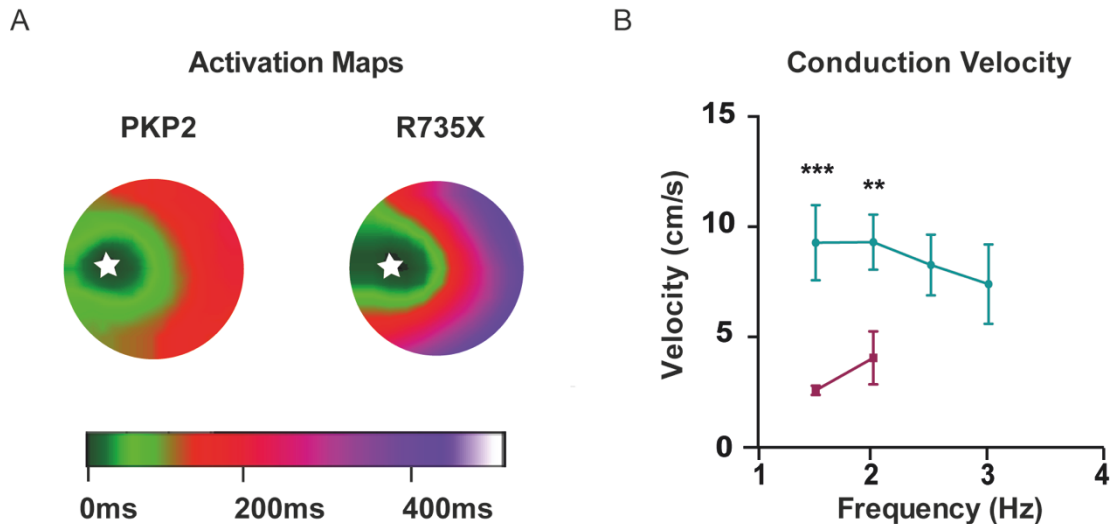


Figure 34. R735X monolayers showed a slower CV. A. Activation maps during 1.5 Hz pacing. Colors represent the time (milliseconds) the impulse takes from the pacemaker place (white star) to the rest of the well. B. Quantification of conduction velocities at different frequencies. N=4 for each group at pacing=1.5Hz. N=3 for each group at pacing = 2 Hz. No R735X monolayer followed the pacing beyond 2 Hz. Data are represented as means \pm s.d. ** $p < 0.01$ and *** $p < 0.001$ by Student's t-test.

Gap junctions are responsible for the electrical coupling of cardiomyocytes and thus, are a key element determining the conduction velocity of the electrical impulse through the cardiac cells. It has been shown that Cx43 (primary component of cardiac gap junctions) is another connexome element that may be disturbed by PKP2 mutations (Cruz et al., 2015) (Fidler et al., 2009) (Oxford et al., 2007). To investigate whether the decrease in the CV of R735X monolayer could be a consequence of a Cx43 defect, we performed immunofluorescence of Cx43 in hiPSC-CMs plated on PDMS-matrigel coated plates for 7 days. We used myosin heavy chain (MHC) immunostaining as a marker of cardiac sarcomeres. Cx43 immunostaining revealed that both the amount and the localization of Cx43 were not significantly different between PKP2 and R735X monolayers (Figure 35). Thus, we believe that the reduction in the conduction velocity exhibited in R735X monolayers is due to the observed impairment in the sodium current.

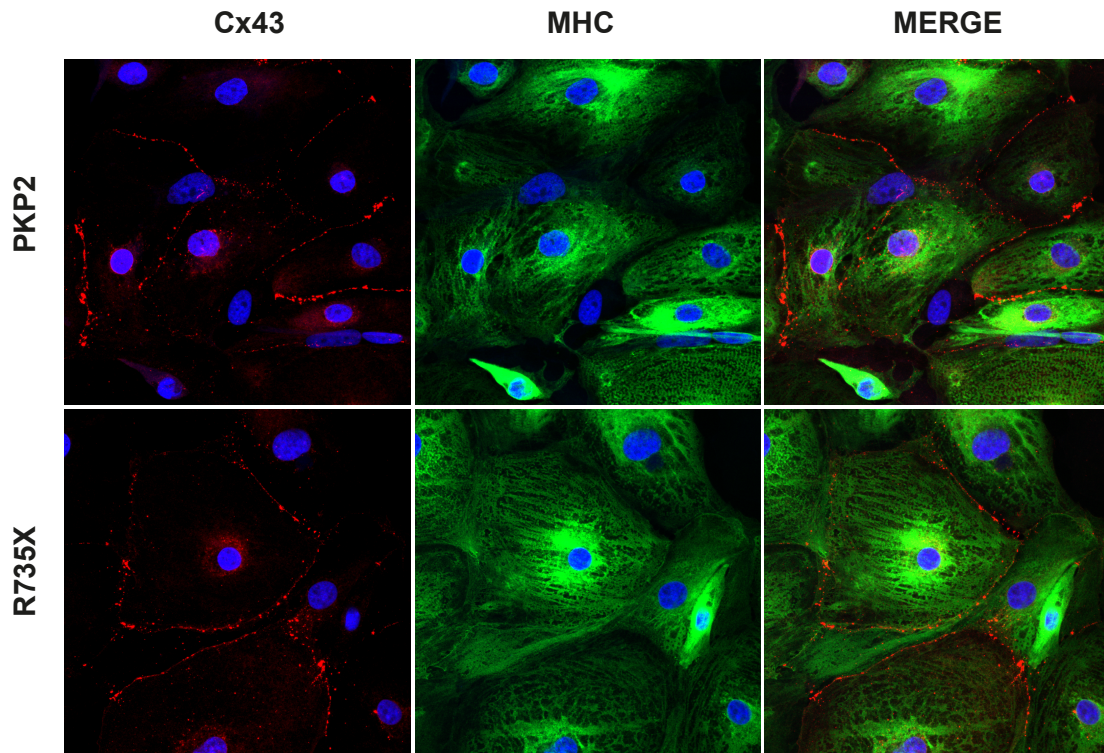


Figure 35. R735X does not alter localization or levels of Cx43 in hiPSC-CM monolayers. Immunofluorescence of Cx43 (red) and MHC (green) in PKP2 (upper panels) and R735X (bottom panels) hiPSC-CMs monolayers. Merge images are showed in left panels.

The study of the rhythmicity of transgenic monolayers also revealed that the increase of the pacing frequency exacerbates the arrhythmic activity in most of mutant monolayers (Figure 36A). Under high frequency pacing (2-3Hz), R735X monolayers underwent arrhythmic events such as intermittent blocks in cells excitation (Figure 36B). As a consequence of the prolongation of the APD, the external pacing is providing a stimulus above the threshold that elicits a second AP (Figure 36B, green star) when the first AP is still in the repolarization phase (the relative refractory period) (Figure 36B, red star). This event leads to an increase in the refractoriness of cells that blocks the cell excitation, impairing the external pacing to evoke a third AP (Figure 36B, orange star) and provoking an arrhythmic event. In addition, we could see multifocal arrhythmias in R735X monolayers. In that case, the endogenous pacemaker of the monolayer competes with the external pacemaker and gets control of the pacing. Most remarkably, the endogenous pacemaker changed its position during the recording time, leading to changes in the direction of the propagation of the impulse (Figure 36C-D). Also, we could find more than one endogenous pacemaker at the same monolayer triggering different waves that met at the same point (Figure 36E). Meanwhile, PKP2 monolayers showed rhythmic activity paired to immobile and unique pacemakers.

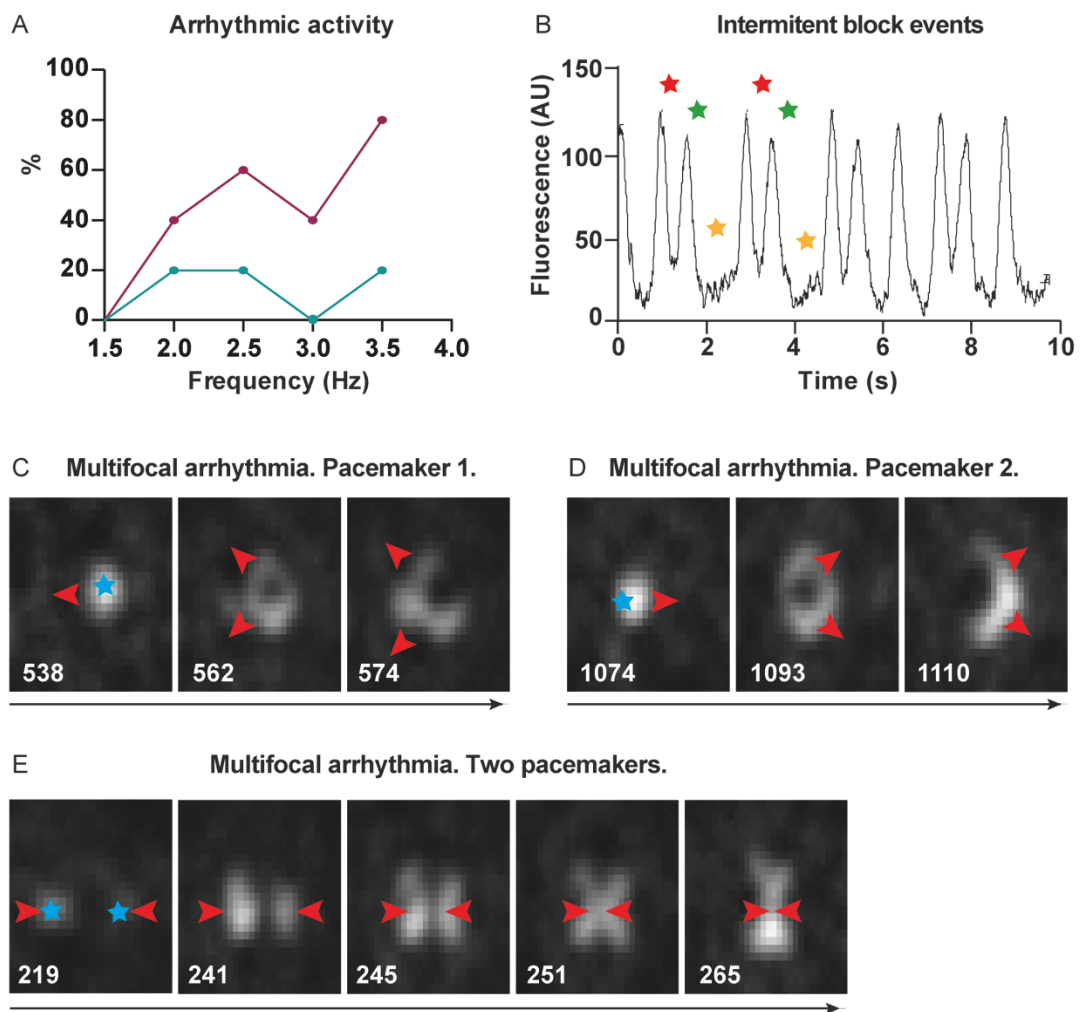


Figure 36. R735X leads to arrhythmic activity in hiPSC-CM monolayers. A. Percentage of monolayers showing arrhythmic activity at different frequencies. B. Example of R735X monolayers undergoing intermittent block events. Red, Green and orange stars indicate first, second and third-blocked AP respectively. C-D. Still frames of movies showing an example of endogenous pacemaker change of position in the same monolayer during the recorded time. E. Still frames of movies showing an example of two endogenous pacemakers at the same time. Red arrows indicate direction of the impulse propagation. Blue stars indicate endogenous pacemakers. Still frame number is indicated in white. Black arrows indicate the sequence of the movie.

In conclusion, optical mapping results indicate that the decrease of sodium current density in hiPSC-CMs reduce the excitability of the mutant monolayers by slowing the depolarization time and reducing the impulse conduction velocity. This phenomenon leads to arrhythmic electrical behavior, such as intermittent block and multifocal arrhythmia. Thus, this experiment highlights the arrhythmogenic effect of R735X in hiPSC-CMs and indicates that an impairment of the fast depolarizing sodium current could be leading to arrhythmias in AC patients harboring the R735X mutation.

DISCUSSION

DISCUSSION

Transgenic hiPSC-CMs platform to model arrhythmic diseases

While previous studies have derived patient specific hiPSC for the modeling of inherited arrhythmias (El-Battrawy et al., 2018) (Itzhaki et al., 2011), we applied a genetic background independent approach to investigate the effect of the R735X mutation. This experimental design avoids heterogeneity related to patient's polymorphisms and allowed us to work with isogenic hiPS cell lines. In the future, we could also compare the effects of the overexpression of different mutations over the same genetic background. Moreover, overexpressing the mutant version of a protein over a wild-type background would help us to distinguish between dominant negative or haploinsufficient related phenotypes. However, both approaches are interesting and complementary, and its combination would help to identify compensatory mechanisms or modulators of the disease.

Modeling inherited cardiac diseases in hiPSC-CMs presents a major concern: immaturity of cells (Goversen et al., 2018). Many strategies have been reported to improve maturity of hiPSC-CMs (Machiraju and Greenway, 2019). In this project, we have used the extracellular matrix mediated maturation method described by Herron et al. (2016) which consists in plating the cells over a soft surface made up of a matrigel-coated PDMS sheet. This system has proven to accelerate the maturation status of the electrophysiological features of hiPSC-CMs which is indispensable for modeling arrhythmic diseases (Herron et al., 2016).

Currently, there is a lack of use of hiPSC-CMs as a model for drug therapy. Among other mayor reasons, generating and studying patient's derived hiPSC-CMs is a very expensive and time-consuming technique (Knollmann, 2013). Here, we have carried out the proof of concept of a potential platform that could quickly generate hiPS cell lines that overexpress inherited arrhythmic disease-related mutations without having to perform skin biopsies, reprogramming of cells and characterization of patient derived hiPS cell lines. Such platform would allow for the study of the molecular mechanism underlying the arrhythmic disease while at the same time performing targeted drug therapy studies. Since the maturity status of hiPSC-CMs interferes in the drug compound responsiveness (da Rocha et al., 2017), the PDMS maturation that we have implemented on these cells may add value to this model as a drug testing platform.

R735X arrhythmogenic effect on hiPSC-CMs

The expression of R735X hiPSC-CMs leads to a consistent reduction (by 70%) in the sodium current density without altering $\text{Na}_v1.5$ channel electrical properties. These results suggest that the diminished I_{Na} is a direct consequence of a reduction in the number of $\text{Na}_v1.5$ channels located at the plasma membrane. In fact, cell surface biotinylation assay (data not shown) revealed a clear tendency of $\text{Na}_v1.5$ to be decreased at the plasma membrane of R735X hiPSC-CM. This phenomenon is significant and consistent in HEK293T and HL-1 cells expressing R735X.

As reported in other hiPSC-CM lines with defect in I_{Na} density (Ma et al., 2018) (Roche et al., 2019), such decrease would slow down cell depolarization. Indeed, analysis of pixel's APs obtained from 2D hiPSC-CMs optical mapping experiments showed that the depolarization phase was two times slower in R735X monolayers, leading to a prolongation of the APD and a reduction in conduction velocity. Optical mapping experiments also revealed that a decrease in I_{Na} leads to a reduction in cells excitability which manifest as spontaneous or paced arrhythmic activity. We observed that the increase of the pacing frequency exacerbates the arrhythmic behavior of mutant monolayers, showing arrhythmogenic events such as intermittent blocks and multifocal arrhythmias. With our data, we propose that the mutant R735X leads to a decrease in the sodium current generated by the voltage-gated sodium channel. This phenomenon decreases the excitability of the cardiomyocytes and consequently, slows down cell depolarization, action potential duration and conduction velocity of the electrical impulses through the cardiomyocytes. This would make the cardiomyocytes unable to follow higher pacing frequencies, which could lead to life-threatening arrhythmogenic events at early stages of AC patients.

To date, several studies have been trying to characterize AC hiPSC lines carrying different PKP2 mutations, but they have focus their investigation in the metabolic alterations –adipogenesis, lipid accumulation – that may happen during the disease (Ma et al., 2013)(Oren et al., 2013)(Kim et al., 2013). However, none of these papers have characterized the electrophysiological alterations that PKP2 mutation may cause in these hiPSC-CMs. One study has shown evidence of a decrease in the sodium current in hiPSC-CM from a AC patient carrying a mutation in PKP2. In this study, they used hESC and patient derived hiPSC-CM infected with the wild-type PKP2 as a control when recording sodium current densities (Cerrone et al., 2014). In contrast, we have compared R735X hiPSC-CMs patch-clamp recordings with the recordings obtained from both Control and PKP2 hiPSC-CM isogenic lines under the same experimental conditions, thereby

avoiding the heterogeneity intrinsic to cardiomyocytes coming from different cells types. It also has been reported that patch-clamp measurements could not be completely accurate given the challenge of proper voltage control resulting from the large cell size of hiPSC-CMs and their short survival during the experiment (Roche et al., 2019)(Cerrone et al., 2014). Patch-clamp data showed in this project are robust because we only included recordings where the voltage was systematically controlled as reflected in the Current-Voltage curves.

To date, there is one study where an AC patient derived hiPSC-CMs 2D monolayer electrical performance was measured. They generated hiPSC-CMs from a patient with the mutation A324fs335X in PKP2 and plated them on a MEA device (Multi Channel Systems MCS GmbH, 2019). They demonstrated a prolonged field potential rise time in the AC hiPSC-CMs (Caspi Oren et al., 2013) but they could not directly measure the excitability, the conduction velocity or identify arrhythmic events with this technique. Therefore, we are presenting for the first time a thorough study of the electrical performance of AC hiPSC-CM 2D monolayers.

AC and BrS: two different diseases?

Brugada syndrome (BrS) is a channelopathy that has been associated with mutations in *SCN5A* genes among others. A decrease in the sodium current in cardiomyocytes has been widely accepted as a hallmark of this syndrome. BrS patients typically presents with syncopal episodes and/or sudden death, a structurally normal heart and a distinctive ECG with a pattern of right bundle branch block with an ST segment elevation in leads V1 to V3 (Brugada et al., 2001). However, after the initial description of BrS, it has been suggested that this syndrome could share several clinical features with AC, implying that these could not be completely distinct diseases (Corrado et al., 2001). Indeed, the screening of 200 patients diagnosed with BrS, no symptoms of AC and no mutations in genes related with BrS (*SCN5A*, *CACNA1c*, *GPD1L* and *MOG1*) revealed that 5 of the patients had single amino acid substitutions in PKP2. They also showed that this BrS related PKP2 mutants lead to a significant reduction of the sodium current in HL-1 cells, when compared with cells transfected with wild-type PKP2 (Cerrone et al., 2014). Thus, in this project we have described an example of a PKP2 mutation identified in AC patients that could lead to BrS clinical manifestations at the early stages of the diseases.

R735X molecular mechanism?

PKP2 integrates into the desmosomal complex at the inner face of the plasma membrane (Godsel et al., 2004). It has been previously described that early truncated mutant versions of PKP2 such as R79X and 179fs proteins fail to localize at the cell borders and are detected at the intracellular space (Joshi-Mukherjee et al., 2008). However, these are very early truncates resulting in less than 30kDa proteins, and may not be representative of the subcellular distribution of larger truncates. In this thesis, we have described that R735X -a PKP2 truncated protein of ~65kDa- is primarily found diffusely at the intracellular space of cells and is only found in some discontinuous spots at cell borders. Thus, we provide an example of the subcellular mislocalization of a larger PKP2 truncated protein, which could have a consequence in the sodium channel function.

Data obtained from FRAP assay of PKP2 proteins tagged with EGFP indicates that EGFP-R735X mobility at the cell-cell contacts is higher than EGFP-PKP2 mobility. Although, their mobile fraction after 120 seconds of bleaching is similar, EGFP-R735X is able to recover half of the final fluorescence 2.5 times faster. Mobile fraction can be composed of free diffusing proteins or transiently immobile proteins that interact in a steady-state with immobile partners (Houtsmuller, 2005). Free diffusing proteins contribute to a fast recovery of the signal and transiently immobile proteins contribute to a slow and more linear recovery of the signal. Therefore, EGFP-R735X recovery kinetics would suggest that the recovery is mostly due to diffusion of mobile molecules along the ROI of stimulation. Meanwhile, EGFP-PKP2 kinetics of recovery has a stronger lineal component which would suggest that the recovery is partially due to redistribution of mobile molecules but also due to the movement of transiently immobile molecules that are being released. FRAP experiments would indicate that PKP2 protein is less mobile because it is interacting with its partners and is being integrated into superior complexes, while the lack of the C-terminal in R735X protein would be avoiding these interactions and impairing its integration into macromolecular structures.

Our data shows that R735X does not disrupt PKP2 localization or mobility pattern, as have been described for other PKP2 mutants (Sato et al., 2009). In fact, the desmosomal structures in the R735X mouse model were not affected when analyzed by transmission electron microscopy and immunofluorescence (Cruz et al., 2015). Moreover, post mortem biopsy of AC patients with mutations in *PKP2* gene showed normal immunoreactive signals for PKP2 (Noorman et al., 2013). Thus, localization and mobility data shows that R735X do not have a direct dominant

negative effect over PKP2, which suggest that R735X may be playing a new role in the cardiomyocyte physiology.

Here we have shown that R735X decreases the amount of exogenous Na_v1.5 located on the plasma membrane of HEK293 and HL-1 cells transiently expressing PKP2 or R735X proteins. Cell surface biotinylation assay also showed that R735X decreases levels of endogenous Na_v1.5 proteins in HL-1 cells and in hiPSC-CMs stably expressing R735X. It has been described that PKP2 and Na_v1.5 co-exist at the same molecular complex since both proteins co-precipitate together in heart lysates and their immunoreactive signals co-localize on the cell borders of isolated adult cardiomyocytes (Sato et al., 2009). However, we observed that tdTomato-R735X failed to co-localize with EGFP-Na_v1.5 in most of the cell border regions, and we did not detect a change in Na_v1.5 mobility pattern in HL-1 cells expressing R735X. Altogether, our data indicates that the effect of R735X on voltage-gated sodium channels is not happening at the plasma membrane level. Nonetheless, we have observed that R735X and Na_v1.5 are able to co-precipitate together. Therefore, we believe that the interaction between R735X and the sodium channel must be taken place away from the cell border, in the intracellular space. Thus, we could hypothesize that this interaction could be affecting the life cycle of the sodium channel protein, which opens up a new filed of investigation.

We have observed that Na_v1.5 levels of total membrane fractions (including plasma membrane, Golgi, ER and mitochondria) from HEK293 cells and Na_v1.5 levels of total protein samples from HL-1 stable cell lines did not differ between cells expressing PKP2 or R735X. However, isolated proteins from the plasma membrane fraction and cell surface proteins showed a significant reduction of Na_v1.5. The data would indicate that R735X is not having a transcriptional or translational effect on Na_v1.5 in these systems, but suggest that R735X could be impairing the proper trafficking of the channel to their appropriate plasma membrane subdomain.

The canonical anterograde Na_v1.5 trafficking has been described as an active transport of Na_v1.5 containing vesicles from the ER/Golgi apparatus through the cell along microtubule tracks (Mercier et al., 2017). Indeed, enhanced tubulin polymerization by the anticancer agent Taxol (TXL) have been shown to decrease Na_v1.5 membrane expression, leading to a two-fold reduction in I_{Na} amplitude, as well as modifying its gating properties. Targeting cardiac Na_v1.5 to specific membrane areas, such as the intercalated disc, involves the anchoring protein Ankyring-G and interacting proteins such as SAP97, N-cadherin and connexin 43, as well as plakophilin-2

and desmoglein-2 (Makara et al., 2014) (S everine et al., 2011) (Malhotra et al., 2004) (Rhatt et al., 2012) (Sato et al., 2009) (Rizzo et al., 2012). At the lateral membrane of cardiomyocytes, $\text{Na}_v1.5$ targeting depends on different macromolecular complexes related to syntrophin/dystrophin expression (Gavillet et al. 2006; Petitprez et al. 2011). In fact, Cerrone et al. showed that PKP2 deficiency led to increased distance between EB-1 clusters (as a marker of microtubules plus-ends), and the N-cadherin plaque midline. This finding indicates that PKP2 haploinsufficiency (directly or indirectly) affects the ability of microtubules to reach the intercalated disc, which could impair delivery of proteins relevant for sodium channel function (Cerrone et al., 2014). How R735X could affect $\text{Na}_v1.5$ trafficking via microtubule or microtubule related proteins needs to be further investigated. On the other hand, it has been recently published that a common early anterograde trafficking mechanism is involved in the transport of $\text{Na}_v1.5$ and Kir2.1 channels to the plasma membrane (Ponce-Balbuena et al., 2018). However, we observed no differences in I_{K1} current density in the I_{Na} deficient R735X hiPSC-CMs. It has been postulated that several pools of $\text{Na}_v1.5$ channels exists and that they are able to reach the plasma membrane from different origins (Golgi apparatus, unconventional Golgi pathway or storage pools)(Mercier et al., 2015). Therefore, if R735X would be interfering in $\text{Na}_v1.5$ trafficking pathway it seems likely to be affecting a different pool of channels that do not associate with Kir2.1 during their trafficking.

In a parallel project developed in our lab, we have observed that HL-1 cells stably expressing R735X have a defect in actin cytoskeleton organization. Concretely, actin microfilaments do not organize above the nucleus of R735X cells as it happens in PKP2 cells, and the ratio F-actin (filamentous) /G-actin (globular, monomeric) is lower in R735X cells (Marquez-Lopez et al. 2019, submitted). To date, several studies have highlighted the importance of the cytoskeleton in the regulation and functioning of the voltage-dependent Na^+ channel. It has been showed that treatment of rat and rabbit ventricular cardiomyocytes with cytochalasin-D (Cyto-D), an agent that interferes with actin polymerization, reduced whole cell peak Na^+ current by 20% (Undrovinas et al., 1995). Cyto-D and gelsolin (used to disrupt the actin cytoskeleton) abolished the perfusion-induced increase in Na^+ current of human jejunal circular smooth muscle cells (Strege et al., 2003). Altogether, such data could suggest that actin disorganization in R735X might be modulating $\text{Na}_v1.5$.

Besides its structural role, PKP2 has been pointed out to participate in different signaling pathways (Bass-Zubek et al., 2009). Its has been suggested that PKP2 may functionally link RhoA-

dependent pathways to drive actin reorganization and regulate DP–IFs interactions required for normal desmosome assembly (Godsel et al., 2010). Moreover, PKP2 has been proposed to serve as a scaffold that recruits PKC (protein kinase C) locally to control the proper assembly and behavior of DP precursors to translocate to nascent desmosomes and properly organize IFs. It has been shown that the absence of PKP2 is accompanied by increased phosphorylation of PKC substrates. Therefore, it has been proposed that, in PKP2 KO cells, PKC would be no longer recruited at DP complexes and would be free to phosphorylate other substrates (Bass-Zubek et al., 2008). On the other hand, Na_v1.5 is integrated into a macromolecular complex interacting with partner proteins that modulate its expression levels, localization, and gating. Such protein complex is the target of extensive post-translational modifications that modulates all these properties. Among many others, PKC phosphorylation of S1503 (human) in the Na_v1.5 III–IV inactivation loop has been described as a modulatory element of the sodium current (Qu, 1996) (Valdivia et al., 2009). PKC activity decreases cardiac I_{Na} in chinese hamster lung cells and in neonatal rat cardiomyocytes (Qu et al., 1994). In some systems, PKC effect on I_{Na} has been related to a decrease in the number of functional channels at the membrane. Hallaq H. et al. (2012) has demonstrated that PKC activation regulates the intracellular distribution of the cardiac Na⁺ channels by preferentially trafficking away Na_v1.5 from the plasma membrane in HEK293 cells (Hallaq et al., 2012). We have demonstrate that R735X co-precipitates with Na_v1.5, likely at the intracellular space, and Bass-Zubek et al. (2008) have shown that PKP2 interacts with PKC by its N-terminal region (Bass-Zubek et al., 2008). Thus, we could hypothesize that R735X may act as an alternative scaffold to PCK, delocalizing and altering PKC activity. As a consequence, PCK-dependent Na_v1.5 phosphorylation could be altered, leading to a decrease in Na_v1.5 at the membrane. To test whether R735X could be trafficking away Na_v1.5 from the plasma membrane and decreasing I_{Na} through PKC, the simplest experiment would be to co-transfect HEK293 cells with SCN5A-S1503A (a PKC resistant mutant) and R735X, and analyze if the amount of Na_v1.5 at the plasma membrane is restored.

In conclusion, we present a hiPSC-CM model of AC with a significant potential in the field of cardiac arrhythmias. We believe this model opens up new possibilities for the study of different mutation-dependent mechanisms and for the testing of new therapies. Moreover, in this thesis project we have provided evidences of the negative effect of the PKP2 AC patient-related mutation R735X over the voltage-gated sodium channel performance and how that could be responsible for the life-threatening arrhythmias during the concealed phase of AC patients.

CONCLUSIONS

CONCLUSIONS

1. The truncated version of Plakophilin-2 (PKP2) protein (R735X) loses its localization at the cell borders, and is mainly found in the cytoplasm, but does not affect the localization of PKP2 protein.
2. R735X protein has a different mobility pattern than PKP2 protein at the plasma membrane, but does not affect PKP2 protein mobility.
3. R735X protein leads to a decrease of $\text{Na}_v1.5$ at the plasma membrane in HEK293T cells as well as in HL-1 cells.
4. Co-localization of R735X with $\text{Na}_v1.5$ is mostly impaired at the plasma membrane of HL-1 cells but they are able to co-precipitate together.
5. R735X protein does not alter $\text{Na}_v1.5$ mobility at the plasma membrane of HL-1 cells.
6. R735X protein leads to a significant decrease in sodium currents in human pluripotent stem cell derived cardiomyocytes (hiPSC-CMs). However, calcium and inward-rectifier potassium currents are not affected in R735X hiPSC-CMs.
7. R735X protein causes an increase in action potential duration by slowing down the depolarization time in hiPSC-CM monolayers, but does not alter their repolarization time. R735X protein leads to a reduction of the conduction velocity in hiPSC-CM monolayers.
8. hiPSC-CM monolayers expressing R735X protein have spontaneous arrhythmic activity, and high frequency pacing exacerbates this arrhythmogenic activity.

CONCLUSIONES

CONCLUSIONES

1. La versión truncada de la proteína Placofilina-2 (proteína R735X) pierde su localización en los bordes de la célula, y se encuentra principalmente en el citoplasma, pero no afecta a la localización de Placofilina-2 (PKP2).
2. La proteína R735X tiene un patrón de movilidad diferente al de la proteína PKP2 en la membrana plasmática, pero no afecta a la movilidad de la proteína PKP2.
3. La proteína R735X provoca la disminución de $\text{Na}_v1.5$ en la membrana plasmática tanto en células HEK293T como en células HL-1.
4. La proteína R735X no co-localiza con $\text{Na}_v1.5$ en la membrana plasmática de células HL-1 pero ambas proteínas son capaces de co-precipitar juntas.
5. La proteína R735X no altera la movilidad de $\text{Na}_v1.5$ en la membrana plasmática de células HL-1.
6. La proteína R735X provoca una reducción significativa en la corriente de sodio en cardiomiocitos derivados de células madre humanas pluripotentes inducidas (del inglés, hiPSC-CMs). Sin embargo, la corriente de calcio y la corriente rectificadora de potasio no están afectadas en hiPSC-CMs mutantes.
7. La proteína R735X causa un incremento de la duración del potencial de acción, prolongando la fase de despolarización sin alterar el tiempo de repolarización. La proteína R735X provoca la disminución de la velocidad de conducción en monocapas de hiPSC-CM.
8. Las monocapas de hiPSC-CMs que expresan la mutación R735X presentan actividad arrítmica de forma espontánea, y el incremento de la frecuencia del marcapasos exacerba dicha actividad arrítmica.

BIBLIOGRAPHY

BIBLIOGRAPHY

Agullo-Pascual, E., Cerrone, M., Delmar, M., 2014. Arrhythmogenic Cardiomyopathy and Brugada Syndrome: Diseases of the connexome. *FEBS Lett* 588, 1322–1330. <https://doi.org/10.1016/j.febslet.2014.02.008>

Alcalde, M., Campuzano, O., Berne, P., García-Pavía, P., Doltra, A., Arbelo, E., Sarquella-Brugada, G., Iglesias, A., Alonso-Pulpon, L., Brugada, J., Brugada, R., 2014. Stop-gain mutations in PKP2 are associated with a later age of onset of arrhythmogenic right ventricular cardiomyopathy. *PLoS ONE* 9, e100560. <https://doi.org/10.1371/journal.pone.0100560>

Allan Bradley, J.C., 2007. Generation of an inducible and optimized piggyBac transposon system. *Nucleic Acids Res.* 35(12): e87. <https://doi.org/10.1093/nar/gkm446>

Bao Jingru, Wang Jizheng, Yao Yan, Wang Yilu, Fan Xiaohan, Sun Kai, He Ding Sheng, Marcus Frank I., Zhang Shu, Hui Rutai, Song Lei, 2013. Correlation of Ventricular Arrhythmias With Genotype in Arrhythmogenic Right Ventricular Cardiomyopathy. *Circulation: Cardiovascular Genetics* 6, 552–556. <https://doi.org/10.1161/CIRCGENETICS.113.000122>

Bass-Zubek, A.E., Godsel, L.M., Delmar, M., Green, K.J., 2009. Plakophilins: multifunctional scaffolds for adhesion and signaling. *Curr Opin Cell Biol* 21, 708–716. <https://doi.org/10.1016/j.ceb.2009.07.002>

Bass-Zubek, A.E., Hobbs, R.P., Amargo, E.V., Garcia, N.J., Hsieh, S.N., Chen, X., Wahl, J.K., Denning, M.F., Green, K.J., 2008. Plakophilin 2: a critical scaffold for PKC α that regulates intercellular junction assembly. *The Journal of Cell Biology* 181, 605–613. <https://doi.org/10.1083/jcb.200712133>

Beckmann, B.-M., Pfeufer, A., Kääb, S., 2011. Inherited Cardiac Arrhythmias. *Dtsch Arztebl Int* 108, 623–634. <https://doi.org/10.3238/arztebl.2011.0623>

Biggs, D.S.C., 2010. 3D Deconvolution Microscopy. *Current Protocols in Cytometry* 52, 12.19.1–12.19.20. <https://doi.org/10.1002/0471142956.cy1219s52>

Brugada, J., Brugada, P., Brugada, R., 2001. Brugada Syndrome: The Syndrome of Right Bundle Branch Block, ST segment Elevation in V1 to V3 and Sudden Death. *Indian Pacing Electrophysiol J* 1, 6–11.

Cerrone, M., Lin, X., Zhang, M., Agullo-Pascual, E., Pfenniger, A., Guský, H.C., Novelli, V., Kim, C., Tirasawasdichai, T., Judge, D.P., Rothenberg, E., Chen, H.-S.V., Napolitano, C., Priori, S., Delmar, M., 2014. Missense Mutations in Plakophilin-2 Cause Sodium Current Deficit and Associate with a Brugada Syndrome Phenotype. *Circulation* 129, 1092–1103. <https://doi.org/10.1161/CIRCULATIONAHA.113.003077>

Cerrone, M., Noorman, M., Lin, X., Chkourko, H., Liang, F.-X., van der Nagel, R., Hund, T., Birchmeier, W., Mohler, P., van Veen, T.A., van Rijen, H.V., Delmar, M., 2012. Sodium current deficit and arrhythmogenesis in a murine model of plakophilin-2 haploinsufficiency. *Cardiovasc. Res.* 95, 460–468. <https://doi.org/10.1093/cvr/cvs218>

Clatot, J., Ziyadeh-Isleem, A., Maugenre, S., Denjoy, I., Liu, H., Dilanian, G., Hatem, S.N., Deschênes, I., Coulombe, A., Guicheney, P., Neyroud, N., 2012. Dominant-negative effect of SCN5A N-terminal mutations through the interaction of Nav1.5 α -subunits. *Cardiovasc Res* 96, 53–63. <https://doi.org/10.1093/cvr/cvs211>

Claycomb, W.C., Lanson, N.A., Stallworth, B.S., Egeland, D.B., Delcarpio, J.B., Bahinski, A., Izzo, N.J., 1998. HL-1 cells: A cardiac muscle cell line that contracts and retains phenotypic characteristics of the adult cardiomyocyte. *Proc Natl Acad Sci U S A* 95, 2979–2984. <https://doi.org/10.1073/pnas.95.6.2979>

Corrado, D., Basso, C., Buja, G., Nava, A., Rossi, L., Thiene, G., 2001. Right Bundle Branch Block, Right Precordial ST-Segment Elevation, and Sudden Death in Young People. *Circulation* 103, 710–717. <https://doi.org/10.1161/01.CIR.103.5.710>

Cox, M., van der Zwaag, P.A., Hauer, R.N.W., 2011. Arrhythmogenic Right Ventricular Dysplasia/Cardiomyopathy. *Circulation* 123, 11. <https://doi.org/10.1161/CIRCULATIONAHA.110.988287>

Cruz, F.M., Sanz-Rosa, D., Roche-Molina, M., García-Prieto, J., García-Ruiz, J.M., Pizarro, G., Jiménez-Borreguero, L.J., Torres, M., Bernad, A., Ruíz-Cabello, J., Fuster, V., Ibáñez, B., Bernal, J.A., 2015. Exercise triggers ARVC phenotype in mice expressing a disease-causing mutated version of human plakophilin-2. *J. Am. Coll. Cardiol.* 65, 1438–1450. <https://doi.org/10.1016/j.jacc.2015.01.045>

da Rocha, A.M., Campbell, K., Mironov, S., Jiang, J., Mundada, L., Guerrero-Serna, G., Jalife, J., Herron, T.J., 2017. hiPSC-CM Monolayer Maturation State Determines Drug Responsiveness in High Throughput Pro-Arrhythmia Screen. *Scientific Reports* 7. <https://doi.org/10.1038/s41598-017-13590-y>

El-Battrawy, I., Zhao, Z., Lan, H., Cyganek, L., Tombers, C., Li, X., Buljubasic, F., Lang, S., Tiburcy, M., Zimmermann, W.-H., Utikal, J., Wieland, T., Borggrefe, M., Zhou, X.-B., Akin, I., 2018. Electrical dysfunctions in human-induced pluripotent stem cell-derived cardiomyocytes from a patient with an arrhythmogenic right ventricular cardiomyopathy. *Europace* 20, f46–f56. <https://doi.org/10.1093/europace/euy042>

Fidler, L.M., Wilson, G.J., Liu, F., Cui, X., Scherer, S.W., Taylor, G.P., Hamilton, R.M., 2009. Abnormal connexin43 in arrhythmogenic right ventricular cardiomyopathy caused by plakophilin-2 mutations. *J Cell Mol Med* 13, 4219–4228. <https://doi.org/10.1111/j.1582-4934.2008.00438.x>

Fressart, V., Duthoit, G., Donal, E., Probst, V., Deharo, J.-C., Chevalier, P., Klug, D., Dubourg, O., Delacretaz, E., Cosnay, P., Scanu, P., Extramiana, F., Keller, D., Hidden-Lucet, F., Simon, F., Bessirard, V., Roux-Buisson, N., Hebert, J.-L., Azarine, A., Casset-Senon, D., Rouzet, F., Lecarpentier, Y., Fontaine, G., Coirault, C., Frank, R., Hainque, B., Charron, P., 2010. Desmosomal gene analysis in arrhythmogenic right ventricular dysplasia/cardiomyopathy: spectrum of mutations and clinical impact in practice. *Europace* 12, 861–868. <https://doi.org/10.1093/europace/euq104>

Gandjbakhch, E., Redheuil, A., Pousset, F., Charron, P., Frank, R., 2018. Clinical Diagnosis, Imaging, and Genetics of Arrhythmogenic Right Ventricular Cardiomyopathy/Dysplasia: JACC State-of-the-Art Review. *J. Am. Coll. Cardiol.* 72, 784–804. <https://doi.org/10.1016/j.jacc.2018.05.065>

Gerull, B., Heuser, A., Wichter, T., Paul, M., Basson, C.T., McDermott, D.A., Lerman, B.B., Markowitz, S.M., Ellinor, P.T., MacRae, C.A., Peters, S., Grossmann, K.S., Michely, B., Sasse-Klaassen, S., Birchmeier, W., Dietz, R., Breithardt, G., Schulze-Bahr, E., Thierfelder, L., 2004. Mutations in the desmosomal protein plakophilin-2 are common in arrhythmogenic right ventricular cardiomyopathy. *Nature Genetics* 36, 1162. <https://doi.org/10.1038/ng1461>

Godsel, L.M., Dubash, A.D., Bass-Zubek, A.E., Amargo, E.V., Klessner, J.L., Hobbs, R.P., Chen, X., Green, K.J., 2010. Plakophilin 2 couples actomyosin remodeling to desmosomal plaque assembly via RhoA. *Mol. Biol. Cell* 21, 2844–2859. <https://doi.org/10.1091/mbc.E10-02-0131>

Godsel, L.M., Getsios, S., Huen, A.C., Green, K.J., 2004. The Molecular Composition and Function of Desmosomes. *Cell Adhesion* 165, 137–193. https://doi.org/10.1007/978-3-540-68170-0_6

Goversen, B., van der Heyden, M.A.G., van Veen, T.A.B., de Boer, T.P., 2018. The immature electrophysiological phenotype of iPSC-CMs still hampers in vitro drug screening: Special focus on IK1. *Pharmacology & Therapeutics* 183, 127–136. <https://doi.org/10.1016/j.pharmthera.2017.10.001>

Grant, A.O., 2009. Cardiac Ion Channels. *Circulation: Arrhythmia and Electrophysiology* 2, 185–194. <https://doi.org/10.1161/CIRCEP.108.789081>

Gray, B., Behr, E.R., 2016. New Insights Into the Genetic Basis of Inherited Arrhythmia Syndromes. *Circulation: Cardiovascular Genetics* 9, 569–577. <https://doi.org/10.1161/CIRCGENETICS.116.001571>

Groeneweg, J.A., Aditya, B., Cynthia A., J., Anneline S., te R., Dennis, D., Crystal, T., Brittney, M., Ans C.P., W., Abhishek C., S., Bina, K., Douwe E., A., Paul G., V., M., de G.N., Karin, de B., L., Z.S., R., K.I., F., van der H.J., D., R.S., Maarten, J.C., J., T.R., A., D.P., A., van V.T., Harikrishna, T., A., W.A., P., J.D., Peter, van T.J., N., H.R., Hugh, C., 2015. Clinical Presentation, Long-Term Follow-Up, and Outcomes of 1001 Arrhythmogenic Right Ventricular Dysplasia/Cardiomyopathy Patients and Family Members. *Circulation: Cardiovascular Genetics* 8, 437–446. <https://doi.org/10.1161/CIRCGENETICS.114.001003>

Hallaq, H., Wang, D.W., Kunic, J.D., George, A.L., Wells, K.S., Murray, K.T., 2012. Activation of protein kinase C alters the intracellular distribution and mobility of cardiac Na⁺ channels. *American Journal of Physiology-Heart and Circulatory Physiology* 302, H782–H789. <https://doi.org/10.1152/ajpheart.00817.2010>

Haugaa, K.H., Haland, T.F., Leren, I.S., Saberniak, J., Edvardsen, T., 2016. Arrhythmogenic right ventricular cardiomyopathy, clinical manifestations, and diagnosis. *Europace* 18, 965–972. <https://doi.org/10.1093/europace/euv340>

Herron, T.J., Rocha, A.M.D., Campbell, K.F., Ponce-Balbuena, D., Willis, B.C., Guerrero-Serna, G., Liu, Q., Klos, M., Musa, H., Zarzoso, M., Bizy, A., Furness, J., Anumonwo, J., Mironov, S., Jalife, J., 2016. Extracellular Matrix–Mediated Maturation of Human Pluripotent Stem Cell–Derived Cardiac Monolayer Structure and Electrophysiological Function. *Circulation: Arrhythmia and Electrophysiology* 9. <https://doi.org/10.1161/CIRCEP.113.003638>

Houtsmuller, A.B., 2005. Fluorescence Recovery after Photobleaching: Application to Nuclear Proteins, in: Rietdorf, J. (Ed.), *Microscopy Techniques*. Springer Berlin Heidelberg, Berlin, Heidelberg, pp. 177–199. <https://doi.org/10.1007/b102214>

Idris, A., Shah, S.R., Park, K., 2018. Right ventricular dysplasia: management and treatment in light of current evidence. *Journal of Community Hospital Internal Medicine Perspectives* 8, 101–106. <https://doi.org/10.1080/20009666.2018.1472513>

Itzhaki, I., Maizels, L., Huber, I., Zwi-Dantsis, L., Caspi, O., Winterstern, A., Feldman, O., Gepstein, A., Arbel, G., Hammerman, H., Boulos, M., Gepstein, L., 2011. Modelling the long QT syndrome with induced pluripotent stem cells. *Nature* 471, 225–229. <https://doi.org/10.1038/nature09747>

Joshi-Mukherjee, R., Coombs, W., Musa, H., Oxford, E., Taffet, S., Delmar, M., 2008. Characterization of the molecular phenotype of two arrhythmogenic right ventricular cardiomyopathy (ARVC)-related plakophilin-2 (PKP2) mutations. *Heart Rhythm* 5, 1715–1723. <https://doi.org/10.1016/j.hrthm.2008.09.009>

Kaese, S., Verheule, S., 2012. Cardiac electrophysiology in mice: a matter of size. *Front Physiol* 3. <https://doi.org/10.3389/fphys.2012.00345>

Kim, C., Wong, J., Wen, J., Wang, S., Wang, C., Spiering, S., Kan, N.G., Forcales, S., Puri, P.L., Leone, T.C., Marine, J.E., Calkins, H., Kelly, D.P., Judge, D.P., Chen, H.-S.V., 2013. Studying arrhythmogenic right ventricular dysplasia with patient-specific iPSCs. *Nature* 494, 105–110. <https://doi.org/10.1038/nature11799>

Kim, S.-I., Ocegüera-Yanez, F., Sakurai, C., Nakagawa, M., Yamanaka, S., Woltjen, K., 2016. Inducible Transgene Expression in Human iPS Cells Using Versatile All-in-One piggyBac Transposons. *Methods Mol. Biol.* 1357, 111–131. https://doi.org/10.1007/7651_2015_251

Knollmann, B.C., 2013. Induced pluripotent stem cell-derived cardiomyocytes: boutique science or valuable arrhythmia model? *Circ. Res.* 112, 969–976; discussion 976. <https://doi.org/10.1161/CIRCRESAHA.112.300567>

Lian, X., Hsiao, C., Wilson, G., Zhu, K., Hazeltine, L.B., Azarin, S.M., Raval, K.K., Zhang, J., Kamp, T.J., Palecek, S.P., 2012. Robust cardiomyocyte differentiation from human pluripotent stem cells via temporal modulation of canonical Wnt signaling. *Proc Natl Acad Sci U S A* 109, E1848–E1857. <https://doi.org/10.1073/pnas.1200250109>

Lian, X., Zhang, J., Azarin, S.M., Zhu, K., Hazeltine, L.B., Bao, X., Hsiao, C., Kamp, T.J., Palecek, S.P., 2013. Directed cardiomyocyte differentiation from human pluripotent stem cells by modulating Wnt/ β -catenin signaling under fully defined conditions. *Nat Protoc* 8, 162–175. <https://doi.org/10.1038/nprot.2012.150>

Oxford, E., Hassan, M., Karen, M., Wanda, C., M., T.S., Mario, D., 2007. Connexin43 Remodeling Caused by Inhibition of Plakophilin-2 Expression in Cardiac Cells. *Circulation Research* 101, 703–711. <https://doi.org/10.1161/CIRCRESAHA.107.154252>

- Ma, D., Liu, Z., Loh, L.J., Zhao, Y., Li, G., Liew, R., Islam, O., Wu, J., Chung, Y.Y., Teo, W.S., Ching, C.K., Tan, B.Y., Chong, D., Ho, K.L., Lim, P., Yong, R.Y.Y., Panama, B.K., Kaplan, A.D., Bett, G.C.L., Ware, J., Bezzina, C.R., Verkerk, A.O., Cook, S.A., Rasmusson, R.L., Wei, H., 2018. Identification of an INa-dependent and Ito-mediated proarrhythmic mechanism in cardiomyocytes derived from pluripotent stem cells of a Brugada syndrome patient. *Scientific Reports* 8. <https://doi.org/10.1038/s41598-018-29574-5>
- Ma, D., Wei, H., Lu, J., Ho, S., Zhang, G., Sun, X., Oh, Y., Tan, S.H., Ng, M.L., Shim, W., Wong, P., Liew, R., 2013. Generation of patient-specific induced pluripotent stem cell-derived cardiomyocytes as a cellular model of arrhythmogenic right ventricular cardiomyopathy. *Eur Heart J* 34, 1122–1133. <https://doi.org/10.1093/eurheartj/ehs226>
- Machiraju, P., Greenway, S.C., 2019. Current methods for the maturation of induced pluripotent stem cell-derived cardiomyocytes. *World J Stem Cells* 11, 33–43. <https://doi.org/10.4252/wjsc.v11.i1.33>
- Makara, M.A., Curran, J., Little, S.C., Musa, H., Polina, I., Smith, S.A., Wright, P.J., Unudurthi, S.D., Snyder, J., Bennett, V., Hund, T.J., Mohler, P.J., 2014. Ankyrin-G Coordinates Intercalated Disc Signaling Platform to Regulate Cardiac Excitability In Vivo. *Circulation Research* 115, 929–938. <https://doi.org/10.1161/CIRCRESAHA.115.305154>
- Malhotra, J.D., Thyagarajan, V., Chen, C., Isom, L.L., 2004. Tyrosine-phosphorylated and Nonphosphorylated Sodium Channel β 1 Subunits Are Differentially Localized in Cardiac Myocytes. *J. Biol. Chem.* 279, 40748–40754. <https://doi.org/10.1074/jbc.M407243200>
- Mercier, A., Bois, P., Chatelier, A., 2017. Sodium Channel Trafficking. *Voltage-gated Sodium Channels: Structure, Function and Channelopathies* 246, 125–145. https://doi.org/10.1007/164_2017_47
- Mercier, A., Clément, R., Harnois, T., Bourmeyster, N., Bois, P., Chatelier, A., 2015. Nav1.5 channels can reach the plasma membrane through distinct N-glycosylation states. *Biochimica et Biophysica Acta (BBA) - General Subjects* 1850, 1215–1223. <https://doi.org/10.1016/j.bbagen.2015.02.009>
- Moriya, H., 2015. Quantitative nature of overexpression experiments. *Mol Biol Cell* 26, 3932–3939. <https://doi.org/10.1091/mbc.E15-07-0512>
- Multi Channel Systems MCS GmbH, 2019. Multiwell-MEA-System Manual. https://www.multichannelsystems.com/sites/multichannelsystems.com/files/documents/manuals/Multiwell-MEA-System_Manual.pdf
- Nerbonne, J.M., Kass, R.S., 2005. Molecular Physiology of Cardiac Repolarization. *Physiological Reviews* 85, 1205–1253. <https://doi.org/10.1152/physrev.00002.2005>
- Nishimura Rick A., Seggewiss Hubert, Schaff Hartzell V., 2017. Hypertrophic Obstructive Cardiomyopathy. *Circulation Research* 121, 771–783. <https://doi.org/10.1161/CIRCRESAHA.116.309348>

Noorman, M., Hakim, S., Kessler, E., Groeneweg, J.A., Cox, M.G.P.J., Asimaki, A., van Rijen, H.V.M., van Stuijvenberg, L., Chkourko, H., van der Heyden, M.A.G., Vos, M.A., de Jonge, N., van der Smagt, J.J., Dooijes, D., Vink, A., de Weger, R.A., Varro, A., de Bakker, J.M.T., Saffitz, J.E., Hund, T.J., Mohler, P.J., Delmar, M., Hauer, R.N.W., van Veen, T.A.B., 2013. Remodeling of the cardiac sodium channel, connexin43, and plakoglobin at the intercalated disk in patients with arrhythmogenic cardiomyopathy. *Heart Rhythm* 10, 412–419. <https://doi.org/10.1016/j.hrthm.2012.11.018>

Oren, C., Irit, H., Amira, G., Gil, A., Leonid, M., Monther, B., Lior, G., 2013. Modeling of Arrhythmogenic Right Ventricular Cardiomyopathy With Human Induced Pluripotent Stem Cells. *Circulation: Cardiovascular Genetics* 6, 557–568. <https://doi.org/10.1161/CIRCGENETICS.113.000188>

Paul J Tesar, M.S.E., 2018. Drug screening for human genetic diseases using iPSC models. *Human Molecular Genetics* 27, R89–R98. <https://doi.org/10.1093/hmg/ddy186>

Petros, S., Deirdre, W., Angeliki, A., Srijita, S.-C., Y., E.H., Alison, E., Nobuhiko, H., Mark, N., Antonios, P., L., S.A., M., E.P., J., M.W., 2006. Clinical Expression of Plakophilin-2 Mutations in Familial Arrhythmogenic Right Ventricular Cardiomyopathy. *Circulation* 113, 356–364. <https://doi.org/10.1161/CIRCULATIONAHA.105.561654>

Platonov, P.G., Haugaa, K.H., Bundgaard, H., Svensson, A., Gilljam, T., Hansen, J., Madsen, T., Holst, A.G., Carlson, J., Lie, Ø.H., Kvistholm Jensen, M., Edvardsen, T., Jensen, H.K., Svendsen, J.H., 2019. Primary Prevention of Sudden Cardiac Death With Implantable Cardioverter-Defibrillator Therapy in Patients With Arrhythmogenic Right Ventricular Cardiomyopathy. *The American Journal of Cardiology* 123, 1156–1162. <https://doi.org/10.1016/j.amjcard.2018.12.049>

Ponce-Balbuena, D., Guerrero-Serna, G., Valdivia, C.R., Caballero, R., Diez-Guerra, F.J., Jiménez-Vázquez, E.N., Ramírez, R.J., da Rocha, A.M., Herron, T.J., Campbell, K.F., Willis, B.C., Alvarado, F.J., Zarzoso, M., Kaur, K., Pérez-Hernández, M., Matamoros, M., Valdivia, H.H., Delpón, E., Jalife, J., 2018. Cardiac Kir2.1 and Nav1.5 Channels Traffic Together to the Sarcolemma to Control Excitability. *Circ Res* 122, 1501–1516. <https://doi.org/10.1161/CIRCRESAHA.117.311872>

Qu, Y., 1996. Phosphorylation of S1505 in the cardiac Na⁺ channel inactivation gate is required for modulation by protein kinase C. *The Journal of General Physiology* 108, 375–379. <https://doi.org/10.1085/jgp.108.5.375>

Qu, Y., Rogers, J., Tanada, T., Scheuer, T., Catterall, W.A., 1994. Modulation of cardiac Na⁺ channels expressed in a mammalian cell line and in ventricular myocytes by protein kinase C. *Proceedings of the National Academy of Sciences* 91, 3289–3293. <https://doi.org/10.1073/pnas.91.8.3289>

Reichart, D., Magnussen, C., Zeller, T., Blankenberg, S., 2019. Dilated Cardiomyopathy - From Epidemiologic to Genetic Phenotypes A Translational Review of Current Literature. *J. Intern. Med.* <https://doi.org/10.1111/joim.12944>

Rhett, J.M., Ongstad, E.L., Jourdan, J., Gourdie, R.G., 2012. Cx43 Associates with Nav1.5 in the Cardiomyocyte Perinexus. *J Membrane Biol* 245, 411–422. <https://doi.org/10.1007/s00232-012-9465-z>

Rizzo, S., Lodder, E.M., Verkerk, A.O., Wolswinkel, R., Beekman, L., Pilichou, K., Basso, C., Remme, C.A., Thiene, G., Bezzina, C.R., 2012. Intercalated disc abnormalities, reduced Na⁺ current density, and conduction slowing in desmoglein-2 mutant mice prior to cardiomyopathic changes. *Cardiovasc Res* 95, 409–418. <https://doi.org/10.1093/cvr/cvs219>

Roche, J. de la, Angsutararux, P., Kempf, H., Janan, M., Bolesani, E., Thiemann, S., Wojciechowski, D., Coffee, M., Franke, A., Schwanke, K., Leffler, A., Luanpitpong, S., Issaragrisil, S., Fischer, M., Zweigerdt, R., 2019. Comparing human iPSC-cardiomyocytes versus HEK293T cells unveils disease-causing effects of Brugada mutation A735V of NaV1.5 sodium channels. *Scientific Reports* 9. <https://doi.org/10.1038/s41598-019-47632-4>

Sato, P.Y., Musa, H., Coombs, W., Guerrero-Serna, G., Patiño, G.A., Taffet, S.M., Isom, L.L., Delmar, M., 2009. Loss of plakophilin-2 expression leads to decreased sodium current and slower conduction velocity in cultured cardiac myocytes. *Circ. Res.* 105, 523–526. <https://doi.org/10.1161/CIRCRESAHA.109.201418>

Séverine, P., Anne-Flore, Z., Jakob, O., Elise, B., Nour, R., Said, E.-H., Maxime, A., Philip, B., Stefan, L., E., L.S., N., H.S., Alain, C., Hugues, A., 2011. SAP97 and Dystrophin Macromolecular Complexes Determine Two Pools of Cardiac Sodium Channels Nav1.5 in Cardiomyocytes. *Circulation Research* 108, 294–304. <https://doi.org/10.1161/CIRCRESAHA.110.228312>

Štefková, K., Procházková, J., Pacherník, J., 2015. Alkaline Phosphatase in Stem Cells [WWW Document]. *Stem Cells International*. <https://doi.org/10.1155/2015/628368>

Strege, P.R., Holm, A.N., Rich, A., Miller, S.M., Ou, Y., Sarr, M.G., Farrugia, G., 2003. Cytoskeletal modulation of sodium current in human jejunal circular smooth muscle cells. *American Journal of Physiology-Cell Physiology* 284, C60–C66. <https://doi.org/10.1152/ajpcell.00532.2001>

Tamargo, J., Caballero, R., Gómez, R., Valenzuela, C., Delpón, E., 2004. Pharmacology of cardiac potassium channels. *Cardiovasc. Res.* 62, 9–33. <https://doi.org/10.1016/j.cardiores.2003.12.026>

Tan, B.Y., Jain, R., den Haan, A.D., Chen, Y., Dalal, D., Tandri, H., Amat-Alarcon, N., Daly, A., Tichnell, C., James, C., Calkins, H., Judge, D.P., 2010. Shared Desmosome Gene Findings in Early and Late Onset Arrhythmogenic Right Ventricular Dysplasia/Cardiomyopathy. *J. of Cardiovasc. Trans. Res.* 3, 663–673. <https://doi.org/10.1007/s12265-010-9224-4>

Tanawuttiwat, T., Te Riele, A.S.J.M., Philips, B., James, C.A., Murray, B., Tichnell, C., Sawant, A.C., Calkins, H., Tandri, H., 2016. Electroanatomic Correlates of Depolarization Abnormalities in Arrhythmogenic Right Ventricular Dysplasia/Cardiomyopathy: EAM Correlates of Depolarization in ARVD. *J Cardiovasc Electrophysiol* 27, 443–452. <https://doi.org/10.1111/jce.12925>

te Riele, A.S.J.M., James, C.A., Philips, B., Rastegar, N., Bhonsale, A., Groeneweg, J.A., Murray, B., Tichnell, C., Judge, D.P., van der Heijden, J.F., Cramer, M.J.M., Velthuis, B.K., Bluemke, D.A., Zimmerman, S.L., Kamel, I.R., Hauer, R.N.W., Calkins, H., Tandri, H., 2013. Mutation Positive Arrhythmogenic Right Ventricular Dysplasia/Cardiomyopathy: The Triangle of Dysplasia Displaced. *J Cardiovasc Electrophysiol* 24, 1311–1320. <https://doi.org/10.1111/jce.12222>

Undrovinas, A.I., Shander, G.S., Makielski, J.C., 1995. Cytoskeleton modulates gating of voltage-dependent sodium channel in heart. *American Journal of Physiology-Heart and Circulatory Physiology* 269, H203–H214. <https://doi.org/10.1152/ajpheart.1995.269.1.H203>

Valdivia, C.R., Ueda, K., Ackerman, M.J., Makielski, J.C., 2009. GPD1L links redox state to cardiac excitability by PKC-dependent phosphorylation of the sodium channel SCN5A. *Am J Physiol Heart Circ Physiol* 297, H1446–H1452. <https://doi.org/10.1152/ajpheart.00513.2009>

Wang, W., James, C.A., Calkins, H., 2019. Diagnostic and therapeutic strategies for arrhythmogenic right ventricular dysplasia/cardiomyopathy patient. *Europace* 21, 9–21. <https://doi.org/10.1093/europace/euy063>

